NASA Technical Memorandum 74044

Experimental Measurements of the Ground Cloud Effluents and Cloud Growth for the May 20, 1975, Titan IIIC Launch at Air Force Eastern Test Range, Florida

Gerald L. Gregory and Richard W. Storey, Jr.

NOVEMBER 1977

NASA

NASA Technical Memorandum 74044

Experimental Measurements of the Ground Cloud Effluents and Cloud Growth for the May 20, 1975, Titan IIIC Launch at Air Force Eastern Test Range, Florida

Gerald L. Gregory and Richard W. Storey, Jr.
Langley Research Center
Hampton, Virginia

National Aeronautics
and Space Administration

**Scientific and Technical
Information Office**

1977

SUMMARY

The report summarizes the effluent measurements and tests of ground cloud behavior made during the May 20, 1975, Titan IIIC (Air Force 777) launch from the Air Force Eastern Test Range (launch complex 40), Florida. The launch took place at 1404 universal time (1004 eastern daylight time). The launch vehicle effluent monitoring experiments were carried out jointly by Langley Research Center, Marshall Space Flight Center, and Kennedy Space Center, all of the National Aeronautics and Space Administration (NASA).

The experiment included surface level and airborne in situ cloud measurements of the exhaust effluents from the Titan IIIC solid rocket boosters. Simultaneous visible spectrum photographic pictures of the ground cloud as well as infrared imaging of the cloud were obtained to study the cloud rise, growth, and direction of travel within the Earth's surface mixing layer. The predictions of cloud growth, direction of travel, and expected surface level effluent concentrations prepared with the NASA multilayer diffusion model were made prior to launch and after launch using measured meteorological conditions. Prelaunch predictions were used to position the effluent monitoring instruments, and the postlaunch predictions were compared with the measured data.

The objectives of the experiment were to gather surface level and airborne in situ cloud effluent measurements for a comparison with the NASA diffusion model predictions as well as to obtain cloud rise and growth data to aid in reducing the uncertainty associated with the several empirical inputs to the diffusion model (for example, cloud stabilization altitude and volume).

Measurement results showed that surface level effluent values were low, often below the detection limits of the instrumentation. The maximum measured surface level hydrogen chloride concentration was 50 parts per billion at about 8 km from the launch pad. Particulate concentrations measured at the surface (attributed to the launch) were below 30 $\mu g/m^3$ at all instrumented sites. Several minutes after launch airborne measurements in the stabilized ground cloud showed maximum hydrogen chloride concentrations of 7 parts per million, maximum nitrogen oxide concentrations of 1 part per million, and average particulate concentrations from 1000 to 3000 $\mu g/m^3$. Measurements showed that by about 1 hr after launch, these effluent values had decayed to less than 0.5 part per million for hydrogen chloride, 0.1 part per million for nitrogen oxide, and approximately 200 to 400 $\mu g/m^3$ for particulates. In addition, airborne particulate measurements indicated that only about 7 to 20 percent of the measured particulates could be attributed to aluminum oxide (i.e., solid rocket motors). The remaining particulates were assumed to be launch debris. The stabilization altitude of the ground cloud (i.e., that cloud determined to be the source of the observed surface level effluents) was measured to be in the range of 1400 to 1900 m. The predicted stabilization altitude (that value used in the postlaunch model calculations) of the ground

cloud centroid was approximately 1300 m. The trajectory of the ground cloud was determined to proceed in a direction of 145° to 165° from the pad and agreed with a predicted trajectory direction of 161°.

Comparisons of the postlaunch model predictions of the surface level effluent values with the measured values showed that on the average for the May 1975 case, the model predictions were high by at least a factor of 5 for maximum hydrogen chloride concentration, and by about a factor of at least 10 for maximum aluminum oxide concentration and total dosage at a site.

INTRODUCTION

The National Aeronautics and Space Administration (NASA) is actively pursuing tropospheric and stratospheric environmental studies in conjunction with rocket firings. The tropospheric program is aimed at measuring and predicting the impact of ground clouds produced at launch on the surface level air quality. The launch vehicle effluent (LVE) monitoring program is conducted by the Langley Research Center (LaRC) with intercenter support from Marshall Space Flight Center (MSFC) and Kennedy Space Center (KSC). The goal of the LVE program is to assess the applicability and accuracy of diffusion models for predicting the dispersion of exhaust effluents from NASA's current and future launch vehicles. The objectives of the program are to develop data to be used in the establishment of potential launch constraints and to develop in-house expertise in the areas relating to the environmental impact of launch activities. The approach employed to meet these objectives is that of measuring rocket exhaust products (produced by large solid rocket motor launch vehicles) at surface level and within the "stabilized ground cloud" formed in the troposphere as the result of the launch. The measurements will be used to make direct comparisons with the diffusion models and NASA rocket plume codes that are used to predict effluent composition and concentrations. In addition, many of the empirical inputs (for example, cloud stabilization altitude and volume) required by the models can be measured in association with the surface level effluent measurements.

This report summarizes the effluent measurements and ground cloud behavior for the Titan IIIC launch (Air Force payload 777) of May 20, 1975. The Titan vehicle was launched from launch complex 40 (LC-40) located at the Air Force Eastern Test Range (AFETR), Florida. Launch time was 1404 UT (1004 EDT). References 1 to 3 describe similar measurements for Titan IIIC launches in 1973 and 1974.

This experiment included surface level and airborne in situ cloud measurements of the exhaust effluents from the Titan IIIC solid rocket motor boosters. Simultaneous visible spectrum photographic pictures of the ground cloud as well as infrared imaging of the cloud were obtained to study the cloud rise, growth, and direction of travel within the Earth's surface mixing layer. The NASA (MSFC) multilayer diffusion model predictions of cloud growth, direction of travel, and expected ground level effluent concentrations were made prior to launch and after launch using measured meteorological conditions.

The authors acknowledge the cooperation and support of personnel from Marshall Space Flight Center, John F. Kennedy Space Center, U.S. Air Force, and the respective contractors for these agencies during the experimental measurement program.

SYMBOLS

Q	sample flow rate, m^3/min or l/min
t	sample time, min
W_c	corrected mass gain, μg
W_H	handling effects correction fator, μg
W_S	uncorrected sample mass gain, μg
X_A	normal ambient particle concentration, $\mu g/m^3$

Abbreviations:

AFETR	Air Force Eastern Test Range
EDT	eastern daylight time
FM	frequency modulated
JPL	Air Force facility number 27200
KSC	John F. Kennedy Space Center
LaRC	Langley Research Center
LC-40	launch complex 40
LVE	launch vehicle effluent
MSFC	Marshall Space Flight Center
NASA	National Aeronautics and Space Administration
P	primary instrument site
ppb	parts per billion (volume/volume)
ppm	parts per million (volume/volume)
QCM	quartz crystal mass monitor
S	secondary instrument site

SRM solid rocket motor

T time relative to launch; $T \equiv 0$ is launch

TVC thrust vector control

UCS universal camera site

UT universal time

PROGRAM DESCRIPTION

Launch Vehicle

Figure 1 shows the Titan IIIC launch vehicle just after lift-off. The rocket exhaust from about the first 10 to 20 sec (depending upon meteorological conditions) of burn is contained in the ground cloud that forms and typically rises to a stabilization height within 15 min after launch. The Titan IIIC launch vehicle consists of a three-stage core using a liquid propulsion system and two solid rocket motors (SRM) attached on opposite sides of the core. The liquid propulsion systems are ignited at high altitude and only the SRM boosters contribute effluents to the ground cloud. The two SRM boosters have a mass flow rate at lift-off of 4160 kg/sec. In addition, the thrust vector control (TVC) system expends nominally 45 kg/sec of nitrogen tetroxide (N_2O_4) into the nozzle flows of both boosters during the formation of the ground cloud. The TVC and SRM mass flow rates are nearly constant during the first 10 to 20 sec of burn. The SRM propellant consists of an ammonium perchlorate oxidizer, an aluminized synthetic-rubber binder fuel, and various other additives to stabilize mass and to control the burning rate. The major constituents after combustion are hydrogen chloride (HCl), aluminum oxide (Al_2O_3), carbon monoxide (CO), carbon dioxide (CO_2), molecular nitrogen (N_2), and water vapor (H_2O). The TVC constituents decompose in the rocket exhaust to nitric oxide (NO) and oxygen (O_2). The motor exit plane composition (ref. 4) is shown in table I as is the exhaust product composition after afterburning plume calculations. (See ref. 5.) Plume afterburning is essentially complete at 1 km from the motor exit plane. The mass of Al_2O_3 is assumed to be conserved in the afterburning calculations. As a result of the afterburning process, almost all the CO is combusted to CO_2, the mass of HCl decreases slightly resulting in an increase in chlorine gas (Cl_2), and NO is produced.

Stabilized Ground Cloud

During the launch of a rocket vehicle, the initial exhaust from the vehicle generates a ground cloud in the immediate vicinity of the launch pad. As a result of its heat content, this cloud rises to a stabilization altitude and drifts and diffuses with the prevailing winds. Depending upon the buoyancy (heat content) of the cloud and the height of the surface mixing layer, the cloud typically stabilizes vertically between altitudes of 500 and 3000 m within 15 min after launch. At stabilization altitude the cloud is termed "a stabilized ground cloud" and is trapped between the Earth's surface and the top

of the surface mixing layer. Initially, the cloud is composed of those species generated by the rocket motor exhaust; however, as the cloud rises, stabilizes, and drifts with the wind, it entrains large quantities of atmospheric air. At the time of stabilization, rocket exhaust effluents make up less than 1 percent of the cloud. Typical Titan III cloud volumes measured at stabilization are 2 to 7 km^3. Under favorable meteorological conditions, the stabilized ground cloud may be visible for 1 hr after launch and be transported 20 to 30 km from the launch pad.

Prelaunch Effluent Predictions

Prelaunch effluent predictions made with the dispersion model (ref. 6) and meteorological forecasts were used to design the effluent sampling experiment. Predictions began at T - 24 hr and continued to T - 3 hr. Meteorological forecasts were based on local wind tower observations, local rawinsonde and tetroon releases, and synoptic weather data as supplied by the National Weather Service network. Marshall Space Flight Center (MSFC) personnel provided both the effluent predictions and the meteorological forecasts (ref. 7). Table II briefly summarizes the prelaunch predictions. Figure 2 summarizes some of the prelaunch wind field soundings used in the meteorological forecasts and indicates wind speed and direction as a function of altitude.

Locations of Surface Level Instruments

The azimuth and distance from the launch pad of each of the 43 sampling sites used in the effluent sampling study are shown in figure 3 and table III. All sites except site AA were selected on the basis of prelaunch dispersion predictions and meteorological forecasts. Site AA, a permanent site for all LC-40 launches, is located on the launch complex perimeter road. During the sampling program, each primary site (P) was manned by two instrument technicians and two test conductors. All other sites (secondary and fallback) were unmanned, and the sampling instrumentation was activated and deactivated remotely from the LVE operations center. Because of the location of LC-40 and the frequency of westerly winds, there is always a high probability that the ground cloud will drift over the ocean. In order to cover this possibility, nine seacraft were obtained as potential primary sampling platforms. As shown in figure 4, the T - 24 hr prediction showed the effluent cloud moving over the ocean. This prediction led investigators to prepare the seacraft for a potential sampling mission. The T - 10.5 hr prediction indicated a cloud trajectory down the coast; such a trajectory required a combination land-sea deployment. At T - 10 hr, the decision was made to locate primary sites 1 to 5 at sea and the instrumentation was placed aboard the seacraft. Final commitment of the seacraft to the sampling mission was withheld until T - 6 hr. At T - 6 hr the seacraft departed the port with the site plan shown in figure 5. The assigned site plan was based on the predicted T - 6 hr trajectory of 174° azimuth with three constraints: (1) meteorological conditions at that time indicated a possible eastward swing of 20° to 30° of the predicted trajectory; (2) water depths in crosshatched areas (fig. 5) were too shallow for safe seacraft operations; and (3) seacraft run time (due to location of shallow water) from area of P-4 and P-5 to the P-1, P-2, and P-3 area was several hours. At T - 4 hr,

the predicted trajectory of the cloud was at an azimuth of 157° from the launch pad; at this time site locations P-1 to P-5 were reviewed and updated and site locations P-6 to P-9 were selected. Figure 6 shows the final primary site plan as well as the predicted surface level HCl isopleths. The same three constraints discussed earlier for the T - 6 hr site plan led to the decision to have seacraft both east (P-1 to P-3) and west (P-4 and P-5) of the shallow water area. The T - 3 hr prediction showed little change in the cloud trajectory, and no further changes in the primary site plan were made during the minus count. As shown in figure 6, site P-3 was moved to P-3' at about T + 42 min. This decision was based on about 40 min of real-time cloud trajectory track and the seacraft captain's willingness to navigate the shallow water area. The seacraft was to head southeast and, at the discretion of the captain, swing west in order to navigate past the shallow water area. At about T + 72 min, this plan was abandoned for safety reasons; the seacraft was then instructed to stop at site P-3' and to continue effluent sampling until completion of the mission.

The remaining 33 sampling sites (shown in fig. 3) were selected using the model predictions and meteorological forecasts from T - 24 hr to T - 3 hr. These site selections are summarized in the following paragraphs.

T - 24 hr prediction.- This prediction was used to select fallback sites CC, DD, and FF. These sites were selected because they were the sites closest to the azimuth (99°) of the predicted (T - 24 hr) cloud path with the required electrical and control power lines. Instruments at these sites required both hard lines for electrical power and control circuits for activation and deactivation of instrumentation.

T - 10.5 hr prediction.- This prediction was used to select instrument sites S-1 to S-10 and S-16 to S-25. Since the T - 10.5 hr predicted cloud trajectory was along the coast (160°), these 20 secondary sites were located from the coast to about 175° which was 15° inland of the coast.

T - 6 hr prediction.- This prediction was used to select instrument sites for the remaining secondary instruments (S-11 to S-15 and S-26 to S-30). Since the predicted cloud path was 174° and those secondary sites selected at T - 10.5 hr adequately covered the regions from the coast line to the predicted cloud path, these additional 10 secondary sites were on the whole located west of the predicted cloud path (173° to 180°). With the selection of these sites, the predicted cloud path (T - 6 hr) was bounded ±10° to 15° with secondary instrument sites.

T - 3 hr prediction.- This prediction was used to update the sampling schedule for all instrument sites and provided cloud path and stabilization altitude data for both the optical tracking and airborne sampling teams.

The postlaunch (T - 0) effluent predictions using the NASA (MSFC) dispersion model and the actual launch time meteorological data are presented in the section of this report entitled "Results and Discussion."

Airborne Sampling Plan

The sampling aircraft, a twin-engine light aircraft, was airborne at approximately T - 30 min. Range safety required the aircraft to be in a holding pattern at an altitude of approximately 1000 m, approximately 6 km west of the launch pad. (See fig. 7.) At T + 1 min the aircraft was released from the holding pattern and was radar vectored toward the launch pad to perform the sampling mission. The sampling plan used by the aircraft was a series of basic downwind and crosswind penetrations of the exhaust cloud. (See fig. 8.) This sampling plan is described as follows:

Pass 1: downwind penetration at the altitude of the center of the ground cloud

Pass 2: crosswind penetration at the altitude of the center of the ground cloud

Pass 3: downwind penetration at Pass 2 altitude minus 150 m

Pass 4: crosswind penetration at Pass 3 altitude

Pass 5: downwind penetration at Pass 4 altitude minus 150 m

Pass 6: crosswind penetration at Pass 5 altitude

Pass 7: downwind penetration at Pass 6 altitude minus 150 m

Pass 8: crosswind penetration at Pass 7 altitude

Pass 9: downwind penetration at the altitude of the center of the ground cloud

Pass 10: crosswind penetration at Pass 9 altitude

Additional odd numbered passes: downwind penetration at Pass 9 altitude

Additional even numbered passes: crosswind penetration at Pass 9 altitude

This sampling plan was based on previous sampling experience which indicated that the aircraft crew could visually identify the exhaust cloud and could estimate while in-flight the altitude of the center of the cloud required for sampling passes 1, 2, and 9. A similar alternate plan was prepared in the event that the necessary visual observations were not possible. In this case, the aircraft would be vectored from the LVE control center based on model predictions, meteorological conditions, real-time optical cloud track, and the collection of surface level effluent data. For the May 1975 mission, the visual flight plan described above was followed for the first 16 penetrations of the cloud. After Pass 16 (approximately T + 65 min), the cloud could not be distinguished from the ambient environment; at this point, the aircraft was

directed (alternate flight plan) to fly downwind passes at a heading of 180° from LC-40. Two passes were flown (altitudes of 300 and 1500 m), each starting at LC-40 and terminating approximately 20 km south of the launch pad. During these passes, the cloud was not located, either visually or with the effluent sampling instrumentation onboard the aircraft. At this point (T + 80 min), the airborne sampling mission was terminated.

Onboard the aircraft was an S-band beacon which was tracked by ground radar to obtain aircraft position as a function of time. However, after Pass 4, overflights of the radar position by the sampling aircraft resulted in frequent loss of signal by the radar, and aircraft position data were not obtained. Table IV shows the flight parameters associated with each aircraft pass. These flight parameters together with the associated effluent measurements will be discussed in detail in the section entitled "Results and Discussion."

Measurement Systems

Surface level effluent measurement systems.- The instruments used at each sampling site are listed in table V. The sampling capabilities of each type of instrument and any laboratory analysis required in reporting the data are described in table VI. Column 1 of table VI lists those references (refs. 8 to 10) which describe the operation of the various instruments. All instruments are commercially available and their characteristics are well documented. Where possible, the performance parameters given in table VI are based on laboratory and field experience with each sampling unit. In lieu of this experience, manufacturer values are quoted. Particle laboratory analysis was directed at: (1) the identification of chemical elements and their relative abundance by neutron activation analyses and (2) the determination of mass loading by gravimetric analysis. Appropriate background samples were taken prior to launch using selected instruments and are presented in the section entitled "Results and Discussion."

Airborne effluent measurement systems.- A sketch of the airborne sampling platform and the location of the various effluent sensors are shown in figure 9. The aircraft and the associated instrumentation are described in detail in reference 11. All the effluent air samples are taken into the aircraft through sampling probes located in the nose of the aircraft. The air sampling probes extend forward of the aircraft nose and sample undisturbed free-stream air. A photograph of the aircraft is shown in figure 10. Table VII describes the characteristics of the airborne effluent monitoring instrumentation. The flight data, meteorological instruments, and data acquisition systems are also described in reference 11.

Optical systems.- Three metric tracking units (Askania cameras) were employed to determine the rise and direction of travel of the effluent ground cloud as a function of time. In addition, a time-sequenced camera (Hassalblad) was positioned at each of the metric tracking sites to obtain color still photographs of the cloud at preselected time intervals after launch. The locations of the tracking units and cameras are shown in figure 11.

An infrared imaging system was mounted on top of the metric tracking units at the north camera site, UCS-9, and the south camera site, JPL. The imagers scan with a field frequency of 16 Hz in the wavelength region from 2.0 to 5.6 μm. The device has a line frequency of 1600 Hz and employs a $10^{o} \times 10^{o}$ 134-mm f/1.8 infrared lens system. Color imaging is recorded on FM (frequency modulated) tape and real-time images are displayed on a color cathode ray tube. Temperature differences of less than 0.2^{o} C can be detected for object temperatures of 30^{o} C.

RESULTS AND DISCUSSION

Postlaunch Effluent Calculation

Effluent dispersion calculations, based on the launch time meteorological conditions, were made after the launch so that the model could be compared with the effluent measurements and the observed cloud behavior. These effluent calculations were performed by MSFC using the diffusion models described in reference 6. These postlaunch effluent calculations are those supplied to LaRC by MSFC several months after launch and reflect the modeling strategy and theory available at that time. These effluent calculations do not reflect model refinements made since the May 1975 launch. The meteorological conditions used in the postlaunch analysis are based on a T + 1 hr, 53-min rawinsonde sounding and T - 0 thermodynamic and kinematic tower data (ref. 7). Figures 12 to 14 and tables VIII to X summarize the postlaunch calculations. Figure 12 shows the meteorological data used in the postlaunch model calculations. Figure 13 shows the predicted HCl surface level isopleths of 0.02, 0.11, and 0.17 ppm. As shown, the maximum surface level HCl concentration was predicted to be 0.23 ppm, 161^{o}, and 14.5 km from the launch pad. Figure 14 gives the surface level cloud center line HCl concentrations and dosages as a function of distance from the launch pad. Table VIII shows the predicted cloud rise and stabilization data. Table VIII also shows two cloud stabilization times and altitudes. The effluent cloud was predicted to have stabilized at about 15 min after launch and at an altitude of 2243.4 m. However, a study of the launch meteorological data (fig. 12) showed a wind shear layer at about 1829 m, and this wind shear was assumed by MSFC to be strong enough to act as a mass boundary in the diffusion model. Thus, only that effluent in the initial cloud below 1829 m is assumed to be transported to the surface in the model predictions. Having considered the vertical distribution of the exhaust effluents emitted below 1829 m, the prevailing meteorological conditions, and the physical processes involved, MSFC personnel determined that the proper stabilization time and altitude for use in the model calculations were approximately 4 min after launch with a cloud centroid altitude of 1318 m. The cloud geometry assumed for the ground cloud (model source cloud) was an ellipsoid with major axes X and Y of 2872 m and a minor axis Z of 1022 m. Figure 15 shows a sketch of the cloud geometry. Table IX shows the predicted ground cloud track and growth as a function of time. Table X gives the predicted HCl and Al_2O_3 surface level concentrations and dosages for each of the surface level instrument sites. The ± value following each entry represents a reasonable error band for the predicted effluent values. This error band is approximately equivalent to a $\pm 10^{o}$ error in predicting the cloud trajectory.

The predicted concentrations and dosages for CO, CO_2, and NO can be obtained from the HCl data by multiplying by the appropriate constants given in table XI. The conversion factors of table XI take into account the afterburning in the plume as discussed in reference 5. The predictions presented in this section will be discussed in more detail as the experimental measurements are discussed.

Cloud Rise, Stabilization, Growth, and Trajectory Measurements

The type of data presented in this section is being used by MSFC to assess and refine (when necessary) some of the empirical inputs to the models (for example, cloud stabilization altitude and volume). This assessment is conducted by MSFC on a continuing basis as each data set is made available. The data discussion of this section is limited to the May 1975 launch predicted and measured data only. Reference to any assessment of the empirical inputs for the model based on either the overall body of data available to date or the May 1975 data is beyond the scope of this report.

The metric tracking cameras and infrared imaging systems tracked the exhaust cloud optically for approximately 50 min after which the cloud could not be distinguished from the ambient background. Figure 16 shows the measured and postlaunch predicted rise of the exhaust cloud to stabilization altitude. The error bars represent one standard deviation calculated from the data taken with the three metric tracking units. Metric tracking data beyond 32 min are not shown. At times greater than 32 min, the one sigma standard deviations were large (±300 m) and inconsistent. These high values indicated that the tracking crews were experiencing difficulty in defining the center of the cloud. Also shown in figure 16 are the altitude and time of aircraft sampling passes 1, 2, 9, and 10. These were the only airborne sampling passes in the first 32 min after launch designed to sample at the altitude of the cloud center. The following points indicated by figure 16 should be noted:

(1) The metric tracking data agree reasonably well with the predicted rise and stabilization of the initial exhaust cloud (2200 m at T + 15 min). In addition, the altitudes of sampling passes 1 and 2 support the predicted data (up to T + 7 min) and confirm the accuracy of the metric tracking data. The metric tracking data lead to the conclusion that the initial cloud stabilized at an altitude of approximately 1900 m, 12 to 14 min after launch. In addition, the metric tracking data (T + 12 to T + 32 min) suggest that the initial cloud remained intact and that the effluents above and below the assumed mass boundary layer (wind shear) at 1829 m are transported in the same direction and together. Based on the wind speed and direction (fig. 12) at 1900 m (measured initial cloud stabilization altitude) and 1318 m (MSFC calculated stabilization altitude), a separation of only 1 km (ground distance, maximum) would occur from T + 12 to T + 32 min. Because of the size of the initial cloud and the location of the metric tracking stations, this separation could not be detected. Thus, the metric tracking data neither validate nor invalidate the MSFC analysis of exhaust cloud stabilization for this launch.

(2) If the assumption is made that the aircraft crew's estimation of the center of the ground cloud is reasonably accurate, then the altitude of

sampling passes 9 and 10 suggests that the ground cloud stabilization altitude is 1400 to 1500 m, an estimate which agrees equally well with the MSFC assumption and the metric tracking data. The flight crew observed that the initial cloud appeared as a double ball (one on top of the other); as time progressed, however, the lower ball flattened and elongated against the bottom of the upper ball while the upper ball flattened itself against the inversion level at the same time. At about T + 7 min the tangent point of the two balls is estimated (based on flight notes) to be 1300 to 1500 m. The altitude of this tangent point appeared to increase slowly with time. The airborne sampling was conducted in the lower cloud.

Therefore, from the available measurement data, there is no evidence to invalidate the assumptions that the initial cloud stabilized above the assumed mass boundary layer (1829 m), that the ground cloud (model source) consisted of effluents only below 1829 m, and that the proper stabilization of the ground cloud was around 1300 m. On the other hand, neither can the measured cloud rise and stabilization data confirm these assumptions although the flight crew's observations tend to support the existence of some type of mass boundary layer in the vicinity of 1300- to 1500-m altitude. In the following discussions of stabilization altitude, cloud growth, and trajectory, the major sources of the data are the metric tracking cameras and other photographs taken from the ground tracking stations. In considering these discussions, the potential for the existence of two separate clouds must be kept in mind.

Figure 17 summarizes the measured cloud rise data for five Titan launches. As shown, during the first 3 to 4 min following the launch, all five clouds rose at nearly 5 m/sec, apparently independent of the existing wind field and vertical thermodynamic structure of the lower atmosphere. After the initial rise, the clouds stabilized at an altitude that was strictly dependent on the buoyancy of the cloud and the vertical thermodynamic structure of the atmosphere.

Figure 18 shows a comparison of measured and predicted crosswind dimensions of the cloud. The measured data were obtained from the time-sequenced photographs taken at camera site JPL, a location approximately in line with the observed cloud trajectory. Thus, these photographs provide essentially a perpendicular view of the crosswind dimensions of the oncoming cloud. The measured data points indicate the average cloud crosswind dimension, and the indicated upper bound is the maximum horizontal crosswind dimension of the irregularly shaped cloud. As shown, the predicted crosswind dimension is nearly constant with respect to time whereas the measurements show an increasing crosswind with time. Crosswind measurements beyond 25 min were not obtained because the cloud was no longer sufficiently distinguishable from the ambient background. If it is assumed, as has been observed from some past launches (see fig. 19), that the measured crosswind dimension approaches an asymptotic value, then from the data represented in figure 18, this value is approximately 3000 m. This value agrees with the predicted crosswind growth. This assumption suggests that the predicted crosswind dimension is in error at the earlier times, thus failing to predict the initial growth of the cloud in the crosswind direction.

Figure 20 shows the measured ground trajectory of the cloud center as determined from the metric tracking cameras. The error bands at T + 20, 40, and 50 min are one sigma standard deviation as determined from the three camera stations. The increases in the standard deviation at the longer times illustrate the larger errors associated with determining cloud position as identification of the cloud from the background becomes more difficult. As observed, the cloud traveled south from the pad at an average speed for the first 50 min of approximately 2.25 m/sec. At T + 50 min, about 7 km from the pad, the cloud could not be distinguished from the background and appeared to have dispersed. Also shown for reference in the figure are the ground locations of aircraft Passes 1 to 4. (These are the only four aircraft passes in which ground position data for the aircraft were obtained.) Figure 21 shows a comparison of the predicted (table IX) and the measured cloud trajectory. The predicted cloud trajectory is about 161° from the pad whereas the measured (metric tracking data) cloud trajectory is about 175°. The predicted trajectory (161°) is consistent with the stabilization altitude assumed by the model of 1318 m, and the measured trajectory is consistent with the stabilization altitude determined by metric tracking of about 1900 m. (See wind direction-altitude profile of fig. 12.)

Figure 22 shows some of the visible photographs of the exhaust cloud. These photographs were taken with a hand-held camera located 179° and 7.8 km from the launch pad. For better figure reproduction, the outline of the exhaust cloud has been traced. The cloud is moving towards the camera.

Ground Level Effluent Measurements

Ambient background.- During the monitoring program, background effluent sampling was conducted to define the ambient concentrations of the three surface-level effluents measured during the launch: HCl, CO, and suspended particulates. Background samplings for these species were conducted at the individual primary sites from about T - 1 hr to about T - 15 min. Ambient HCl and CO concentrations were below the lower detection limit of the instrumentation: 5 ppb and 0.5 ppm, respectively. Figure 23 shows a typical ambient particle background. The data are from the mass monitor (particles 0.1 to 10 μm in diameter) located at site P-1 and show an average particle loading of about 30 $\mu g/m^3$ with instantaneous loadings as high as approximately 60 $\mu g/m^3$. To obtain the aluminum content of the ambient particle background, nuclepore sampling (suspended particles greater than 0.01 μm in diameter) was performed several days prior to launch and was submitted to neutron activation analysis for aluminum quantitation. Three background samples were taken and one of these was submitted to neutron activation analysis. In addition, 10 nuclepore filters were loaded into filter holders, stored with the launch filters, and then unloaded and weighed after launch to determine handling effects. To identify the aluminum, two of these 10 filters were subjected to neutron activation analysis. Table XII summarizes the background and handling loadings, and table XIII gives the aluminum results from neutron activation analysis.

Launch particulate loading.- The mass monitors located at sites P-1 through P-9 showed no increase in particulate loading as the result of the launch as only normal ambient fluctuations (similar to those of fig. 23) were

noted. The lower detection limit for the launch particulates is taken to be the average particulate background concentration; thus, the concentration of launch particulates at these nine sites is assumed to be less than 30 $\mu g/m^3$. Particulate samples from the eight-stage cascade impactor were of insufficient quantity for analysis and the light scattering photometers at sites P-1 to P-3 showed no launch effluents. All but one nuclepore sample (S-29) showed mass gains above the ambient and handling effects of table XII. Table XIV shows the nuclepore data. All nuclepore filters were weighed before and after launch in a class-100 clean room and then only after the sample had equilibrated to the clean room environment. Column 6 of table XIV is the uncorrected mass gain of the filter (postlaunch weight minus prelaunch weight). Column 7 is the corrected mass gain obtained from column 6 by correcting for handling and normal ambient background effects. Equation (1) is used to calculate corrected mass gain, where W_H and X_A were taken to be 13 µg and 30.1 $\mu g/m^3$, respectively (from table XII):

$$W_c = (W_S - W_H) - X_A Qt \qquad (1)$$

where

W_c corrected mass gain, µg

W_S uncorrected sample mass gain, µg

W_H handling effects correction factor, µg

X_A normal ambient particle concentration, $\mu g/m^3$

Q sample flow rate, m^3/min

t sample time, min

All the corrected mass gains in table XIV are above one sigma standard deviation (table XII) of the ambient background and handling and thus are statistically significant samples and potential samples of particulates from the launch. These samples were subjected to neutron activation analysis to identify the quantity of aluminum present in each sample. Table XV shows the results. Again equation (1) is used to calculate the corrected aluminum mass, but in this case W_H and X_A are 1.91 µg and 0.07 $\mu g/m^3$ of aluminum, respectively (from table XIII). Only seven sites showed aluminum above background and handling, and only the sample at site AA showed aluminum content of sufficient quantity for further discussion. For example, at site P-1 the 2.39-µg aluminum mass (corrected mass gain) represents only about 2 percent of the total corrected mass gain (111.4 µg) of the filter, and aluminum handling and background corrections accounted for 50 percent of the total aluminum sample. Therefore, with the exception of site AA, for reporting purposes in the remaining portions of this report, all the aluminum present in a nuclepore sample is assumed to be from the launch, and the aluminum deposition (dosage) at a site is assumed to be equal to or less than that value reported in column 2 of table XV (uncorrected filter mass gain). To obtain Al_2O_3 deposition from column 2 of table XV, the aluminum content is multiplied by 1.9 (1.9 g of Al_2O_3 contain

1 g of aluminum). For example, for site P-1 the Al_2O_3 deposition is reported as less than 8.6 μg.

Carbon monoxide.- The CO instrumentation at sites P-1 to P-5 showed no CO as the result of the launch. Therefore, at these sites ground level CO concentrations as the result of the launch were less than 0.5 ppm (lower detection limit).

Hydrogen chloride.- Except for site AA (on the launch pad) HCl dosages were below 80 ppm-sec, the detection limit of the bubbler sampling system. The HCl dosage at site AA was 130 ± 75 ppm-sec as determined from two bubblers. Although pH paper measurements are qualitative, they are useful in determining those areas where HCl is present. Acid spotting of pH paper occurred at sites AA, P-2, P-4, P-6, S-4, S-5, S-8, S-10, S-24, and S-25. In most cases the acid spotting was light, a result indicating low effluent concentrations in comparison with other launches. Figure 24 shows the site plan and indicates the sites where pH paper spotting occurred. The pH paper results identified primary sites P-2, P-4, P-6, and P-7 as those most likely to have detected HCl with the concentration monitoring instrumentation.

No HCl was detected at site P-1, P-3, P-3', P-5, P-6, P-7, P-8, or P-9 using the concentration monitoring instrumentation. The lower detection limit for HCl was 5 ppb at sites P-1, P-3, P-3', P-5, and P-8; 30 ppb at sites P-7 and P-9; and 40 ppb at site P-6. The higher detection limit at some of the sites was the result of operator error or noise in the data acquisition system. HCl was believed to be detected by the chemiluminescent HCl detector at sites P-2 and P-4. Figure 25 shows the HCl data trace at site P-2 from T + 40 to T + 140 min. No HCl above 5 ppb (lower detection limit) was detected prior to T + 40 min. Those times of suspected HCl detection are noted in the figure. The low HCl concentrations observed at the surface, the instrument drift, and the instrument response time at these low concentrations led to the conclusion that the maximum HCl concentration at site P-2 was about 50 ppb and the HCl dosage was below 1 ppm-sec. Figure 26 shows the HCl data trace from site P-4. The instrument's output shows a continuous positive drift from about T - 0 to about T + 53 min and then returns and remains at 0 for the duration of the sampling at site P-4 (T + 128 min). This drift is probably 0 drift of the instrument with some HCl superimposed over it. The 0 drift and superimposed HCl cannot be separated with any reasonable accuracy. Because of the speculative nature of the data and because pH paper spotting did occur at site P-4, HCl was probably detected by the chemiluminescent detector, but concentration and dosage were less than 30 ppb and 10 ppm-sec, respectively.

Based upon the low levels of HCl observed at sites P-2 and P-4, any HCl occurring at sites P-6 and P-7 would most likely have been below the detection limit of the chemiluminescent instruments at those locations; thus, the pH paper results and chemiluminescent instrument data are consistent.

Wind direction and wind speed.- Since sites P-1 to P-5 were located on seacraft, wind measurements were not made. Wind measurements (surface level at an altitude of approximately 3 m) made at sites P-6, P-7, and P-8 were consistent among the sites and agreed with the launch meteorological data shown

in figure 12. The measurements indicated a wind speed of 2.5 to 4.0 m/sec from about 300° to 340°.

Airborne Effluent Measurements

As discussed earlier, the aircraft was equipped to monitor HCl, suspended particulates, NO, NO_x, CO, and CO_2. The characteristics of the airborne instrumentation were discussed earlier (table VIII) as were the flight parameters (table IV) associated with each sampling pass. Figure 27 shows the data obtained during the second airborne sampling pass and illustrates the type of data obtained during each sampling pass. Data traces for 16 sampling passes are shown in appendix A. The CO/CO_2 instrument malfunctioned during the mission and no data were obtained. Only the NO_x data for each sampling pass are shown as the NO/NO_x measurements indicate that essentially all the NO_x is attributed to NO. With reference to figure 27, the effluent data indicate that the effluent concentrations show an in-cloud structure (i.e., concentration varies as a function of position in the cloud). This observed structure is a function of the irregular shape of the cloud and the actual distribution of effluents in the cloud as well as of the response time of the various instruments. The NO/NO_x and nephelometer (particles) data show nearly identical cloud structure. Because of the detection limit of the HCl instrument (0.5 ppm), the scale on which the data were recorded (0 to 20 ppm), and the low in-cloud HCl concentrations, the HCl measurements indicate a similar cloud structure, but they do not provide as much detail as the nephelometer and NO/NO_x instruments.

The airborne QCM particulate measurements were influenced by moisture collection and evaporation from the crystal sensor. During some of the airborne sampling passes, the QCM data showed a series of peaks and valleys (in the concentration plotted against time profile) not observed in the other data (faster responding instruments) taken aboard the aircraft. The peaks are attributed to the accumulation of particulates as well as moisture and aerosol, and the large valleys (negative particle loadings in some cases) probably result from the subsequent evaporation of the moisture and aerosol. The net effect is that some of the QCM data are probably not a valid representation of the in-cloud particulate structure. Appendix A discusses this moisture effect in some detail and identifies those sampling passes where the moisture effect is most serious. The QCM data of figure 27 (Pass 2) are from one of the sampling passes not believed to be seriously affected by the moisture problem. Because the HCl concentrations are near the detection limit of the HCl instrument and because of the moisture problem with the QCM, the nephelometer and NO/NO_x data represent more closely the actual in-cloud structure for the particulates and gas species, respectively. As seen in figure 27 and appendix A, the particulates and gas species show nearly identical in-cloud effluent structure. The lag or lead times of the rise and fall of the various effluent concentrations result from the different response times of the instruments as well as the location of the instruments onboard the aircraft (nose compartment or cabin). The aircraft data presented in the report have not been corrected for these lag/lead time effects.

HCl results.- Figure 28 shows the maximum HCl concentration and total dosage measured during each sampling pass. The maximum observed HCl concentration and dosage were 7 ppm (Pass 1) and 28 ppm-sec (Pass 3), respectively. Based on the performance of the HCl detector, the calibration of the instrument, and the residence time of the aircraft in the cloud, the lower detection limits for the measurements are 0.5 ppm and 10 ppm-sec. Instrument performance suggests that the HCl data are accurate to about ±15 percent. Although the data of figure 28 represent data taken at various altitudes (different portions of the cloud) and at various orientations with respect to the cloud path (crosswind and downwind passes), the low HCl concentrations and the rapid decay of the in-cloud concentration preclude any analysis of the data to determine an in-cloud HCl distribution profile (vertically, alongwind, or crosswind).

NO_x results.- Figure 29 shows the maximum NO_x concentrations and total dosage measured during each sampling pass. The maximum observed NO_x concentration (hence NO, since, as stated earlier, almost all the NO_x is NO) and dosage were 1020 ppb and 14 ppm-sec, respectively. During the first pass the detector was off-scale and the observed concentration was above 500 ppb (not shown in fig. 29). Based on the instrument performance, the lower detection limits for the instrument are 20 ppb and 0.4 ppm-sec. Accuracy is of the order of 5 to 10 percent of reading. As shown in figure 29, the maximum NO_x concentration decreases with time; furthermore, within the accuracy of the data and airborne sampling plan, no conclusive trends are observed with regard to sampling altitude or sampling orientation (crosswind compared with downwind pass) within the cloud. The NO_x dosage data also show no trends with respect to sampling altitude or orientation within the cloud.

Particulate mass loading results.- Table XVI summarizes the particulate measurement results. Table XVI(a) gives the average in-cloud concentration for the total particulate burden as well as the Al_2O_3 burden. These data were obtained with the concentrator instrument (nuclepore filter). With this instrument, single filters were exposed to multiple sampling passes (successive passes). Each filter was exposed just prior to the start of the first pass for that filter and remained exposed until the end of the last pass for that filter. The ambient background particulate mass collected between sampling passes is negligible compared with the collected mass from the cloud. The airborne nuclepore filters (concentrator instrument) were handled and analyzed in the manner previously discussed (surface level nuclepore filters). The concentrator data are representative of the average in-cloud particulate concentration but provide no information on maximum in-cloud (instantaneous) concentration. As in the surface level measurements, only a portion of the total suspended particulates collected was Al_2O_3; the remaining particulates are assumed to be debris. The aircraft concentrator data indicate that only 7 to 21 percent by mass of the collected particulates can be attributed to the launch vehicle (Al_2O_3). Figures 30 and 31 show the time decay of the average particulate concentration for total suspended particulates and Al_2O_3 particulates, respectively.

Table XVI(b) shows the average in-cloud particulate loading as determined by the QCM and nephelometer instruments. The QCM data analysis is discussed

in appendix A. This analysis technique reduces the moisture effect on the data but does not eliminate it. The nephelometer data are those shown in appendix A, averaged for each sampling pass. The nephelometer measures the light scattering coefficient of the particulates and from these measurements approximates the mass loading (refs. 12 and 13). Nephelometer-obtained mass loadings are generally accurate to about a factor of 2. Figure 32 shows a comparison of the average in-cloud particulate concentration as determined by the three instruments. The data of figure 32 lead to the conclusion that the average in-cloud particulate concentration ranges from about 1000 to 3000 $\mu g/m^3$ several minutes after launch and decays to about 200 to 400 $\mu g/m^3$ at an hr after launch.

The airborne data, the moisture problem observed for the QCM, and the assumptions required in the analysis of the nephelometer data do not allow definitive conclusions to be drawn about the maximum particulate concentration observed during each sampling pass. Based on the data of appendix A, the maximum particulate concentration in the cloud is probably 1500 to 3000 $\mu g/m^3$ several minutes after launch and decays to around a few hundred $\mu g/m^3$ after 1 hr.

Model-Measurement Comparison

Prior to the presentation of any model-measurement comparison, brief comments on the validity of direct (point) model-measurement comparisons are appropriate. Since the MSFC model is a Gaussian plume model, it is most suited (by design) for predicting the average outcome of an event, given a number of chances to study the same event; the validity of a comparison based on a single measurement of the event must therefore be questioned. Comparisons based on different launches do not satisfy this requirement because a different launch is for all practical purposes a new event that should be studied many times. This argument has frequently led to the contention that comparisons of a single measurement with the model prediction at a given site constitute an invalid assessment of the model. Although this statement may be theoretically correct, the justification for point-to-point model-measurement comparisons is within the potential use of the model. The model may be used to predict the environmental impact of a given launch, and the predictions at given locations may be a key input to launch constraint decisions based on air quality. Applications of this type require point-to-point comparisons.

A second point to note concerning the model-measurement comparison is that when considering point-to-point comparison (type presented in this report), it is difficult, if not impossible, to separate completely the diffusion and meteorological aspects of the model. Disagreement between modeling and measurement results can be attributed to meteorological inaccuracies, diffusion modeling inaccuracies, or a combination of both. In the comparisons presented in the next section, no attempt has been made to isolate the cause of any observed discrepancies between model and measurement. It is noted only that the meteorological inputs for the postlaunch diffusion model analysis appear reasonable for this launch and were based on a postlaunch analysis of all available meteorological data and observations.

Surface level effluents.- Table XVII summarizes the HCl and Al_2O_3 measurement results previously discussed for those sites where effluent predictions were made (table X). This section of the report compares the measured and predicted results for each of the surface level sites. Two comparisons are considered, one qualitative and one quantitative. First, however, the predictions of table X must be converted to engineering units compatible with the measured data of table XVII. The existing HCl units of table X (ppm and ppm-sec) are already compatible. For predicted Al_2O_3 maximum concentration and dosage (deposition), the appropriate units are $\mu g/m^3$ and μg, respectively. Appendix B discusses these conversions and table XVIII shows the resulting Al_2O_3 predicted values.

The first model-measurement comparison is qualitative and takes into account the error band of $\pm 10^o$ for cloud trajectory mentioned earlier. For this comparison a site is classified into one of three groups: (1) measurement is lower than the predicted band ($\pm 10^o$ error band on trajectory), (2) measurement is within the prediction band, and (3) measurement is higher than the prediction band. Table XIX summarizes these comparisons. As shown, the model never predicted low. Two points should be noted regarding the comparison. First, the HCl dosage comparison results depend on the detection limit of the bubbler sampling system. Because of the unrealistically high detection limit (80 ppm-sec), a larger number of the comparison points fall into the "within band" category than is the actual case. For example, if the same HCl dosage comparisons were made where the dosage detection limit was only 10 ppm-sec, only 17 of the 40 comparison points fall into the "within band" category and the remaining 23 points fall into the "high" category. Second, a similar case exists for the Al_2O_3 dosage comparisons because the reported Al_2O_3 dosage data of table XVII are based on all the aluminum sampled at a site (no background corrections).

Considering the foregoing comparison which suggests that the model predictions are generally higher than the measured data, it is desirable to quantify the model predictions with reference to the measured data. The model accuracy may be a function of the actual effluent concentrations existing during the launch; that is, the model (as compared with the measured data) may be a factor of 100 in error at concentrations of a few parts per billion while only a factor of 5 in error at a few parts per million. In the same way, the reverse may be the case with the model being more accurate at the lower concentrations. In the second type of model-measurement comparison, the comparison sites (surface measurement sites) are categorized into two groups: sites at which predicted (model) HCl concentrations are below 0.1 ppm and sites where predicted HCl concentrations are 0.1 ppm or above. (The maximum predicted HCl concentration at any measurement site was about 0.2 ppm.) The following guidelines apply for the comparison:

(1) The parameter selected for the comparison is the ratio of the predicted effluent value to the measured value at a site. Thus, a ratio greater than one indicates an overprediction by the model.

(2) The predicted values used in the comparisons are from table X (HCl) and table XVIII (Al_2O_3). The 10^o azimuth error band is not considered in the comparison.

(3) The measurement values used in the comparison are those of table XVII; and for those cases where the measurements are reported as "less than," the comparison ratio will be reported as "greater than."

(4) No comparisons are shown for HCl dosage, as the high detection limit of the dosage measurement negates any meaningful conclusions.

Table XX shows the results of the comparison. Based on the data of the table, then on the average for those sites where HCl concentrations are predicted to be below 0.1 ppm, the model predictions for maximum HCl concentration are high by at least a factor of 7 (as compared with the measurements); maximum Al_2O_3 concentration, high by at least a factor of 3; and for the Al_2O_3 dosage, high by at least a factor of 8. For sites where HCl concentrations are predicted to be 0.1 ppm or above, the model was high by at least a factor of 5, 12, or 18 for the respective predictions. In only one case (site P-2 for maximum HCl concentration) did the model underpredict. For this case the measured maximum HCl concentration was 50 ppb, and the model predicted 30 ppb.

Conclusions about the overall accuracy of the model as compared with the measured data must be carefully formulated based on the May 1975 data. The following points should be kept in mind:

(1) Measured and predicted effluent concentrations are usually low, often by a factor of 10 or more below the levels at which concentrations of effluents begin to be considered environmental concerns.

(2) In most cases, measurements at a given site used in the comparison study are conservatively high. An upper value for launch effluents at the site is reported rather than the actual value which was often below the detection limit of the instruments. Thus, for these cases, the model is reported as being "at least" some factor higher than the measured value.

(3) Although the model-measurement comparison may at first appear to suggest that the model is better or worse (in comparison to the measurements) for the various concentration ranges, this is not a valid conclusion from the May 1975 data set. The detection limit of the instrumentation may bias this conclusion for this data set (due to low concentrations).

(4) The one case (P-2, maximum HCl concentration) in which the measurements confirm an underprediction by the model is not a valid indicator that the model may be an underpredictor. The concentration at this site is low, well below those levels of environmental concern and may approach the noise level of the model. As shown in the first type of model-measurement comparison, the measured HCl concentration at P-2 was within the prediction uncertainty band ($\pm 10^{o}$ cloud trajectory) assumed for the model.

The authors believe that two appropriate conclusions from the model-measurement comparisons can be drawn: first, the model consistently overpredicted for this launch; second, for the levels of effluents observed, the model was high by at least a factor of 5 for maximum HCl concentration at a site, and high by about at least a factor of 10 for Al_2O_3 concentration and dosage.

In addition to providing the direct comparison of the predicted and measured surface level effluent values, the analysis of the overall body of surface level effluent data results in two important observations. First, if the surface level effluent measurements are considered in terms of determining the most probable cloud trajectory, then from the pH paper results (fig. 24) and the other measurements, the cloud trajectory was probably between 145° and 165°. This finding is in reasonable agreement with the predicted cloud trajectory of 161°. Second, pH paper results pointed to detection of acidic particles or aerosols at surface level as far as 15 km downwind from the pad.

Airborne effluents.- Direct comparisons between the airborne effluent measurements and corresponding model predictions are not presented because at this time the in-cloud model predictions are not available.

CONCLUDING REMARKS

In summarizing the effluent data obtained during the May 1975 launch, it is noted that although the surface level effluent concentrations were low, often below the detection limit of the instrumentation, sufficient data (hydrogen chloride and aluminum oxide) were obtained for a limited assessment of the diffusion model predictions. The prelaunch meteorological data and cloud trajectory forecasts were such that the majority of the surface level instrumentation was located under the actual cloud trajectory. The airborne sampling mission was highly successful - 16 sampling passes through the cloud in which measurements were made for hydrogen chloride, nitrogen oxide, and aluminum oxide.

The maximum observed surface level hydrogen chloride concentration was 50 parts per billion at about 8 km from the launch pad. The corresponding hydrogen chloride dosage at the site was less than 1 ppm-sec. The predicted hydrogen chloride values at this site were 30 parts per billion and 16.8 ppm-sec. The maximum predicted hydrogen chloride concentration at any of the surface level instrumented sites was 0.2 part per million. Surface level concentration measurements of aluminum oxide were below 30 $\mu g/m^3$ at all instrumented sites. Dosage measurements of aluminum oxide were always below 9 µg and typically below 3 to 4 µg. Predicted aluminum oxide values were typically of the order of 100 to 300 $\mu g/m^3$ and 30 to 40 µg. Measurement results indicated surface level carbon monoxide concentrations to be below 0.5 part per million. The presence of acidic particulates or aerosols was detected as far as 15 km from the launch pad. However, the acidic particulate or aerosol fallout was slight, barely detectable.

The 16 airborne sampling passes of the stabilized ground cloud occurred from between 4.5 and 64 min after launch and covered an altitude range of about 900 to 1600 m. Hydrogen chloride concentrations ranged from 7 parts per million to less than 0.5 part per million. Hydrogen chloride dosages ranged from 29 ppm-sec to less than 10 ppm-sec. Nitrogen oxide concentrations ranged from about 1 part per million to 0.1 part per million. Particulate concentration values differ somewhat depending on the instrument used but based on the results the average particulate (total suspended) concentrations in the cloud ranged from 1000 to 3000 $\mu g/m^3$ several minutes after launch to about

200 to 400 $\mu g/m^3$ at an hr after launch. Chemical analyses of collected airborne particulates suggested that only 7 to 20 percent of the total particulates in the cloud were aluminum oxide from the solid rocket motors. The remaining particulates were assumed to be launch debris.

The stabilization altitude of the ground cloud was measured to be in the range of 1400 to 1900 m. Discrepancies existed in the various data used to determine stabilization altitude; hence, the relatively large uncertainty in the measured stabilization altitude. As observed at earlier launches, the initial rise rate (first 3 to 4 min) of the cloud appears to be independent of meteorological conditions and was approximately 5 m/sec. The cloud trajectory was predicted (postlaunch) to be about 161° from the launch pad. The ground level effluent measurements supported this trajectory: the data show a cloud trajectory between 145° and 165°.

Because a low level of exhaust effluents occurred at the surface, results from model-measurement comparisons were somewhat limited. However, model-measurement comparisons showed the model to predict generally high effluent values at surface level. Based on the available data, the model for the May 1975 launch was found on the average to be high by at least a factor of 5 for maximum hydrogen chloride concentration at a site and about at least a factor of 10 for maximum aluminum oxide concentration and total dosage.

Langley Research Center
National Aeronautics and Space Administration
Hampton, VA 23665
September 29, 1977

APPENDIX A

AIRBORNE DATA

Quartz Crystal Mass Monitor

The quartz crystal mass monitor (QCM) is in principle an impactor particulate collector. The sample is drawn into the instrument by a pump and impacted (collected) on the sensing crystal. Located behind the sensing crystal is a second crystal which serves as a frequency reference and temperature compensator. The two crystals, in separate resonant circuits, produce a beat frequency which is increased when mass is added to the sensing crystal. This beat frequency is converted to an analog voltage proportional to the total mass collected (μg). The analog signal is further differentiated to give a signal proportional to instantaneous mass loading ($\mu g/m^3$ as function of time). Operation of the QCM in the presence of moisture and volatile liquid aerosols can affect the output of the instrument. The sensing crystal is responsive to any mass change (positive or negative) whether the change involves a solid particle, a water droplet, or a volatile liquid aerosol. In a moisture laden environment (like some SRM clouds), water and volatile aerosols can condense on the crystal sensor together with the particulates, resulting in high particulate mass concentration readings. The moisture and aerosols can then evaporate from the crystal, and the evaporation causes an apparent decrease in the observed concentration. Some of the airborne QCM data (figs. 33 to 47 and fig. 27) from the May 1975 Titan IIIC launch show evidence of a moisture effect, the data for sampling passes 3, 4, and 5 in particular. An examination of the QCM data for these passes shows two distinct features which suggest the moisture effect is occurring:

(1) Comparison of the QCM data with the nephelometer data (nephelometer is the faster responding instrument) shows that the QCM instrument shows particle concentration variations (as function of time) not observed by the nephelometer. This additional structure is believed to be the result of moisture and aerosol collection and re-evaporation.

(2) The return of the QCM instrument's output to 0 or below while the nephelometer and NO_x instruments show substantial effluent readings is also indicative of the moisture effect. Based on the design of the QCM, readings below 0 particle concentrations are a strong indication of mass loss from the sensing crystal.

The net result of the moisture effect is that for this launch, the validity of the airborne QCM data (concentration as function of time) must be questioned. For sampling passes 3, 4, and 5 the indicated maximum particulate concentration is high, and the peak-valley appearance of the data traces is the result of the moisture effect rather than the actual in-cloud particulate structure. For the other passes it is best assumed that the moisture effect may also influence the QCM data to some extent. Although a comparison of the QCM and nephelometer data (in-cloud structure) for some passes, like Pass 2, shows that both instruments represent a nearly identical in-cloud structure, it is best not to conclude from the data that a moisture effect is not present. For these reasons,

the QCM data plots are presented in this appendix and only limited conclusions are formed in the body of the text concerning maximum in-cloud particulate concentrations. Based on the data, an appropriate conclusion is that the maximum in-cloud particulate concentration is about 1500 to 3000 $\mu g/m^3$ several minutes after launch, decreasing to several hundred $\mu g/m^3$ at an hr after launch.

Although the moisture effect may have a pronounced effect on the QCM particle concentration profiles, its effect on the total mass of particulate collected per pass was not as severe. Once the aircraft exited from the cloud, any collected moisture or liquid aerosol appears to rapidly evaporate from the crystal. Therefore, an average in-cloud particulate loading was obtained with some confidence by taking the difference between the accumulated mass on the sensing crystal before and after a pass (after the data trace indicates the moisture and liquid aerosols were evaporated) and dividing by the air volume sampled while the aircraft was in the cloud. The data reduction technique in this appendix is the basis of the QCM data presented in the main body of the report. (See table XVI(b).)

For future airborne launch sampling missions, the QCM inlet probe is being redesigned to eliminate (or reduce) the moisture and volatile aerosol condensation problem.

Data Plots

Figures 33 to 47 and figure 27 show the airborne data traces for HCl, NO_x, and particulates (QCM and nephelometer). These plots are the basis of the discussions presented in the main text under the section entitled "Airborne Effluent Measurements." Nephelometer data for Pass 16 are omitted from figure 47 (operational problems). For Pass 1 both the nephelometer and QCM readings went off scale, and for Pass 6 the QCM data went off scale.

APPENDIX B

SAMPLE CALCULATION FOR Al_2O_3

As shown in table X, the Al_2O_3 predicted effluent values are given in terms of mg/m^3 (for concentration) and $mg\text{-}sec/m^3$ (for dosage). To compare these predicted values with the Al_2O_3 measurements of table XVII, the predicted concentrations must be converted to engineering units compatible with the output of the monitoring instrumentation, namely $\mu g/m^3$ for concentration and μg of Al_2O_3 for dosage. For concentration, the conversion calculations require only that the Al_2O_3 concentrations of table X be multiplied by 1000 to convert mg/m^3 to $\mu g/m^3$. For the dosage conversion, equation (B1) applies:

$$\text{Dosage} = D \times Q \times 1000 \times 0.001 \frac{1}{60} \qquad \text{(B1)}$$

where

Dosage — mass of Al_2O_3 predicted to be sampled at site using instrument with sample flow rate F, μg

D — predicted dosage from table X, $mg\text{-}sec/m^3$

Q — instrument sample flow rate (table XIV), l/min

10^3 — conversion factor for mg to μg

10^{-3} — conversion factor for liter to m^3

60 — conversion factor for min to sec

For site P-1, D is 40.8 ± 45.2 $mg\text{-}sec/m^3$ (table X), Q is 25.9 l/min (table XIV), and equation (B1) gives the dosage at 17.6 ± 19.5 μg of Al_2O_3. Table XVIII summarizes the resulting Al_2O_3 predictions in units compatible with the measurements of table XVII.

REFERENCES

1. Gregory, Gerald L.; and Storey, Richard W., Jr.: Effluent Sampling of Titan IIIC Vehicle Exhaust. NASA TM X-3228, 1975.

2. Stewart, Roger B.; Sentell, Ronald J.; and Gregory, Gerald L.: Experimental Measurements of the Ground Cloud Effluents and Cloud Growth During the February 11, 1974 Titan-Centaur Launch at Kennedy Space Center. NASA TM X-72820, 1976.

3. Bendura, Richard J.; and Crumbly, Kenneth C.: Ground Cloud Effluent Measurements During the May 30, 1974, Titan III Launch at the Air Force Eastern Test Range. NASA TM X-3539, 1977.

4. Stephens, J. Briscoe, ed.: Atmospheric Diffusion Predictions for the Exhaust Effluents From the Launch of a Titan IIIC, Dec. 13, 1973. NASA TM X-64925, 1974.

5. Gomberg, Richard I.; and Stewart, Roger B.: A Computer Simulation of the Afterburning Processes Occurring Within Solid Rocket Motor Plumes in the Troposphere. NASA TN D-8303, 1976.

6. Dumbauld, R. K.; Bjorklund, J. R.; and Bowers, J. F.: NASA/MSFC Multilayer Diffusion Models and Computer Program for Operational Prediction of Toxic Fuel Hazards. NASA CR-129006, 1973.

7. Stephens, J. Briscoe; Adelfang, S. I.; and Goldford, A. I.: Compendium of Meteorological Data for the Titan IIIC (AF-777) Launch in May 1975. NASA TM X-73338, 1976.

8. Gregory, Gerald L.; Hudgins, Charles H.; and Emerson, Burt R., Jr.: Evaluation of a Chemiluminescent Hydrogen Chloride and a NDIR Carbon Monoxide Detector for Environmental Monitoring. 1974 JANNAF Propulsion Meeting, Volume I, Part II, CPIA Publ. 260 (Contract N00017-72-C-4401), Appl. Phys. Lab., Johns Hopkins Univ., Dec. 1974, pp. 681-704. (Available from DDC as AD B002 590.)

9. Reyes, Robert J.; Miller, Richard L.; and Beatty, David C.: Monitoring of HCl From Solid Propellant Launch Vehicles. 1974 JANNAF Propulsion Meeting, Volume I, Part II, CPIA Publ. 260 (Contract N00017-72-C-4401), Appl. Phys. Lab., Johns Hopkins Univ., Dec. 1974, pp. 705-722. (Available from DDC as AD B002 590.)

10. Hulten, William C.; Storey, Richard W.; Gregory, Gerald L.; Woods, David C.; and Harris, Franklin S., Jr.: Effluent Sampling of Scout "D" and Delta Launch Vehicle Exhausts. NASA TM X-2987, 1974.

11. Wornom, Dewey E.; Woods, David C.; Thomas, Mitchel E.; and Tyson, Richard W.: Instrumentation of Sampling Aircraft for Measurement of Launch Vehicle Effluents. NASA TM X-3500, 1977.

12. Charlson, R. J.; Ahlquist, N. C.; Selvidge, H.; and MacCready, P. B., Jr.: Monitoring of Atmospheric Aerosol Parameters With the Integrating Nephelometer. J. Air Pollution Control Assn., vol. 19, no. 12, Dec. 1969, pp. 937-942.

13. Tombach, Ivar: Measurement of Some Optical Properties of Air Pollution With the Integrating Nephelometer. AIAA Paper No. 71-1101, Nov. 1971.

TABLE I.- TITAN SRM EXHAUST COMPOSITION

[Percent by mass of nozzle exit plane flow]

Product	Nozzle exit plane[a]	Plume at 1 km from exit plane[b]
Aluminum oxide (Al_2O_3)	30.4	30.4
Carbon monoxide (CO)	27.9	(c)
Hydrogen chloride (HCl)	21.0	20.4
Nitrogen (N_2)	8.4	(d)
Water vapor (H_2O)	6.7	31.9
Carbon dioxide (CO_2)	2.9	48.0
Chlorine (Cl_2)	(c)	2.3
Oxygen (O_2)	(c)	(d)
Nitrogen oxide (NO)	(c)	1.2
Others	2.7	.6
	100.0	[e]134.8

[a]Data from reference 4.
[b]Data from reference 5.
[c]Less than 0.1.
[d]Assumed to be part of air.
[e]Total greater than 100 percent because of chemical addition of air in afterburning.

TABLE II.- SUMMARY OF MSFC EFFLUENT DISPERSION PREDICTIONS, MINUS COUNT

T minus time, hr	Cloud stabilization altitude, m	Cloud path from LC-40 (true), deg	Peak HCl concentration, ppm	Location of peak from LC-40, km
T - 24	1549	99	0.04	13.0
T - 10.5	1549	160	.05	11.5
T - 6	1204	174	.66	7.7
T - 4	1204	157	.20	7.1
T - 3	1204	159	.91	7.0

TABLE III.- MEASUREMENT SITE LOCATION RELATIVE TO LAUNCH COMPLEX 40

Site designation[a]	Azimuth (true), deg	Distance, km
AA	80.0	0.1
CC	95.0	.7
DD	13.4	1.4
FF	39.0	.8
P-1	145.0	12.0
P-2	145.0	8.0
P-3	145.0	16.0
P-3'	146.0	18.9
P-4	164.0	16.0
P-5	175.0	16.0
P-6	162.6	11.8
P-7	164.6	6.8
P-8	172.3	8.2
P-9	176.2	13.9
S-1	175.5	2.7
S-2	160.0	3.0
S-3	165.0	5.0
S-4	170.0	5.5
S-5	166.0	5.9
S-6	165.0	6.9
S-7	164.5	7.6
S-8	164.0	8.0
S-9	163.5	8.7
S-10	163.0	9.7
S-11	179.0	6.8
S-12	184.0	8.3
S-13	173.5	9.0
S-14	183.5	10.4
S-15	180.0	9.1
S-16	175.0	6.0
S-17	169.5	6.8
S-18	175.0	7.1
S-19	170.0	8.2
S-20	170.0	9.4
S-21	175.0	11.3
S-22	173.5	13.0
S-23	169.0	12.5
S-24	163.0	13.0
S-25	158.0	12.7
S-26	180.0	10.5
S-27	177.0	12.5
S-28	183.0	12.6
S-29	180.0	13.9
S-30	182.5	13.9

[a]In figure 3, S (secondary) designation has been omitted.

TABLE IV.- AIRBORNE SAMPLING PARAMETERS

Pass number	Sampling altitude,[a] m	Aircraft ground speed,[b] m/sec	Type of pass	Cloud location[c] from LC-40		Time[d] of cloud penetration, T + min
				km	Deg, true	
1	1129 ± 17	50 ± 4	Downwind	2.42	166	T + 4.4
2	1362 ± 17	51 ± 4	Crosswind	2.45	174	T + 6.4
3	1249 ± 28	52 ± 2	Downwind	3.28	169	T + 8.1
4	1245 ± 14	52 ± 1	Crosswind	3.12	166	T + 9.8
5	1048 ± 26	54 ± 5	Downwind	----	---	T + 12.5
6	1064 ± 8	50 ± 2	Crosswind	----	---	T + 14.5
7	899 ± 11	54 ± 1	Downwind	----	---	T + 17.1
8	894 ± 8	52 ± 1	Crosswind	----	---	T + 19.2
9	1490 ± 15	52 ± 1	Downwind	----	---	T + 28.2
10	1546 ± 11	50 ± 3	Crosswind	----	---	T + 30.1
11	1524 ± 26	52 ± 2	Downwind	----	---	T + 32.4
12	1525 ± 12	49 ± 2	Crosswind	----	---	T + 34.8
13	1531 ± 6	51 ± 1	Downwind	----	---	T + 37.6
14	1543 ± 10	52 ± 1	Crosswind	----	---	T + 39.9
15	1539 ± 7	52 ± 1	Downwind	----	---	T + 42.2
16	1588 ± 28	54 ± 2	Crosswind	----	---	T + 63.4

[a]Sampling altitude ± altitude variation during pass.

[b]Ground speed ± speed variation during pass.

[c]Approximate cloud location based on radar track of aircraft; data not available after Pass 4 due to radar dropout.

[d]Approximate time, reference to launch, at which aircraft entered cloud.

TABLE V.- EQUIPMENT SITE PLAN

Site designation	Instrument type	Species and/or item measured
P-1	Chemiluminescent	HCl
	Coulometer	HCl
	Bubbler	HCl
	pH paper	HCl
	Nondispersive infrared	CO
	Quartz crystal mass monitor	Particles
	Light photometer (right angle scattering)	Particles
	Impactor-cascade, eight stage	Particles
	Nuclepore filter	Particles
	Wind vane, anemometer	Wind speed, direction
P-2	Chemiluminescent	HCl
	Coulometer	HCl
	Bubbler	HCl
	pH paper	HCl
	Nondispersive infrared	CO
	Quartz crystal mass monitor	Particles
	Light photometer (forward scattering)	Particles
	Impactor-cascade, eight stage	Particles
	Nuclepore filter	Particles
	Wind vane, anemometer	Wind speed, direction
P-3	Chemiluminescent	HCl
	Bubbler	HCl
	pH paper	HCl
	Nondispersive infrared	CO
	Quartz crystal mass monitor	Particles
	Light photometer (forward scattering)	Particles
	Impactor-cascade, eight stage	Particles
	Nuclepore filter	Particles
	Wind vane, anemometer	Wind speed, direction

TABLE V.- Concluded

Site designation	Instrument type	Species and/or item measured
P-4 and P-5	Chemiluminescent	HCl
	Bubbler	HCl
	pH paper	HCl
	Nondispersive infrared	CO
	Quartz crystal mass monitor	Particles
	Impactor-cascade, eight	Particles
	Nuclepore filter	Particles
	Wind vane, anemometer	Wind speed, direction
P-6, P-7, and P-8	Chemiluminescent	HCl
	Bubbler	HCl
	pH paper	HCl
	Quartz crystal mass monitor	Particles
	Impactor-cascade, eight stage	Particles
	Nuclepore filter	Particles
	Wind vane, anemometer	Wind speed, direction
P-9	Chemiluminescent	HCl
	Bubbler	HCl
	pH paper	HCl
	Quartz crystal mass monitor	Particles
	Nuclepore filter	Particles
AA	Bubbler	HCl
	pH paper	HCl
	Nuclepore filter	Particles
CC, DD, FF, and S-1 to S-30	Bubbler	HCl
	pH paper	HCl
	Nuclepore filter	Particles

TABLE VI.- INSTRUMENT CAPABILITIES

(a) Gas instruments

Instrument type and species measured	Source	Range	Detection limit	Response to 90-percent reading	Required analysis
Chemiluminescent, HCl	Reference 8	0.005 to 50 ppm	0.005 ppm	1 to 30 sec[c] above 0.05 ppm	None
Microcoulometer, HCl	Reference 9	0.1 to 20 ppm	0.1 ppm	1 min	None
Bubbler, HCl	Reference 10	>80 ppm-sec	80 ppm-sec	Not applicable	Coulometric
pH paper, HCl	Reference 10	Qualitative	1 ppm	Not applicable	None
Nondispersive infrared, CO	Reference 8	0.5 to 200 ppm	0.5 ppm	30 sec	None

(b) Particle instruments

Instrument type	Source	Particle size range, diameter, μm	Detection limit	Response to 90-percent reading	Required analysis
Light photometer (right angle scattering)[a]	Reference 10	0.5 to 6.5	1 particle	1 msec	Computer processing
Light photometer (forward scattering)[b]	Reference 10	0 3 to 10.0	1 particle	1 msec	Computer processing
Mass monitor[a]	Reference 10	0.1 to 10.0	10 $\mu g/m^3$	5 sec	None
Nuclepore filter[a]	Reference 10	Suspended particulates >0.01	10 μg	Not applicable	Gravimetric, NAA[b]
Impactor-cascade, eight stage[a]	Reference 10	0.43 to 11.0	50 μg	Not applicable	Gravimetric, NAA
Impactor-rotating drum, four stage[a]	Reference 10	0 5 to 14.0	50 μg	Not applicable	Gravimetric, NAA

(c) Meteorological instruments

Instrument type and species	Range	Detection limit
Microvane,[a] wind direction	0.5 to 45 m/sec	0 5 m/sec
Three-cup anemometer,[a] wind speed	0° to 342°	1°

[a]Instrument specification based on manufacturer's data.
[b]Neutron activation analysis.
[c]Response time is function of concentration; at 0.05 ppm, 30 sec; below 0.05 ppm, several minutes.

TABLE VII.- AIRBORNE INSTRUMENT CHARACTERISTICS

Instrument and species	Range[a]	Detection limit	Response to 90-percent reading	Required analysis
Chemiluminescent, HCl	0.5 to 200 ppm	0.5 ppm	1 sec	None
Infrared, CO-CO_2	5 to 500 ppm CO 325 to 700 ppm CO_2	5 ppm CO [b]3 ppm CO_2	1.5 sec	None
Chemiluminescent, NO-NO_x	0.002 to 5 ppm	0.002 ppm	1 sec	None
Quartz crystal mass monitor, particles	0.1- to 10-μm diam	10 $\mu g/m^3$	5 sec	None
Nephelometer, particles	0.4- to 1-μm diam suspended particulates	100 particles	0.2 sec	None
Concentrator filter, particles	>0.4-μm diam	10 μg	Not applicable	Gravimetric, NAA[c]

[a]For particle instruments, range given in particle size diameter.
[b]Change above ambient.
[c]Neutron activation analysis.

TABLE VIII.- PREDICTED CLOUD RISE AND STABILIZATION

Time after launch, T + min:sec	Cloud centroid altitude, m
T + 0:04	121.9
T + 0:05	142.6
T + 0:20	304.8
T + 0:27	368.5
T + 0:49	511.8
T + 1:03	592.5
T + 1:07	609.6
T + 1:21	683.1
T + 2:08	883.6
T + 2:16	914.4
T + 2:55	1058.3
T + 3:45	1219.2
T + 3:50	1235.7
[a]T + 4:19	[a]1318.0
T + 5:33	1524.0
T + 5:40	1543.2
T + 7:39	1828.8
T + 8:59	2005.6
T + 9:11	2030.6
T + 9:21	2051.6
T + 10:01	2133.6
T + 10:10	2150.7
[b]T + 15:23	[b]2243.4

[a]Cloud stabilization time and altitude for ground cloud used as source term for model.

[b]Cloud stabilization time and altitude for initial effluent cloud.

TABLE IX.- PREDICTED CLOUD TRACK AND GROWTH

Time after launch, T + min:sec	Cloud location relative to LC-40		Cloud dimensions	
	Azimuth (true), deg	Distance, km	Crosswind diameter, m	Alongwind diameter, m
[a]T + 4:19	168	0.96	2872	2872
T + 9:19	162	1.97	2873	4559
T + 14:19	162	2.99	2876	4629
T + 19:19	162	4.01	2883	4743
T + 24:19	161	5.03	2891	4897
T + 29:19	161	6.04	2902	5099
T + 34:19	161	7.06	2915	5315
T + 39:19	161	8.08	2931	5569
T + 44:19	161	9.10	2949	5849
T + 49:19	161	10.11	2969	6151
T + 54:19	161	11.13	2992	6472
T + 59:19	161	12.14	3017	6809
T + 64:19	161	13.17	3043	7160

[a]Cloud stabilization time (ground cloud).

TABLE X.- PREDICTED HCl AND Al_2O_3 EFFLUENT CONCENTRATION AND DOSAGE LEVELS AT SURFACE LEVEL INSTRUMENT SITES[a]

Site designation	HCl prediction for -		Al_2O_3 prediction for -	
	Maximum concentration, ppm	Dosage, ppm-sec	Maximum concentration, mg/m^3	Dosage, $mg\text{-}sec/m^3$
P-1	0.04 ± 0.04	19.2 ± 21.3	0.08 ± 0.09	40.8 ± 45.2
P-2	0.03 ± 0.02	16.8 ± 11.2	0.07 ± 0.05	35.8 ± 23.7
P-3	0.03 ± 0.05	16.7 ± 24.3	0.07 ± 0.10	35.4 ± 51.6
P-3'	0.04 ± 0.05	18.5 ± 23.5	0.08 ± 0.10	39.4 ± 49.9
P-4	0.21 ± 0.09	104 ± 44.6	0.45 ± 0.19	221 ± 94.7
P-5	0.05 ± 0.04	26.5 ± 22.1	0.11 ± 0.09	56.2 ± 46.9
P-6	0.21 ± 0.09	105 ± 42.6	0.45 ± 0.18	222 ± 90.6
P-7	0.10 ± 0.03	47.1 ± 13.0	0.20 ± 0.06	100 ± 27.6
P-8	0.08 ± 0	38.8 ± 1.6	0.17 ± 0.01	82.6 ± 3.9
P-9	0.05 ± 0.05	23.1 ± 22.6	0.10 ± 0.10	49.1 ± 47.9
S-1	0	0.1 ± 0	0	0.2 ± 0
S-2	0	0.5 ± 0.1	0	1.1 ± 0.2
S-3	0.03 ± 0.01	16.0 ± 3.6	0.07 ± 0.02	33.9 ± 7.7
S-4	0.04 ± 0	18.1 ± 1.9	0.08 ± 0.01	38.4 ± 4.1
S-5	0.06 ± 0.01	29.8 ± 7.0	0.13 ± 0.03	63.2 ± 14.8
S-6	0.10 ± 0.03	48.8 ± 13.6	0.21 ± 0.06	104 ± 28.9
S-7	0.12 ± 0.04	60.3 ± 17.7	0.26 ± 0.08	128 ± 37.7
S-8	0.14 ± 0.04	68.6 ± 22.1	0.30 ± 0.10	146 ± 47.0
S-9	0.16 ± 0.05	78.0 ± 26.3	0.34 ± 0.11	166 ± 56.0
S-10	0.18 ± 0.07	91.1 ± 34.0	0.39 ± 0.15	194 ± 72.3
S-11	0.02 ± 0.02	9.9 ± 7.4	0.04 ± 0.03	21.1 ± 15.8
S-12	0.01 ± 0.02	3.6 ± 9.2	0.02 ± 0.04	7.6 ± 19.7
S-13	0.07 ± 0.02	32.4 ± 9.1	0.14 ± 0.04	68.9 ± 19.4
S-14	0.01 ± 0.02	3.2 ± 11.9	0.01 ± 0.05	6.8 ± 25.3
S-15	0.02 ± 0.03	10.2 ± 14.7	0.04 ± 0.06	21.6 ± 31.2
S-16	0.03 ± 0.01	14.2 ± 2.8	0.06 ± 0.01	30.3 ± 6.0
S-17	0.07 ± 0.01	34.3 ± 3.6	0.15 ± 0.02	72.9 ± 7.7
S-18	0.04 ± 0.01	20.9 ± 5.7	0.09 ± 0.02	44.4 ± 12.1
S-19	0.10 ± 0.01	48.4 ± 4.7	0.21 ± 0.02	103 ± 10.1
S-20	0.11 ± 0.01	56.5 ± 5.0	0.24 ± 0.02	120 ± 10.6
S-21	0.06 ± 0.03	29.8 ± 17.0	0.13 ± 0.07	63.2 ± 36.2
S-22	0.07 ± 0.03	35.3 ± 16.9	0.15 ± 0.07	74.9 ± 36.0
S-23	0.15 ± 0.02	72.1 ± 10.7	0.31 ± 0.05	153 ± 22.7
S-24	0.22 ± 0.09	108 ± 45.7	0.46 ± 0.20	229 ± 97.1
S-25	0.21 ± 0.08	104 ± 41.0	0.45 ± 0.18	220 ± 87.2
S-26	0.02 ± 0.04	10.0 ± 17.7	0.04 ± 0.08	21.3 ± 37.7
S-27	0.04 ± 0.04	19.4 ± 21.9	0.08 ± 0.09	41.2 ± 46.5
S-28	0.01 ± 0.03	3.7 ± 15.0	0.02 ± 0.06	7.8 ± 31.8
S-29	0.02 ± 0.04	8.4 ± 21.1	0.04 ± 0.09	17.9 ± 44.9
S-30	0.01 ± 0.03	3.3 ± 15.2	0.01 ± 0.07	6.9 ± 32.2

[a]± notation is used to represent ±10° cloud trajectory uncertainty; no prediction is less than 0; for example, 0.1 ± 0.2 is interpreted as

(1) Prediction at the site is 0.1 ppm.

(2) Allowing an approximate ±10° variation in cloud trajectory, the prediction varies from 0 to 0.3 ppm.

TABLE XI.- EFFLUENT CONVERSION FACTORS[a]

Species	Conversion factor
CO	<0.01
CO_2	2.3
NO	0.06

[a]Example: NO concentration (or dosage), 0.06 HCl concentration (or dosage) with HCl, CO, CO_2, NO concentration in ppm and HCl, CO, CO_2, NO dosage in ppm-sec.

TABLE XII.- BACKGROUND AND HANDLING RESULTS,

NUCLEPORE SAMPLING SYSTEM

Source	Mean	Standard deviation
Handling effect[a]	13 μg	8.5 μg
Ambient background[b]	30.1 $\mu g/m^3$	3.1 $\mu g/m^3$

[a]Based on 10 samples.
[b]Based on 3 samples.

TABLE XIII.- BACKGROUND AND HANDLING RESULTS, ALUMINUM CONTENT

Source	Average content	Minimum	Maximum
Handling effect[a]	1.91 μg	1.74 μg	2.08 μg
Ambient background[b]	0.07 $\mu g/m^3$	Not applicable	Not applicable

[a]Based on 2 samples.
[b]Based on 1 sample.

TABLE XIV.- LAUNCH NUCLEPORE DATA

Site designation	Filter activation, min	Filter deactivation, min	Filter sample time, min	Flow rate, l/min	Uncorrected sample mass gain, W_S, µg	Corrected mass gain, W_c, µg
AA	T - 1	T + 5	6	45.0	166	144.9
CC	T - 1	T + 5	6	48.1	54	32.3
DD	T - 1	T + 5	6	25.2	49	31.5
FF	T - 1	T + 5	6	47.0	35	13.5
P-1	T + 38	T + 162	124	25.9	221	111.4
P-2	T + 33	T + 115	82	23.5	150	79.0
P-3, P-3'	T + 68	T + 153	96	24.0	142	59.8
P-4	T + 64	T + 128	128	24.6	194	86.5
P-5	T + 64	T + 170	58	23.6	147	93.1
P-6	T + 46	T + 122	122	23.0	169	71.5
P-7	T + 25	T + 73	48	25.5	116	66.3
P-8	T + 34	T + 122	88	26.0	137	55.1
P-9	T + 18	T + 154	136	21.0	216	117.0
S-1	T + 15	T + 54	39	21.0	104	66.4
S-2	T + 15	T + 54	39	19.0	61	25.7
S-3	T + 15	T + 54	39	21.0	113	75.4
S-4	T + 15	T + 54	39	21.0	73	35.4
S-5	T + 36	T + 68	32	22.0	85	50.9
S-6	T + 36	T + 68	32	22.0	155	120.8
S-7	T + 46	T + 73	27	22.0	85	54.1
S-8	T + 46	T + 73	27	20.0	97	67.8
S-9	T + 46	T + 73	27	21.0	82	51.9
S-10	T + 57	T + 105	48	21.0	82	38.7
S-11	T + 15	T + 54	39	22.0	89	50.2
S-12	T + 36	T + 68	32	21.0	78	44.8
S-13	T + 46	T + 73	27	22.0	61	30.1
S-14	T + 57	T + 105	48	20.0	61	19.1
S-15	T + 57	T + 105	48	21.0	92	48.7
S-16	T + 15	T + 54	39	21.0	61	23.4
S-17	T + 36	T + 68	32	19.0	71	39.7
S-18	T + 36	T + 68	32	21.0	72	38.8
S-19	T + 46	T + 73	27	21.0	92	61.9
S-20	T + 57	T + 105	48	21.0	87	43.7
S-21	T + 66	T + 118	52	22.0	110	62.6
S-22	T + 78	T + 125	47	20.0	103	61.7
S-23	T + 78	T + 125	47	21.0	112	69.3
S-24	T + 78	T + 125	47	21.0	146	103.3
S-25	T + 66	T + 118	52	21.0	131	85.2
S-26	T + 66	T + 118	52	20.0	108	63.7
S-27	T + 66	T + 118	52	21.0	106	60.2
S-28	T + 66	T + 118	52	20.0	103	58.7
S-29	T + 78	T + 125	47	21.0	42	-----[a]
S-30	T + 78	T + 125	47	20.0	108	66.7

[a]No data entry means corrected mass gain is attributed to handling and background effects only.

TABLE XV.- NUCLEPORE NEUTRON ACTIVATION RESULTS, ALUMINUM

Site designation	Uncorrected sample mass gain, µg of Al	Corrected mass gain, µg of Al (a)
AA	36.8	34.87
CC	1.3	-----
DD	1.1	-----
FF	1.34	-----
P-1	4.52	2.39
P-2	2.68	.64
P-3, P-3'	1.68	-----
P-4	3.68	1.55
P-5	1.6	-----
P-6	2.02	-----
P-7	1.30	-----
P-8	2.38	.31
P-9	1.78	-----
S-1	1.72	-----
S-2	1.00	-----
S-3	1.62	-----
S-4	1.06	-----
S-5	1.58	-----
S-6	1.54	-----
S-7	1.08	-----
S-8	1.98	.03
S-9	1.84	-----
S-10	.98	-----
S-11	1.04	-----
S-12	.88	-----
S-13	1.02	-----
S-14	(b)	(b)
S-15	.78	-----
S-16	1.08	-----
S-17	.81	-----
S-18	.81	-----
S-19	1.04	-----
S-20	1.22	-----
S-21	.85	-----
S-22	1.23	-----
S-23	1.86	-----
S-24	1.64	-----
S-25	2.14	.15
S-26	.81	-----
S-27	.97	-----
S-28	1.19	-----
S-29	(c)	(c)
S-30	1.38	-----

[a]No data entry means corrected aluminum mass gain less than 0; aluminum on filter is attributed to handling and background only.

[b]Neutron activation data not available.

[c]Based on total mass gain (table XIV), sample not statistically significant.

TABLE XVI.- AIRCRAFT PARTICULATE DATA

(a) Concentrator (nuclepore) data

Pass number	Average in-cloud particle loading, $\mu g/m^3$	Average in-cloud Al_2O_3 loading, $\mu g/m^3$
1, 2	2874	194
3, 4	911	110
5, 6	1159	147
7, 8	Not available	81
9, 10	815	53
11, 12, 13	228	47
14, 15, 16	237	26

(b) Average in-cloud particulate loading

Pass number	QCM data, $\mu g/m^3$	Nephelometer data, $\mu g/m^3$
1	1645	681
2	945	501
3	290	376
4	350	264
5	815	253
6	875	417
7	568	302
8	430	228
9	624	165
10	1045	141
11	887	153
12	791	165
13	330	70
14	1146	200
15	283	130
16	797	Not available

TABLE XVII.- SUMMARY OF MEASUREMENT RESULTS AT GROUND LEVEL

Site designation	HCl measurements		Al_2O_3 measurements	
	Maximum concentration,[a] ppm	Dosage, ppm-sec	Maximum concentration,[a] $\mu g/m^3$	Dosage,[b] μg
P-1	<0.005	<80	<30	<8.6
P-2	.050	<1	<30	<5.1
P-3	<.005	<80	<30	<3.2
P-3'	<.005	<80	<30	<3.2
P-4	<.030	<10	<30	<7.0
P-5	<.005	<80	<30	<3.0
P-6	<.040	<80	<30	<3.8
P-7	<.030	<80	<30	<2.5
P-8	<.005	<80	<30	<4.5
P-9	<.030	<80	<30	<3.4
S-1	NA	<80	NA	<3.3
S-2	NA	<80	NA	<1.9
S-3	NA	<80	NA	<3.1
S-4	NA	<80	NA	<2.0
S-5	NA	<80	NA	<3.0
S-6	NA	<80	NA	<2.9
S-7	NA	<80	NA	<2.1
S-8	NA	<80	NA	<3.8
S-9	NA	<80	NA	<3.5
S-10	NA	<80	NA	<1.9
S-11	NA	<80	NA	<2 0
S-12	NA	<80	NA	<1.7
S-13	NA	<80	NA	<1.9
S-14	NA	<80	NA	(c)
S-15	NA	<80	NA	<1.5
S-16	NA	<80	NA	<2.1
S-17	NA	<80	NA	<1.5
S-18	NA	<80	NA	<1.5
S-19	NA	<80	NA	<2.0
S-20	NA	<80	NA	<2.3
S-21	NA	<80	NA	<1.6
S-22	NA	<80	NA	<2.3
S-23	NA	<80	NA	<3.5
S-24	NA	<80	NA	<3.1
S-25	NA	<80	NA	<4.1
S-26	NA	<80	NA	<1.5
S-27	NA	<80	NA	<1.8
S-28	NA	<80	NA	<2.3
S-29	NA	<80	NA	(c)
S-30	NA	<80	NA	<2.6

[a]NA: not applicable because site was not instrumented for concentration measurement.

[b]Column 2 of table XV converted to Al_2O_3 dosage; (column 2 of table XV) × (1.9).

[c]Neutron activation analysis not performed.

TABLE XVIII.- PREDICTED Al_2O_3 CONCENTRATIONS AND DOSAGES[a]

Site designation	Maximum concentration, $\mu g/m^3$	Dosage, μg
P-1	80 ± 90	17.6 ± 19.5
P-2	70 ± 50	14.0 ± 9.3
P-3	70 ± 100	14.2 ± 20.6
P-3'	80 ± 100	15.8 ± 20
P-4	450 ± 190	90.7 ± 38.8
P-5	110 ± 90	22.1 ± 18.5
P-6	450 ± 180	85.2 ± 34.7
P-7	200 ± 60	42.5 ± 11.7
P-8	170 ± 10	35.8 ± 1.7
P-9	100 ± 100	17.2 ± 16.8
S-1	0	0.1 ± 0
S-2	0	0.3 ± 0.1
S-3	70 ± 20	11.9 ± 2.7
S-4	80 ± 10	13.4 ± 1.4
S-5	130 ± 30	23.2 ± 5.4
S-6	210 ± 60	38.1 ± 10.6
S-7	260 ± 80	47.0 ± 13.8
S-8	300 ± 100	48.5 ± 15.7
S-9	340 ± 110	58.0 ± 19.6
S-10	390 ± 150	67.7 ± 25.3
S-11	40 ± 30	7.7 ± 5.8
S-12	20 ± 40	2.7 ± 6.9
S-13	140 ± 40	25.3 ± 7.1
S-14	10 ± 50	2.3 ± 8.4
S-15	40 ± 60	7.6 ± 10.9
S-16	60 ± 10	10.8 ± 2.1
S-17	150 ± 20	23.1 ± 2.4
S-18	90 ± 20	15.5 ± 4.2
S-19	210 ± 20	36.1 ± 3.5
S-20	240 ± 20	42.0 ± 3.7
S-21	130 ± 70	23.2 ± 13.3
S-22	150 ± 70	25.0 ± 12.0
S-23	310 ± 50	53.6 ± 7.9
S-24	460 ± 200	80.3 ± 34.0
S-25	450 ± 180	77.0 ± 30.5
S-26	40 ± 80	7.1 ± 12.6
S-27	80 ± 90	14.4 ± 16.3
S-28	20 ± 60	2.6 ± 10.6
S-29	40 ± 90	6.3 ± 15.7
S-30	10 ± 70	2.3 ± 10.7

[a]No prediction less than 0; that is, 80 ± 90 means predicted value ranged from 0 to 170 when 10° cloud trajectory error was considered.

TABLE XIX.- MODEL-MEASUREMENT COMPARISON, QUALITATIVE

Comparison parameter	Number of comparison points	Predictions as compared to measurements		
		High	Within band	Low
Maximum HCl concentration	10	5	5	0
HCl dosage	40	2	38	0
Maximum Al_2O_3 concentration	10	6	4	0
Al_2O_3 dosage	38	25	13	0

TABLE XX.- MODEL-MEASUREMENT COMPARISON, QUANTITATIVE

(a) Sites at which predicted HCl concentration less than 0.1 ppm

Site designation	$\frac{\text{Predicted}}{\text{Measured}}$ ratio		
	Maximum HCl concentration[a]	Maximum Al_2O_3 concentration[a]	Al_2O_3 dosage
P-1	>8.0	>2.6	>2.0
P-2	.6	>2.3	>2.7
P-3	>6.0	>2.3	>4.4
P-3'	>8.0	>2.6	>4.9
P-5	>10	>3.6	>7.3
P-8	>16	>5.6	>7.9
P-9	>1.6	>3.3	>5
S-1	NA	NA	>.03
S-2	NA	NA	>.1
S-3	NA	NA	>3.8
S-4	NA	NA	>6.7
S-5	NA	NA	>7.7
S-11	NA	NA	>3.8
S-12	NA	NA	>1.5
S-13	NA	NA	>13
S-14	NA	NA	(b)
S-15	NA	NA	>5.0
S-16	NA	NA	>5.1
S-17	NA	NA	>15
S-18	NA	NA	>10
S-21	NA	NA	>14
S-22	NA	NA	>10
S-26	NA	NA	>4.7
S-27	NA	NA	>8
S-28	NA	NA	>1.1
S-29	NA	NA	(b)
S-30	NA	NA	>70.8

[a]Not applicable because measurement of parameter not made at site.

[b]Measured data not available.

TABLE XX.- Concluded

(b) Sites at which predicted HCl concentration 0.1 ppm or higher

Site designation	$\frac{\text{Predicted}}{\text{Measured}}$ ratio		
	Maximum HCl concentration[a]	Maximum Al_2O_3 concentration[a]	Al_2O_3 dosage
P-4	>7.0	>15	>12
P-6	>5.2	>15	>22
P-7	>3.3	>6.6	>17
S-6	NA	NA	>13
S-7	NA	NA	>22
S-8	NA	NA	>12
S-9	NA	NA	>16
S-10	NA	NA	>35
S-19	NA	NA	>18
S-20	NA	NA	>18
S-23	NA	NA	>15
S-24	NA	NA	>25
S-25	NA	NA	>18

[a]Not applicable because measurement of parameter not made at site.

L-74-2088

Figure 1.- Titan IIIC vehicle at lift-off, T + 7 sec.

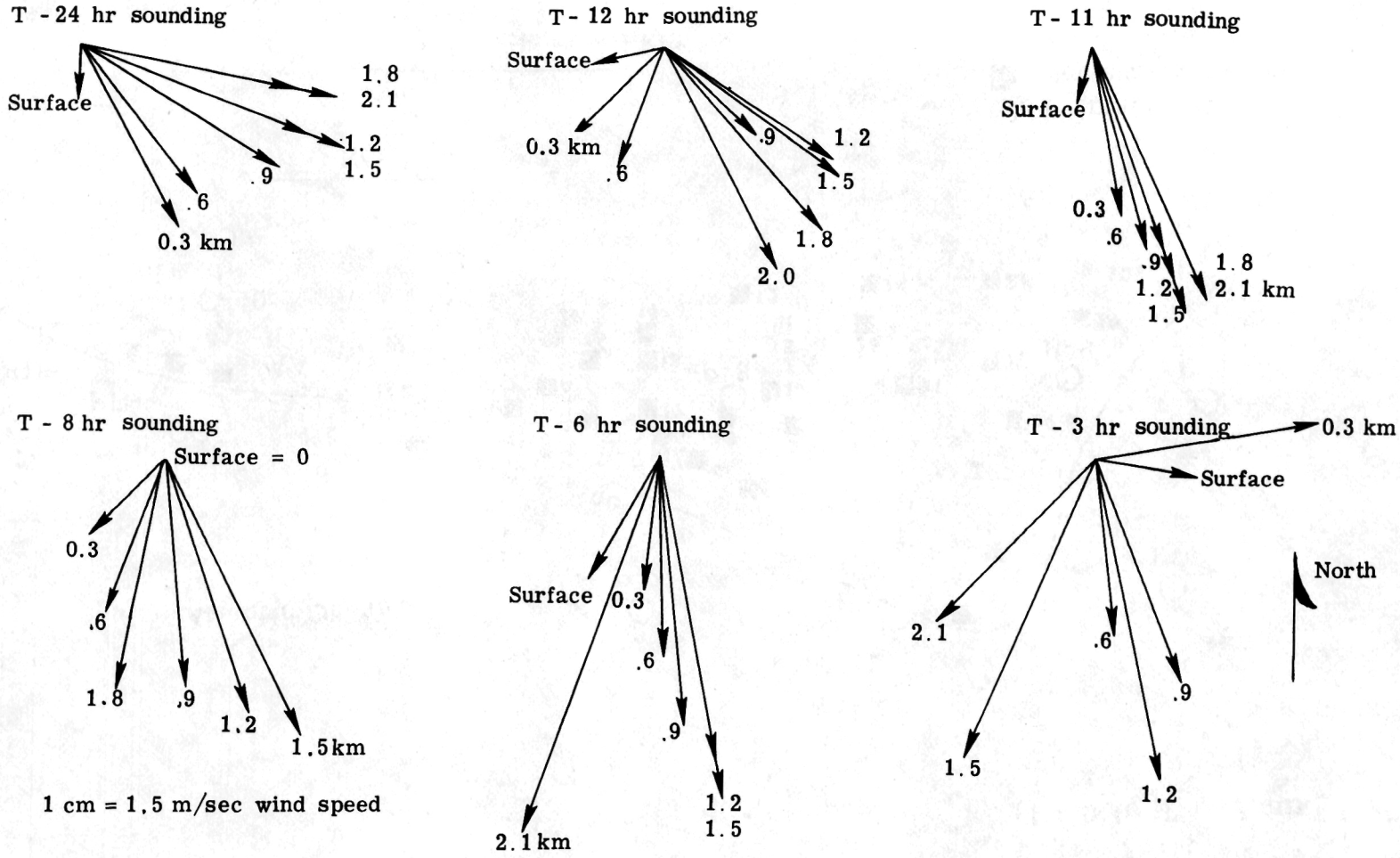

Figure 2.- Wind velocity and direction as function of altitude for different prelaunch times.

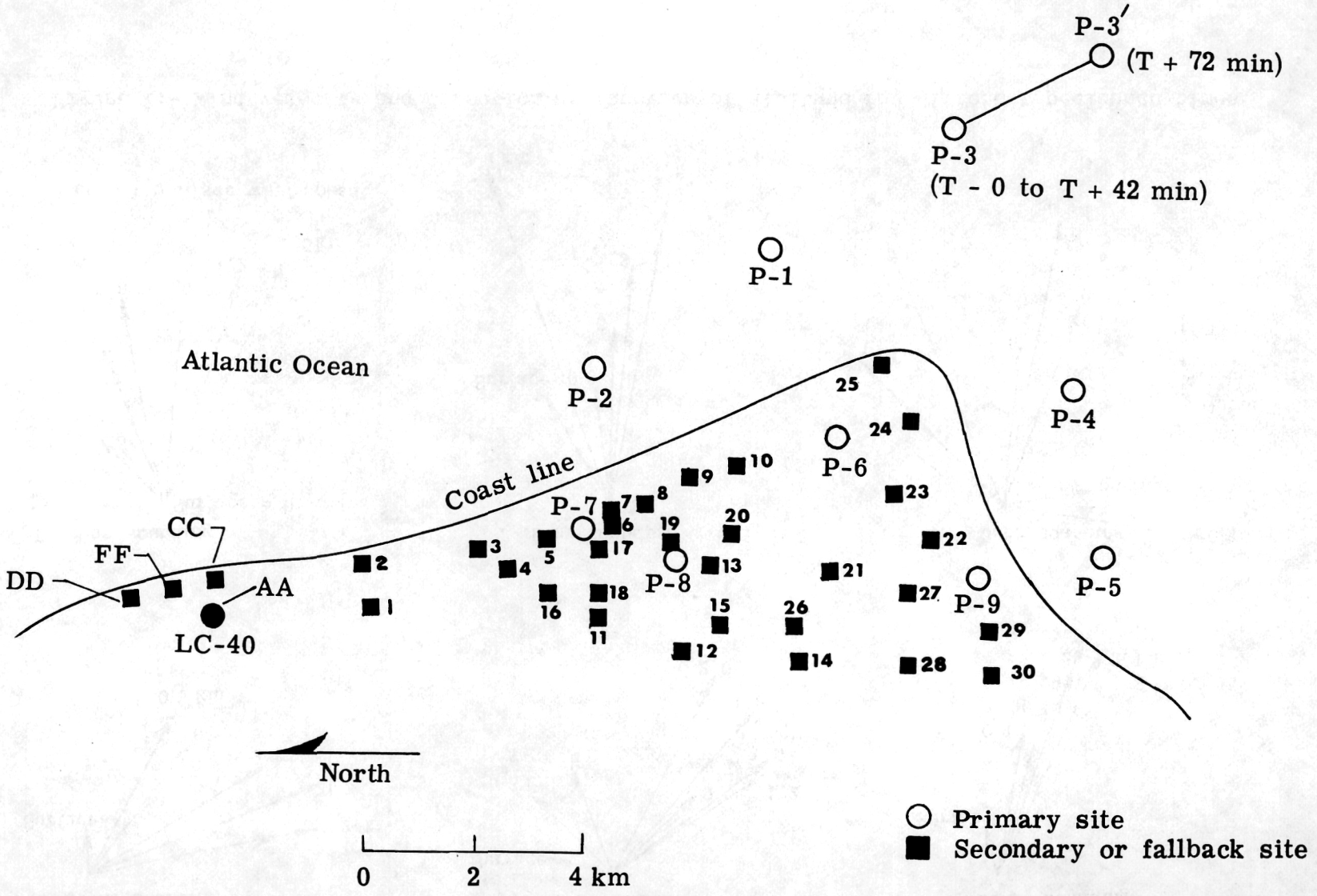

Figure 3.- Sampling instrumentation site plan.

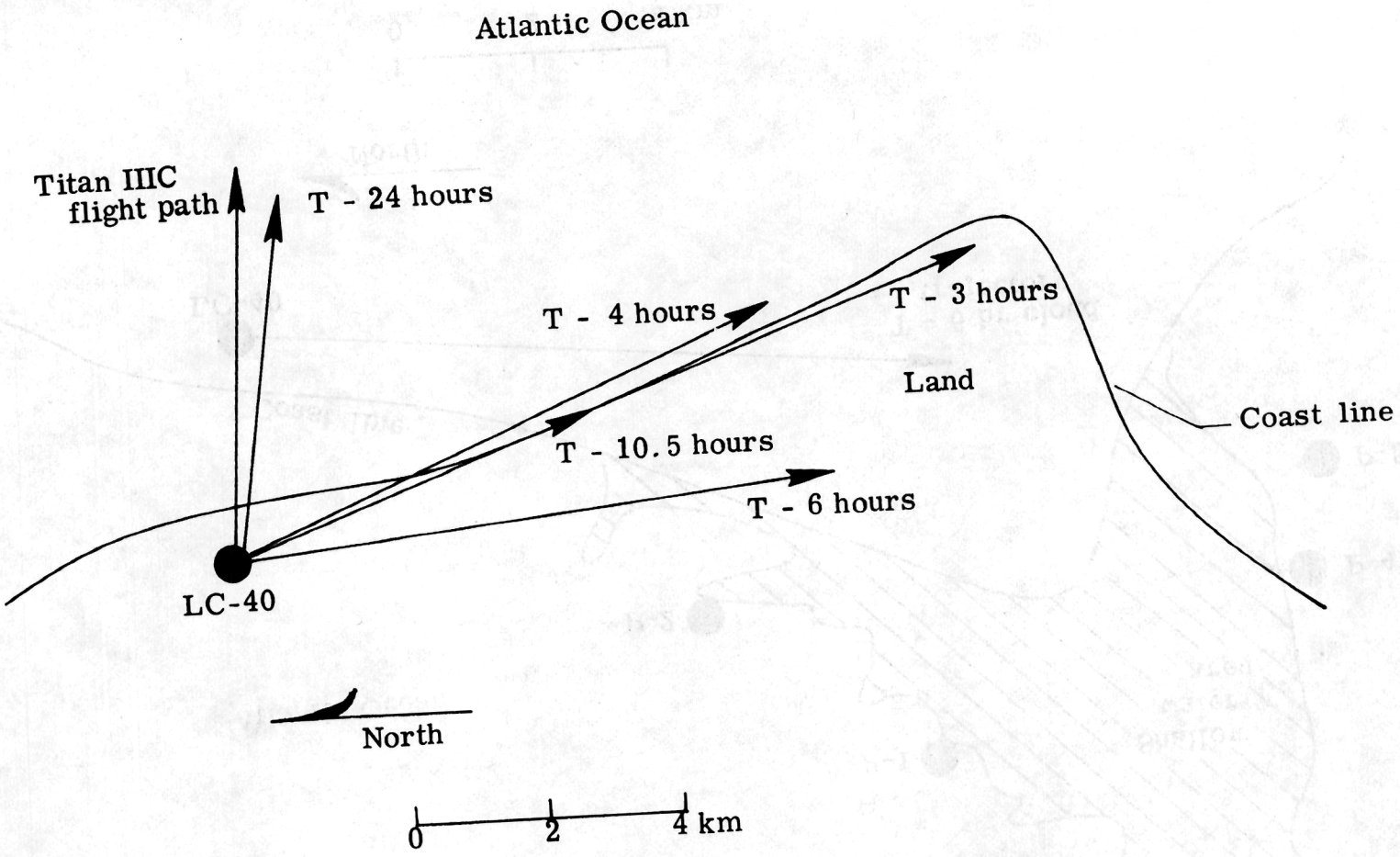

Figure 4.- Prelaunch cloud trajectory predictions.

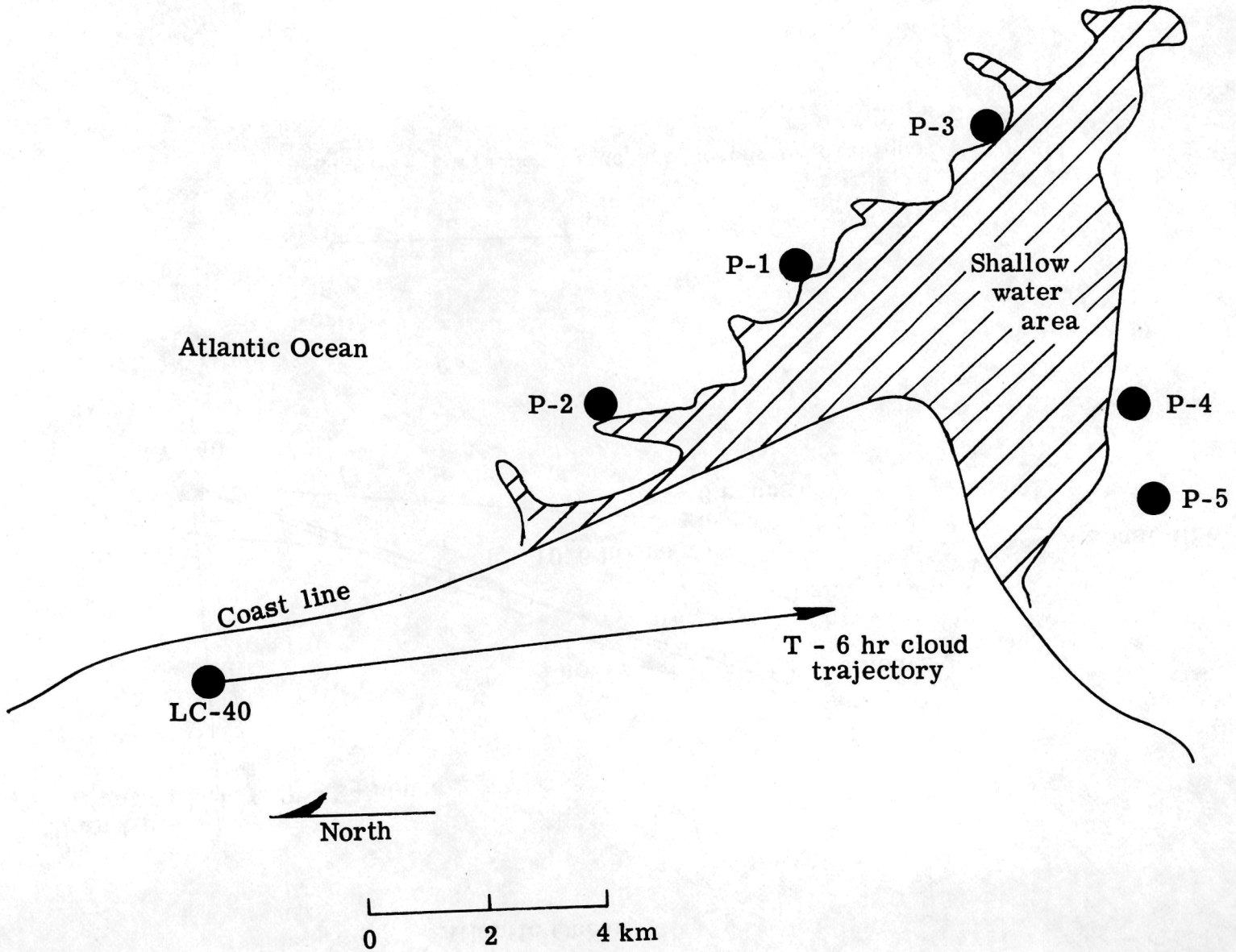

Figure 5.- T - 6 hr primary site plan.

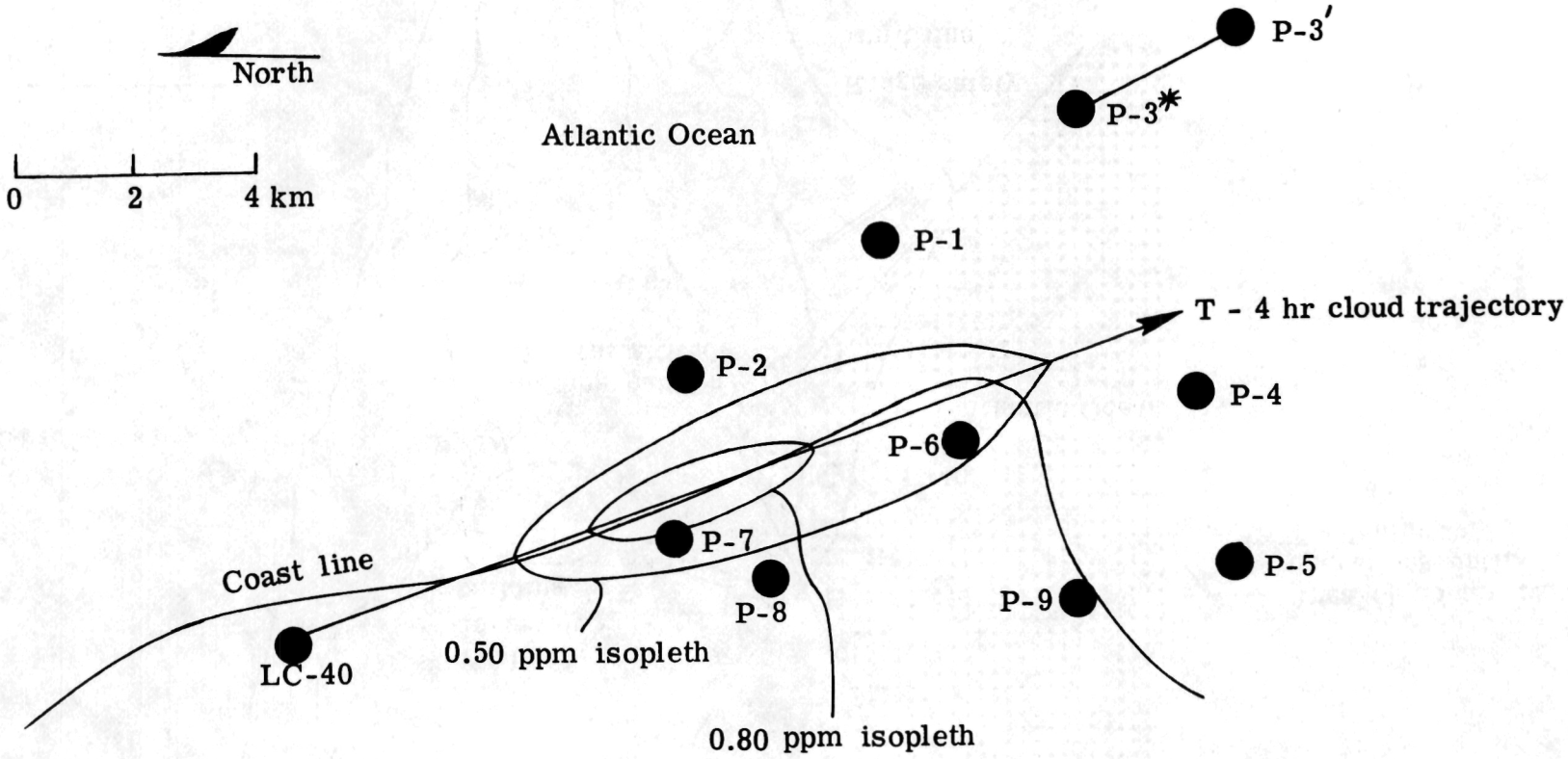

Figure 6.- Final primary site plan and T - 4 hr effluent predictions. P-3 relocated at T + 42 min; on site at P-3' at T + 72 min.

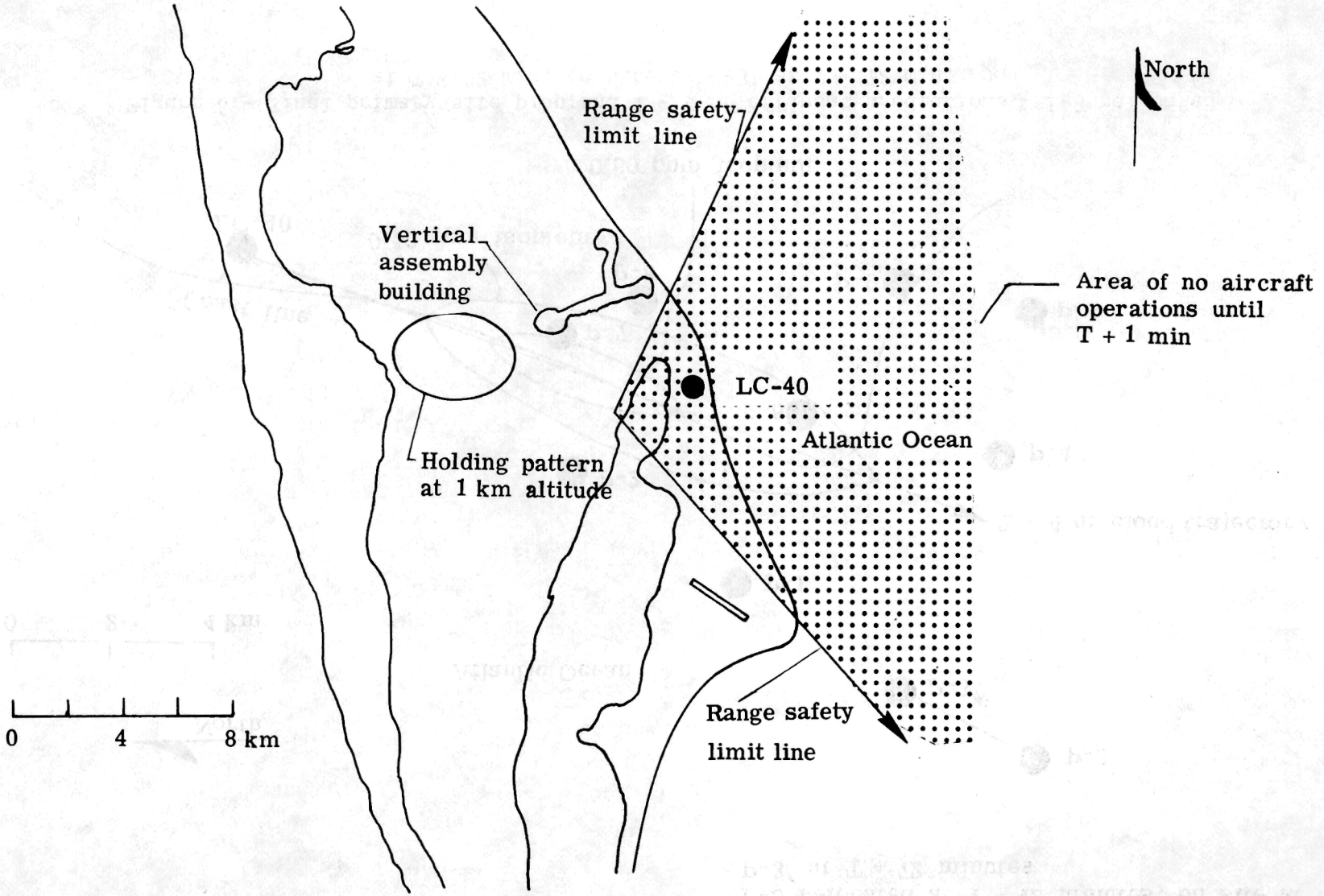

Figure 7.- Aircraft holding pattern.

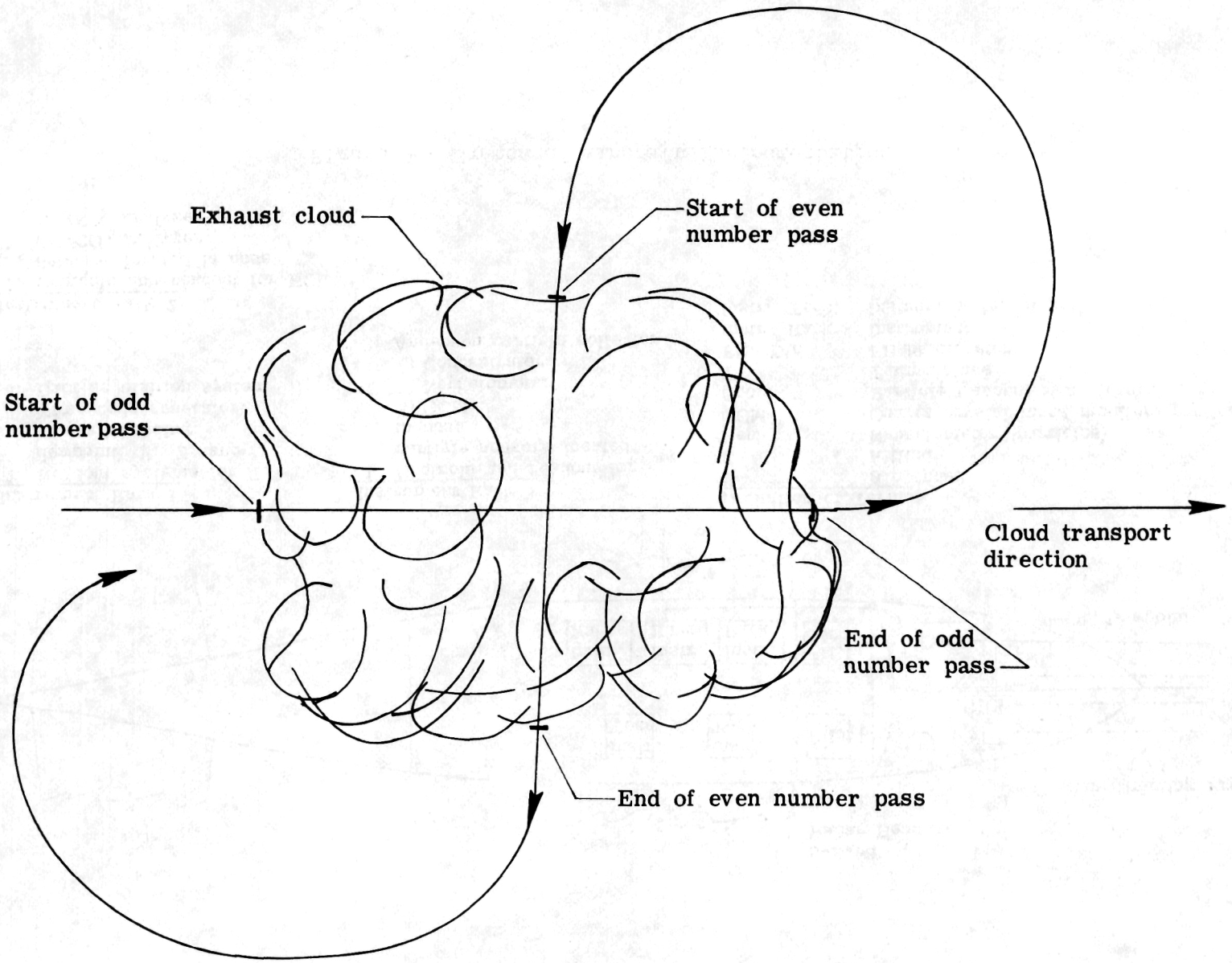

Figure 8.- Basic aircraft sampling plan, downwind-crosswind (plan view). Alternate odd and even number passes may be at varying altitudes.

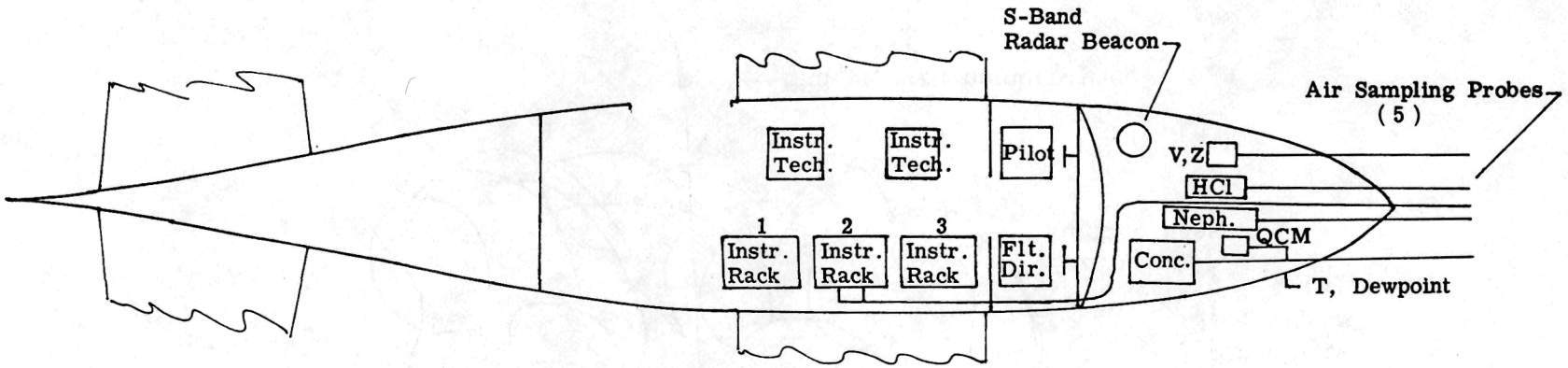

Instrument Rack 1
1. Readout systems for T, dewpoint, V, Z, and aircraft heading
2. Time code generator
3. Data acquisition system

Instrument Rack 2
1. Controls and readout for HCl; detector located in nose
2. CO/CO_2 analyzer
3. NO/NO_x analyzer

Instrument Rack 3
1. Controls and readout for particle sensors located in nose
   a) QCM
   b) Nephelometer
   c) Concentrator
2. Andersen particle collector

Definition of Terms:

V	Air speed
Z	Altitude
Neph	Nephelometer (particles)
QCM	Quartz crystal mass monitor (particles)
Conc.	Particle Concentrator (filters)
T	Temperature
Flt. Dir.	Flight director
Instr. Rack	Instrument rack
Instr. Tech.	Instrument technician

Figure 9.- Sketch of aircraft instrumentation.

L-77-310

Figure 10.- Sampling aircraft.

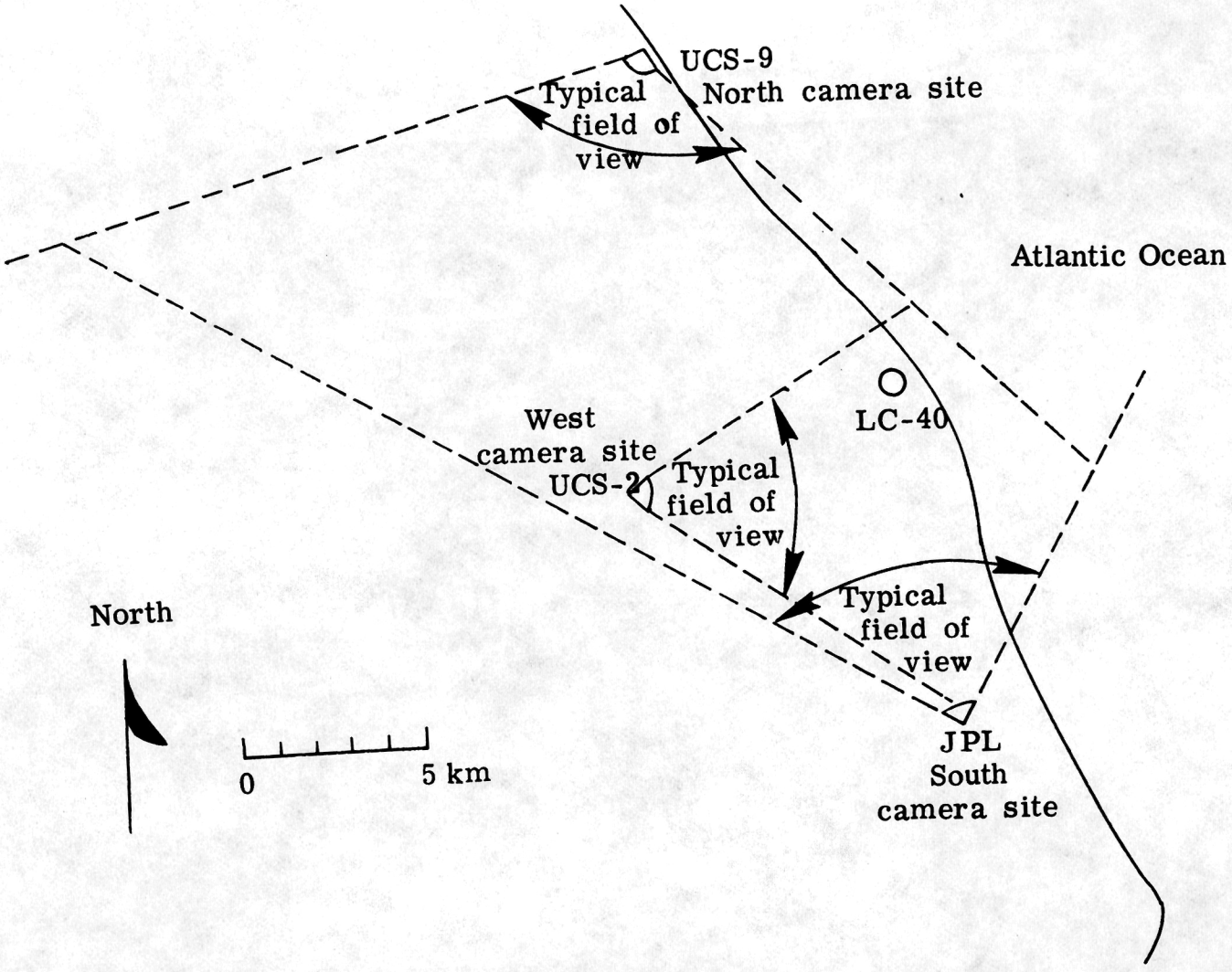

Figure 11.- Camera site plan.

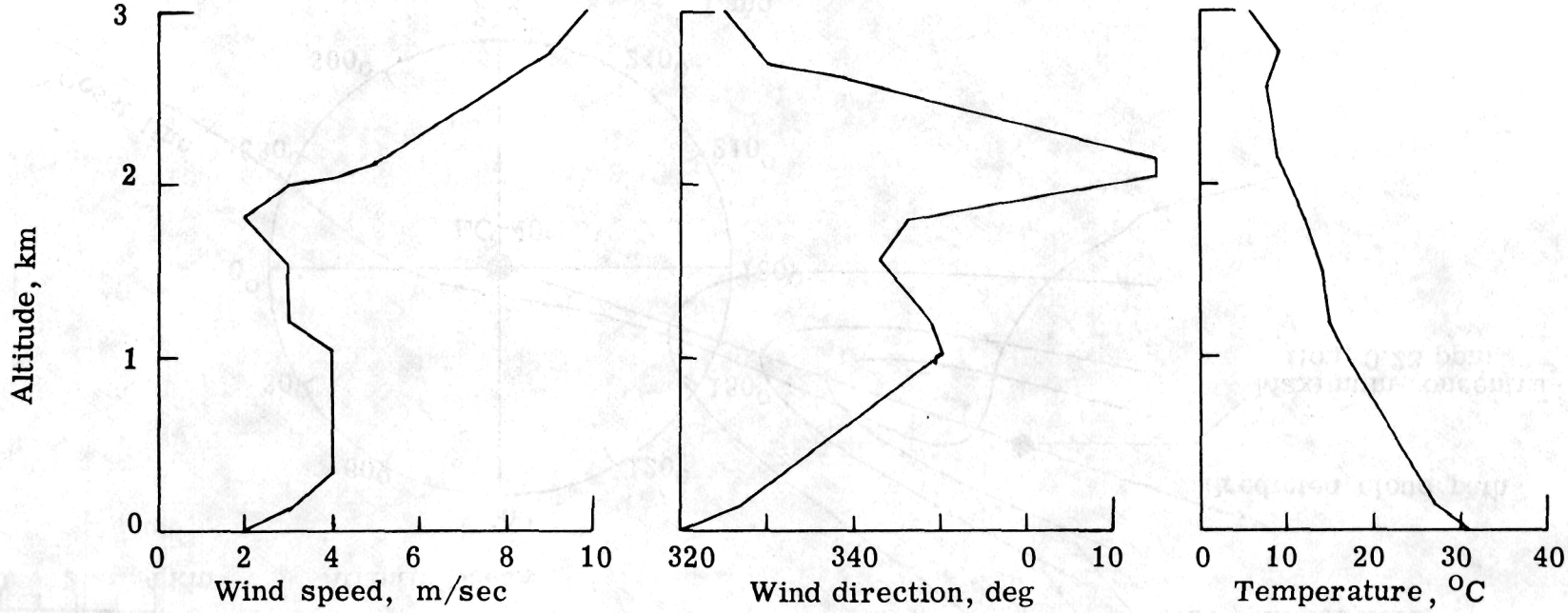

Figure 12.- Meteorological data used for postlaunch model.

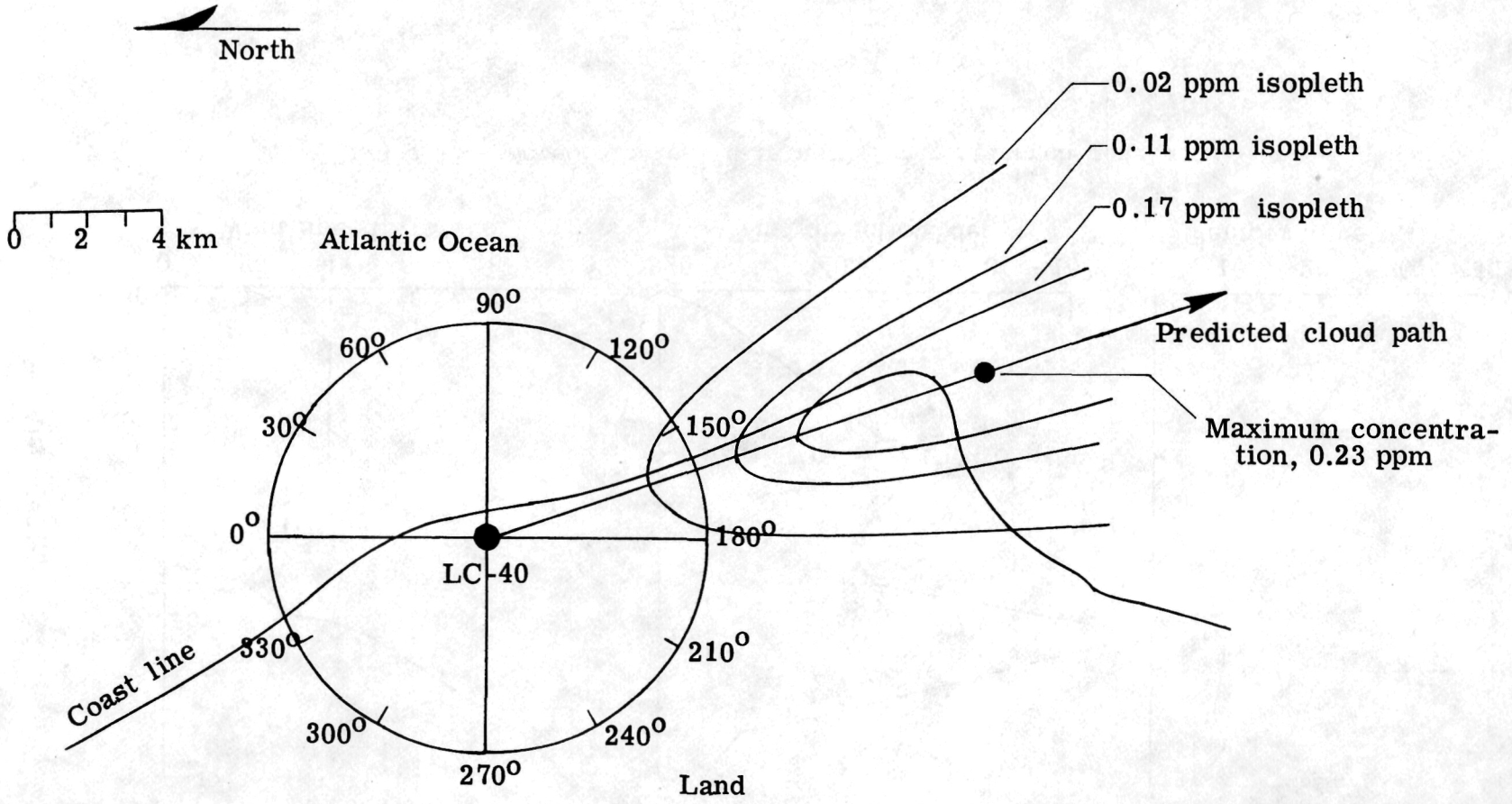

Figure 13.- Surface level HCl isopleths.

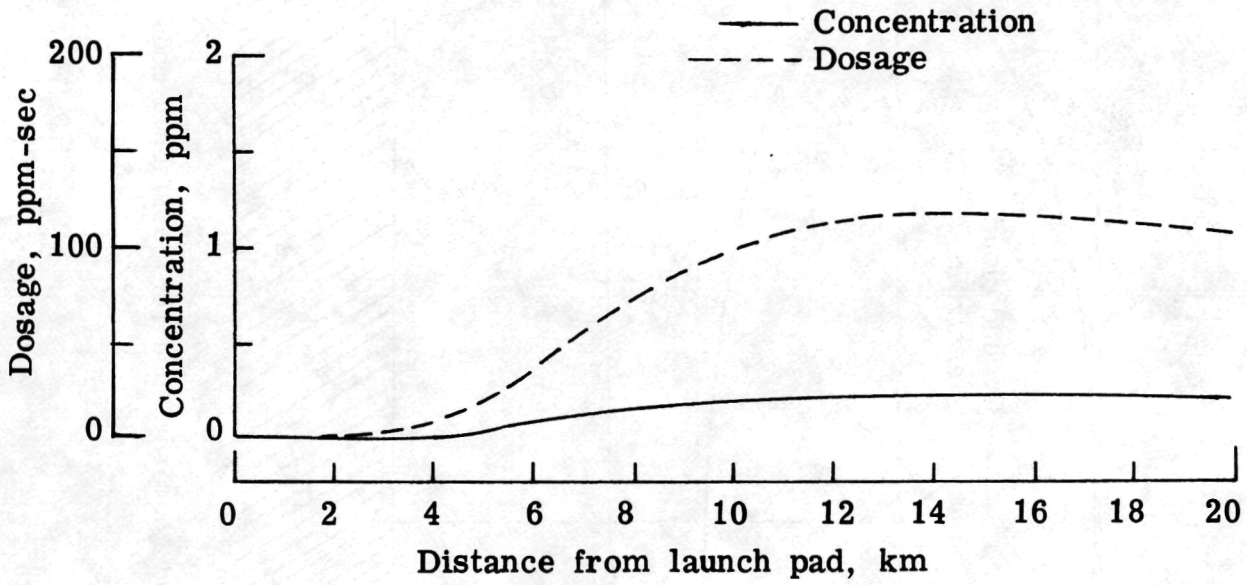

Figure 14.- Surface level HCl concentrations and dosage. Cloud center line.

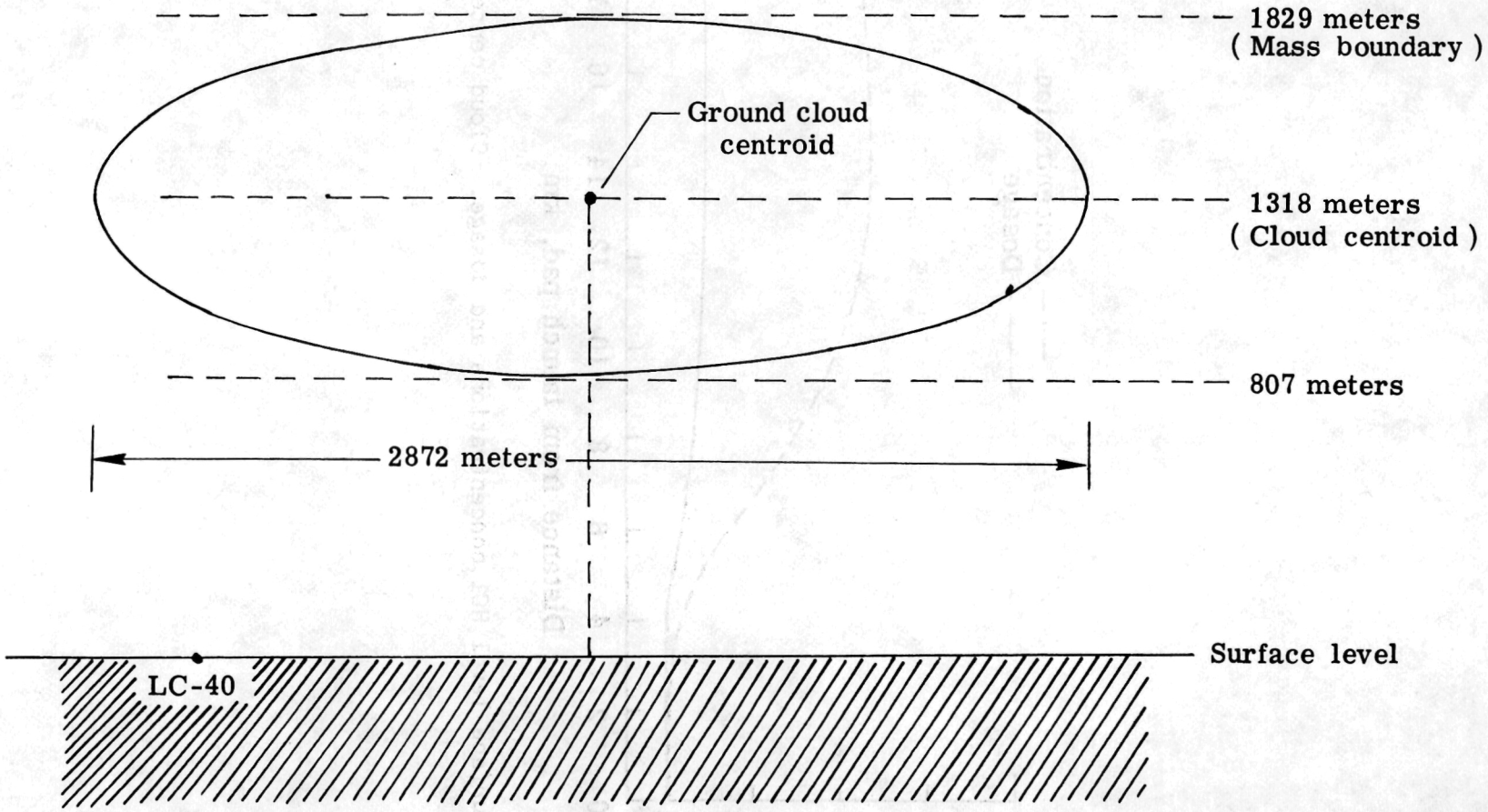

Figure 15.- Source cloud geometry used for postlaunch model calculations.

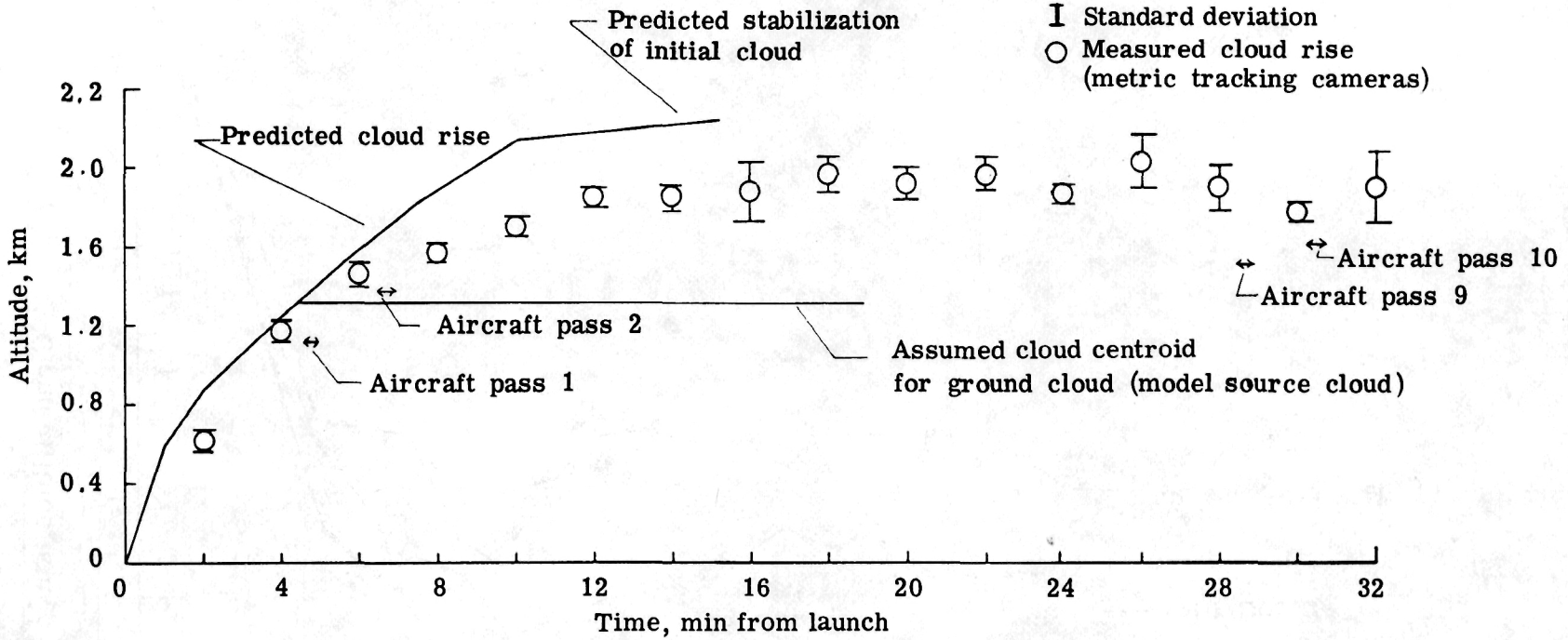

Figure 16.- Cloud stabilization altitude data, May 1975.

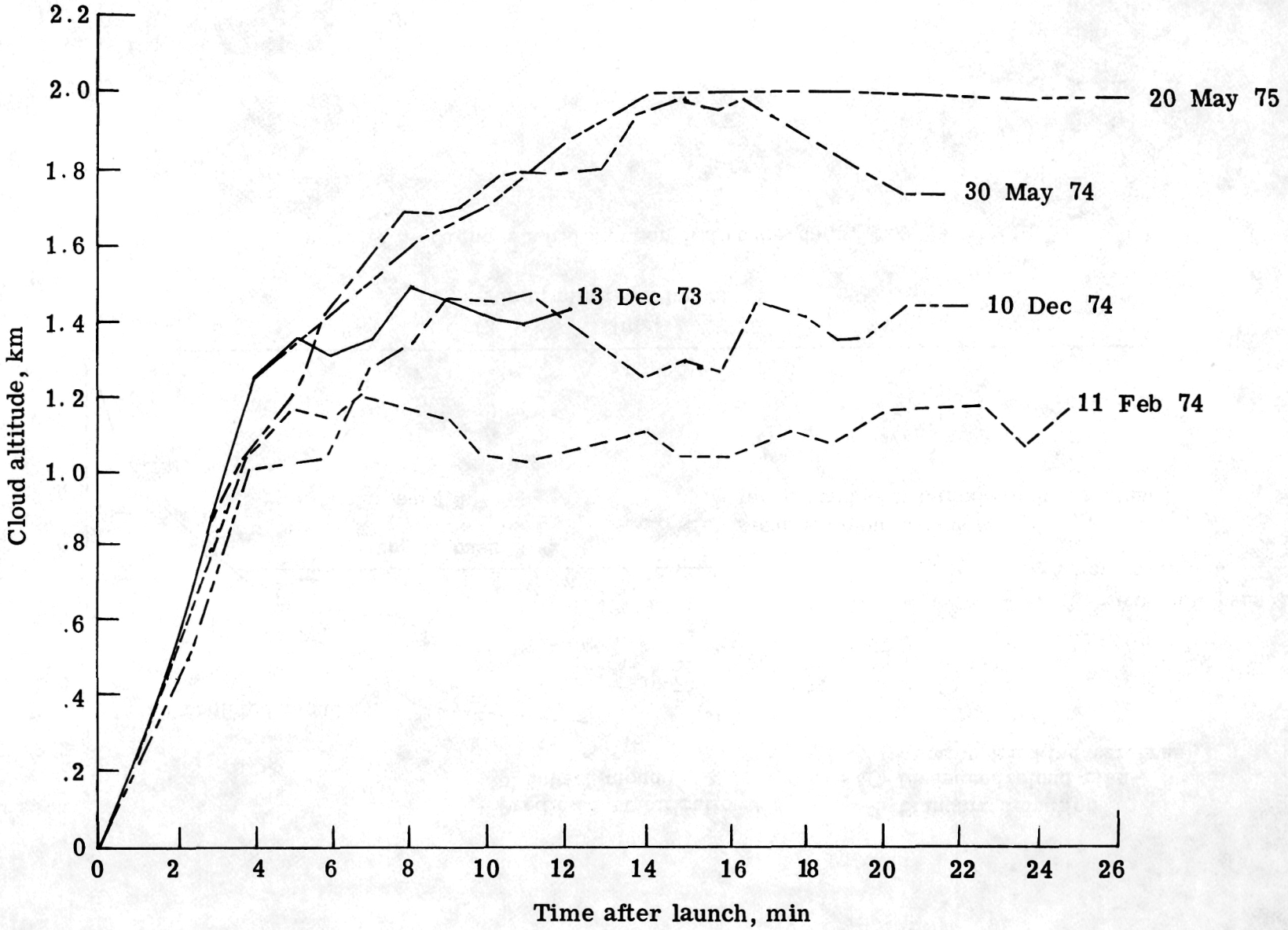

Figure 17.- Summary of cloud stabilization altitude data. Five Titan IIIC launches.

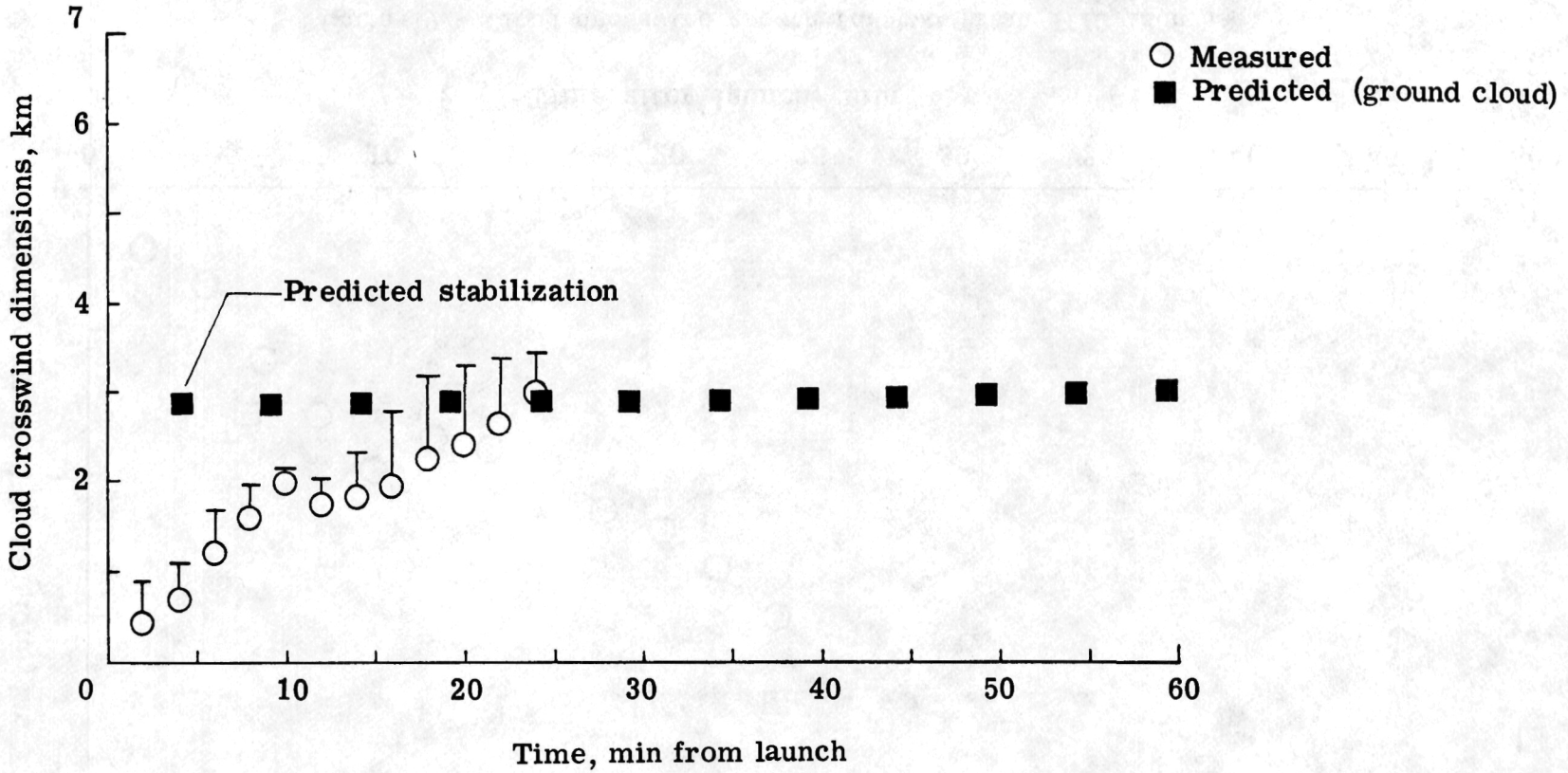

Figure 18.- Cloud crosswind growth, May 1975.

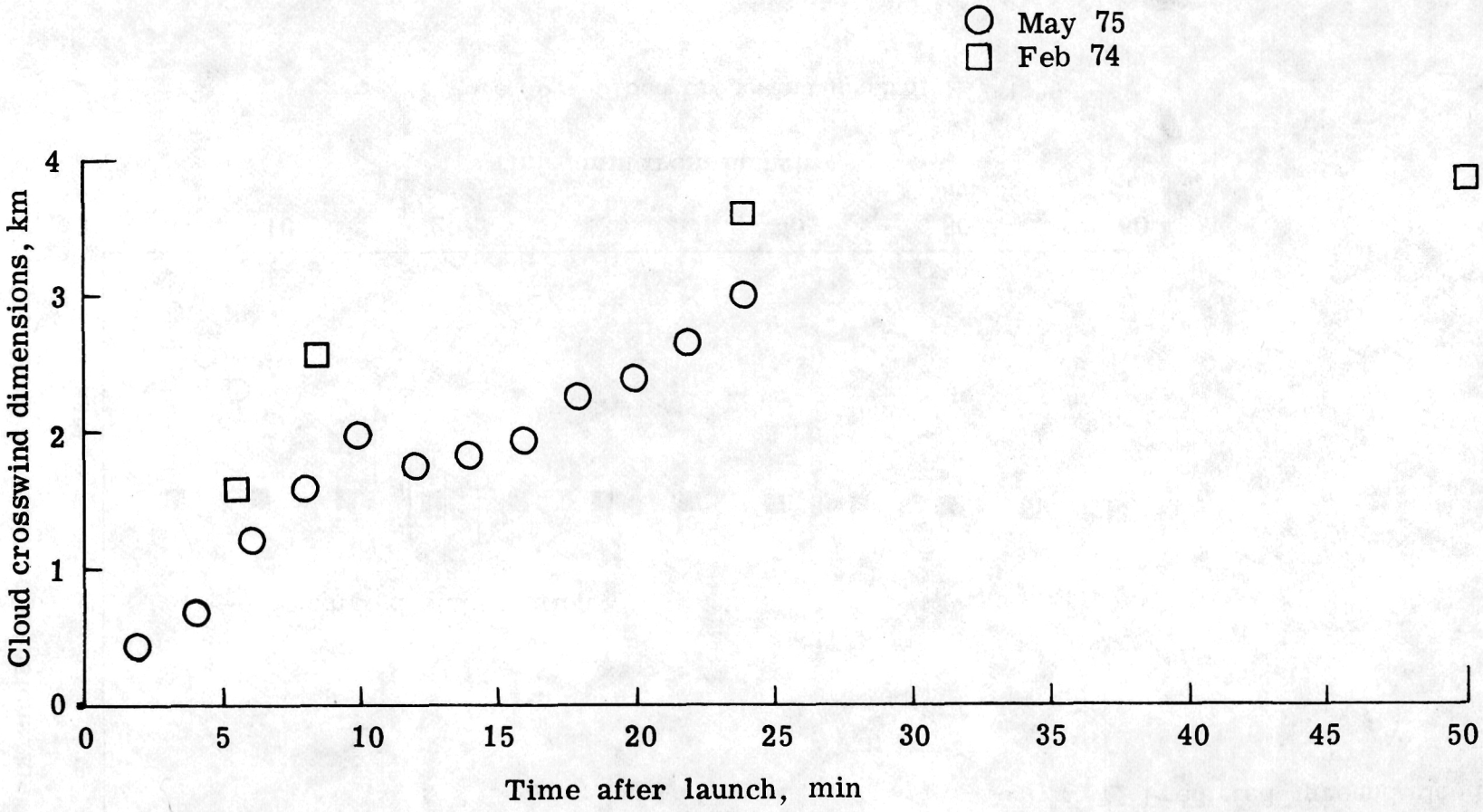

Figure 19.- Cloud crosswind growth for two Titan IIIC launches.

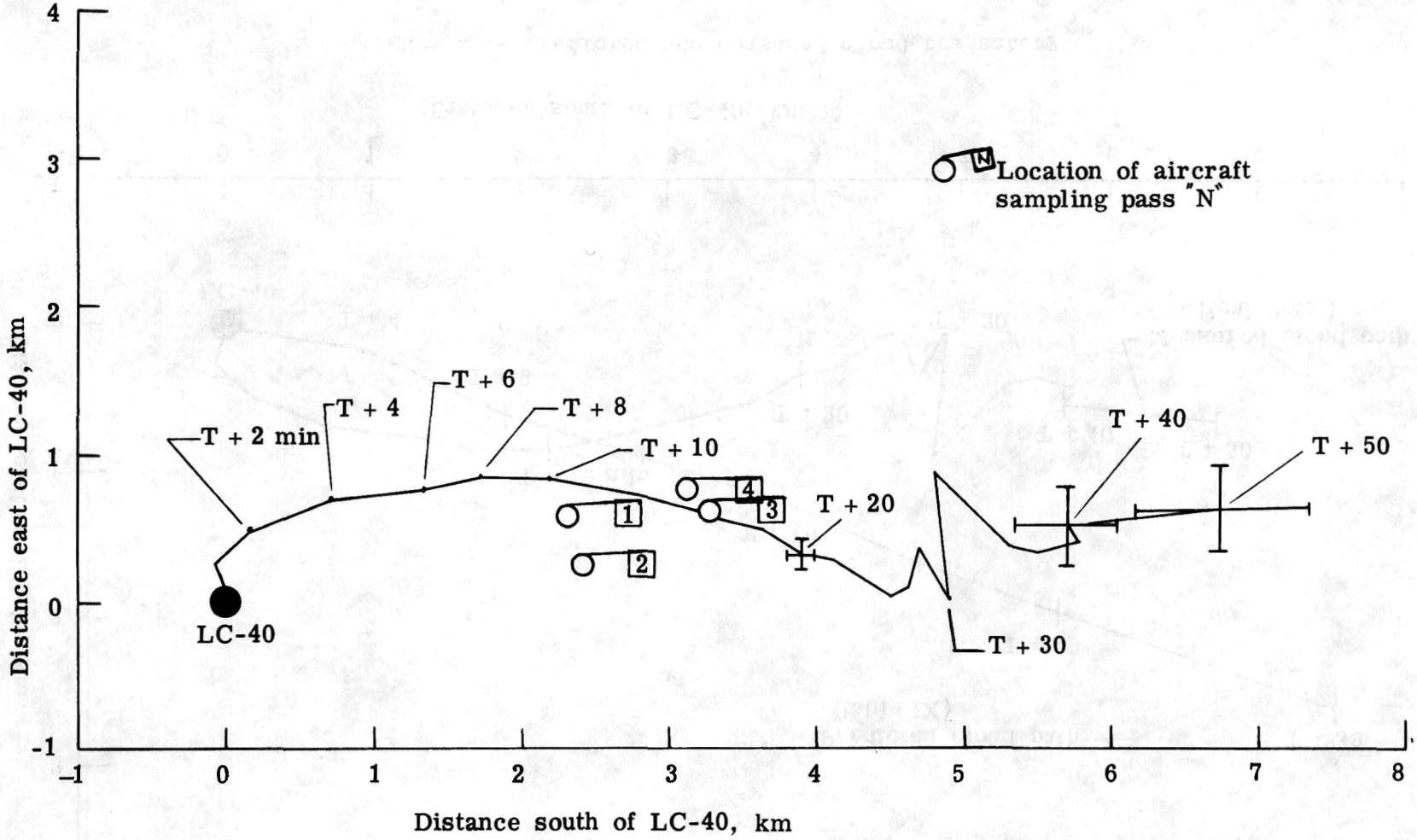

Figure 20.- Cloud trajectory measurements.

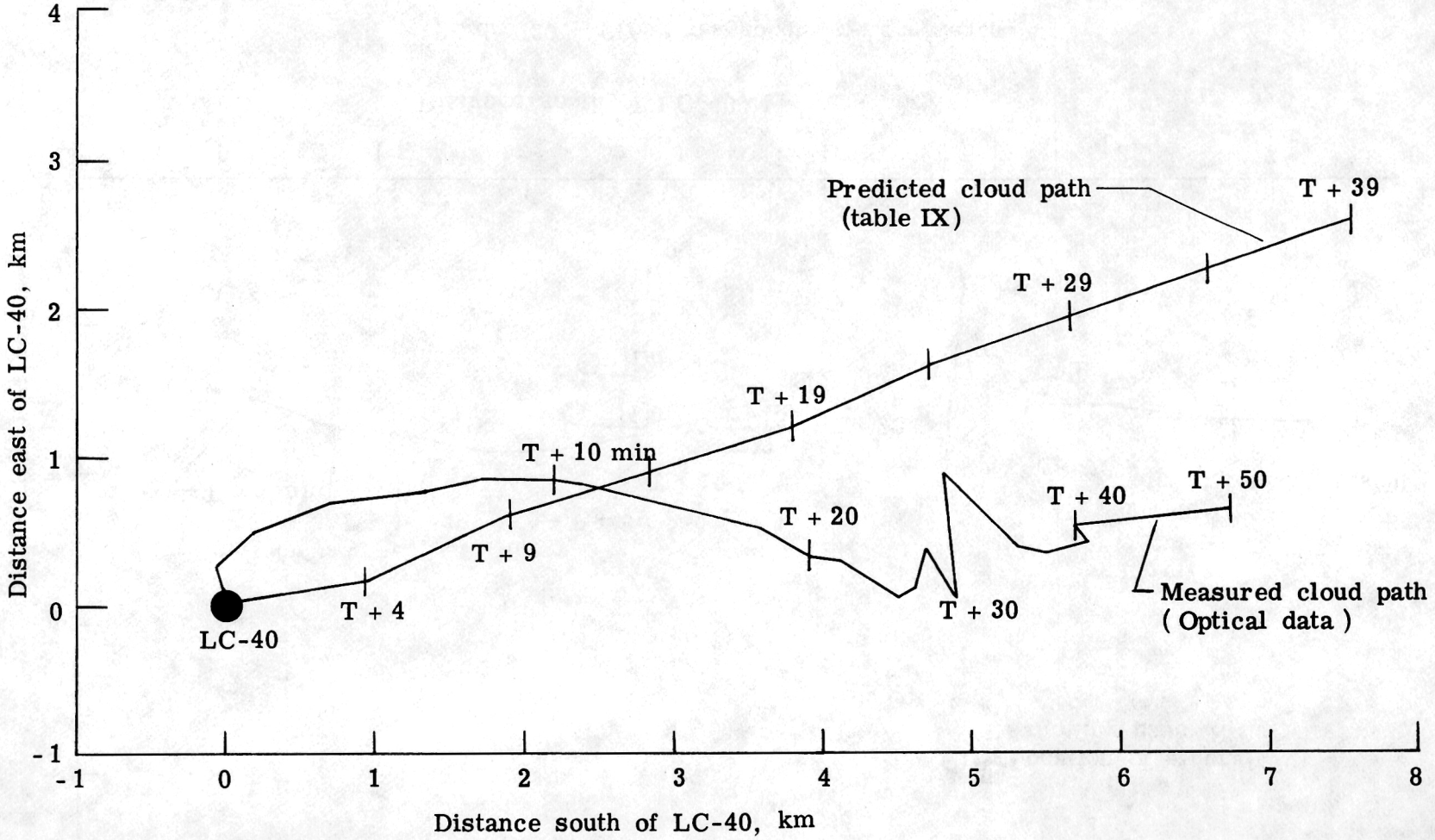

Figure 21.- Predicted and measured cloud trajectory.

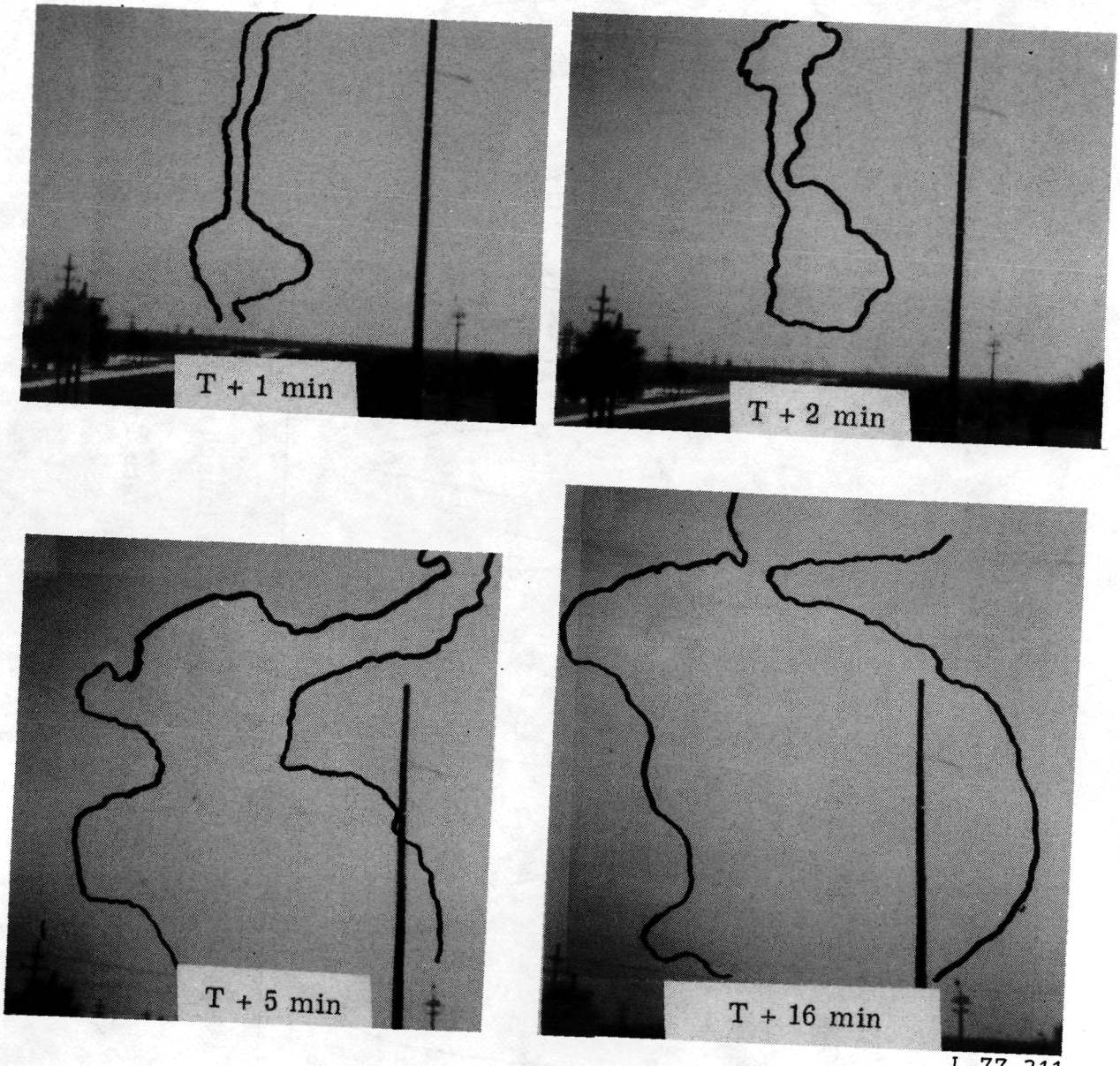

L-77-311

Figure 22.- Visible cloud photography.

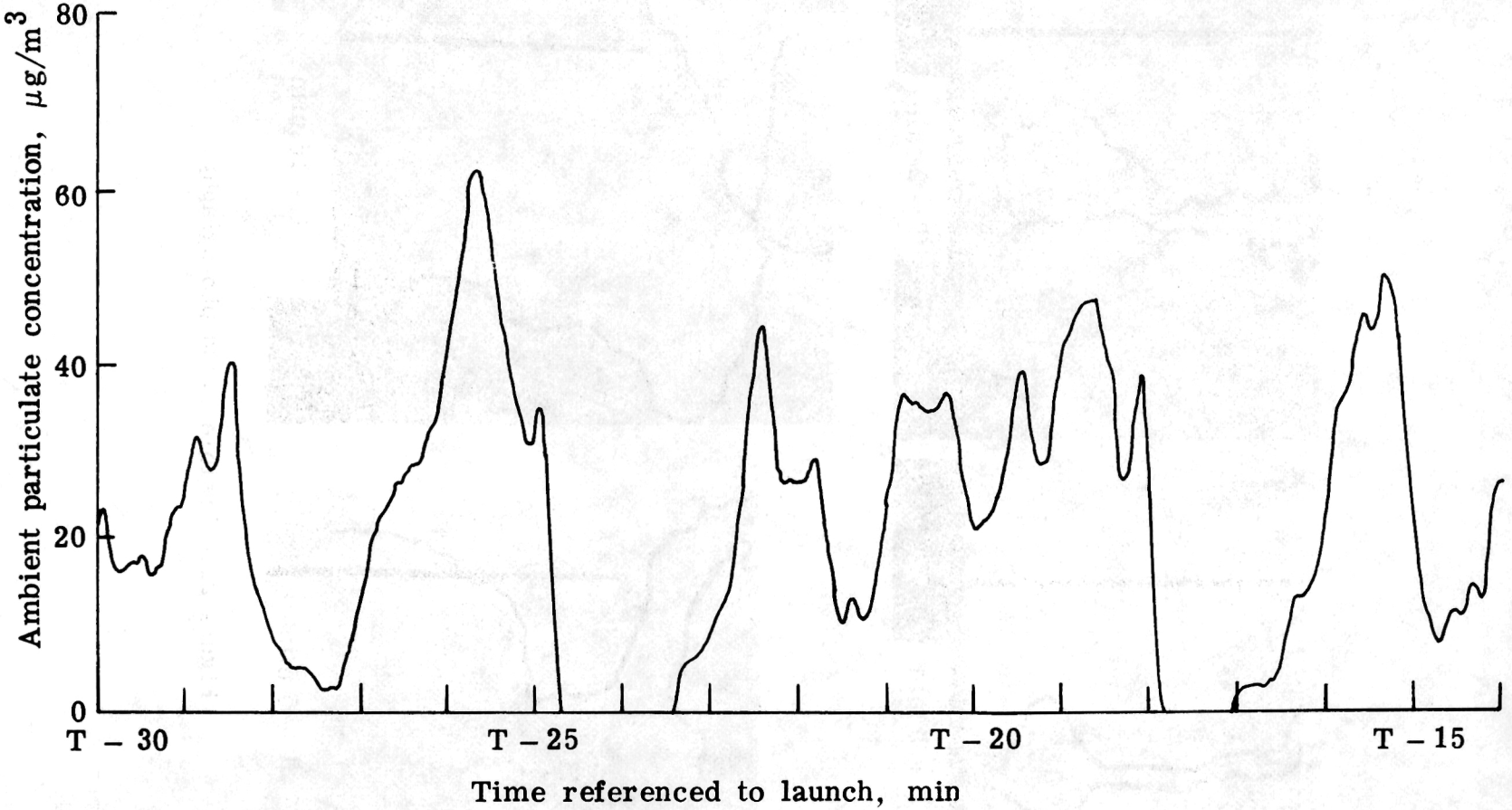

Figure 23.- Prelaunch ambient particulate loading. Mass monitor data.

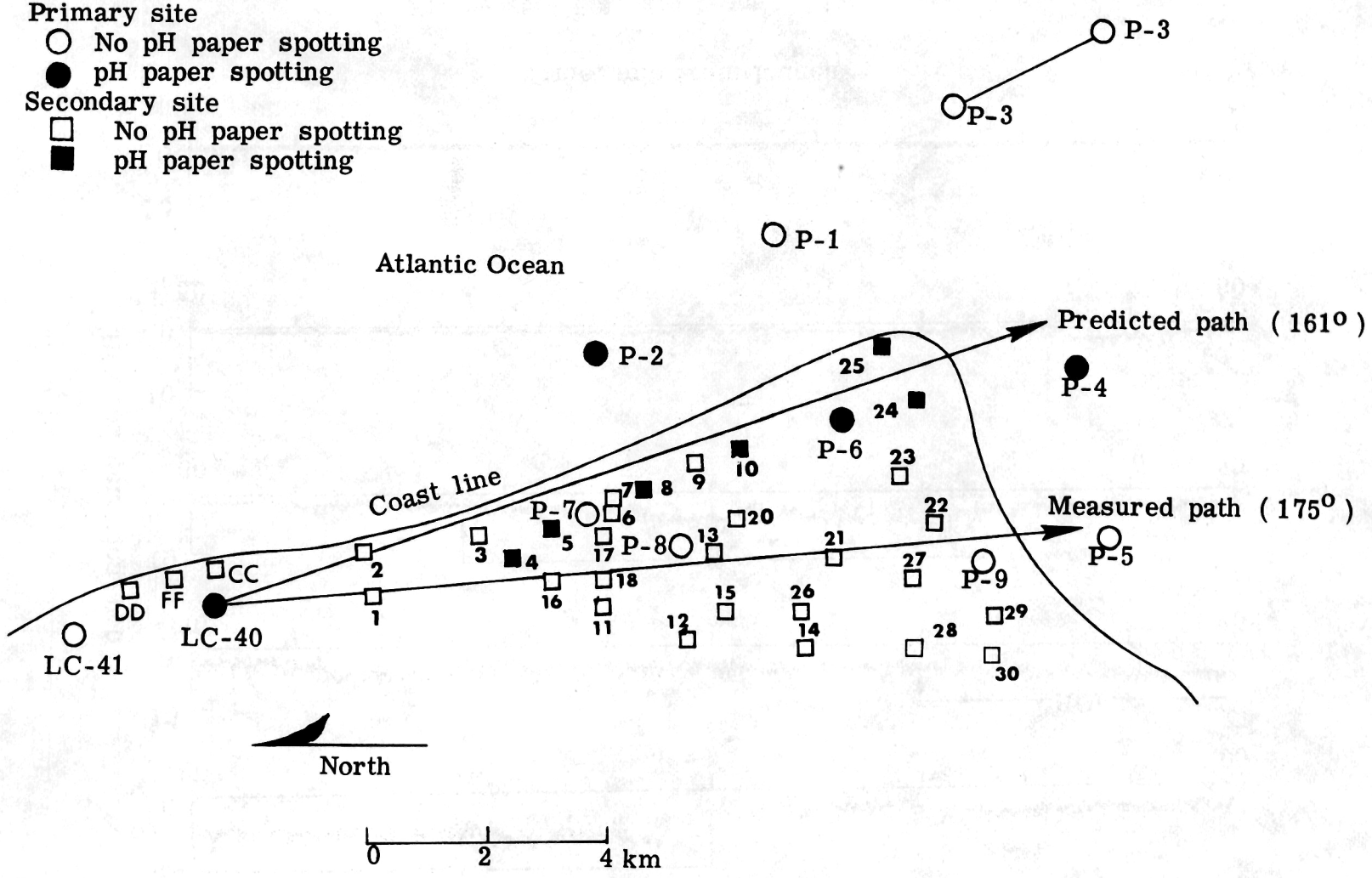

Figure 24.- pH paper results.

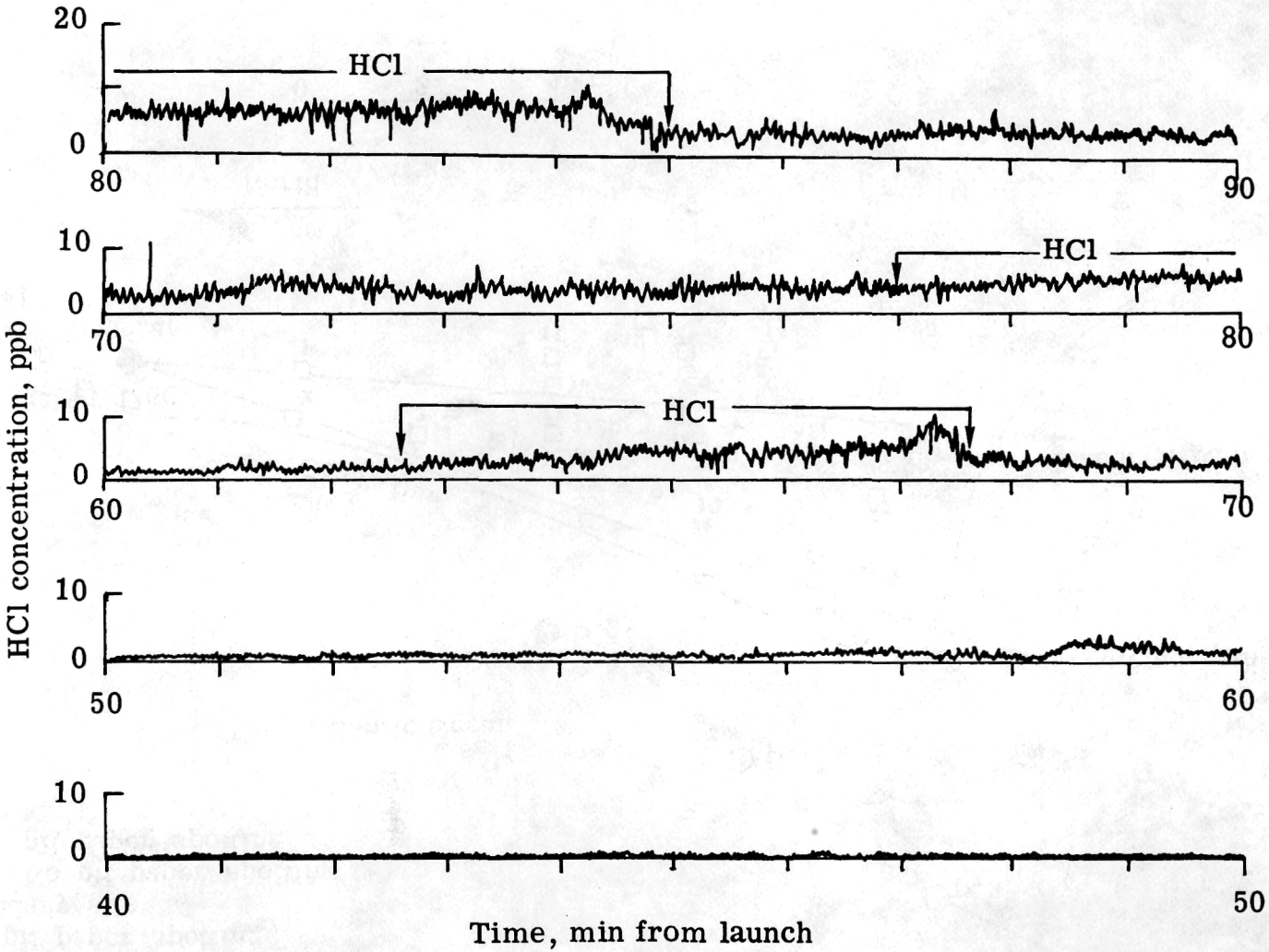

Figure 25.- HCl data trace. Site P-2.

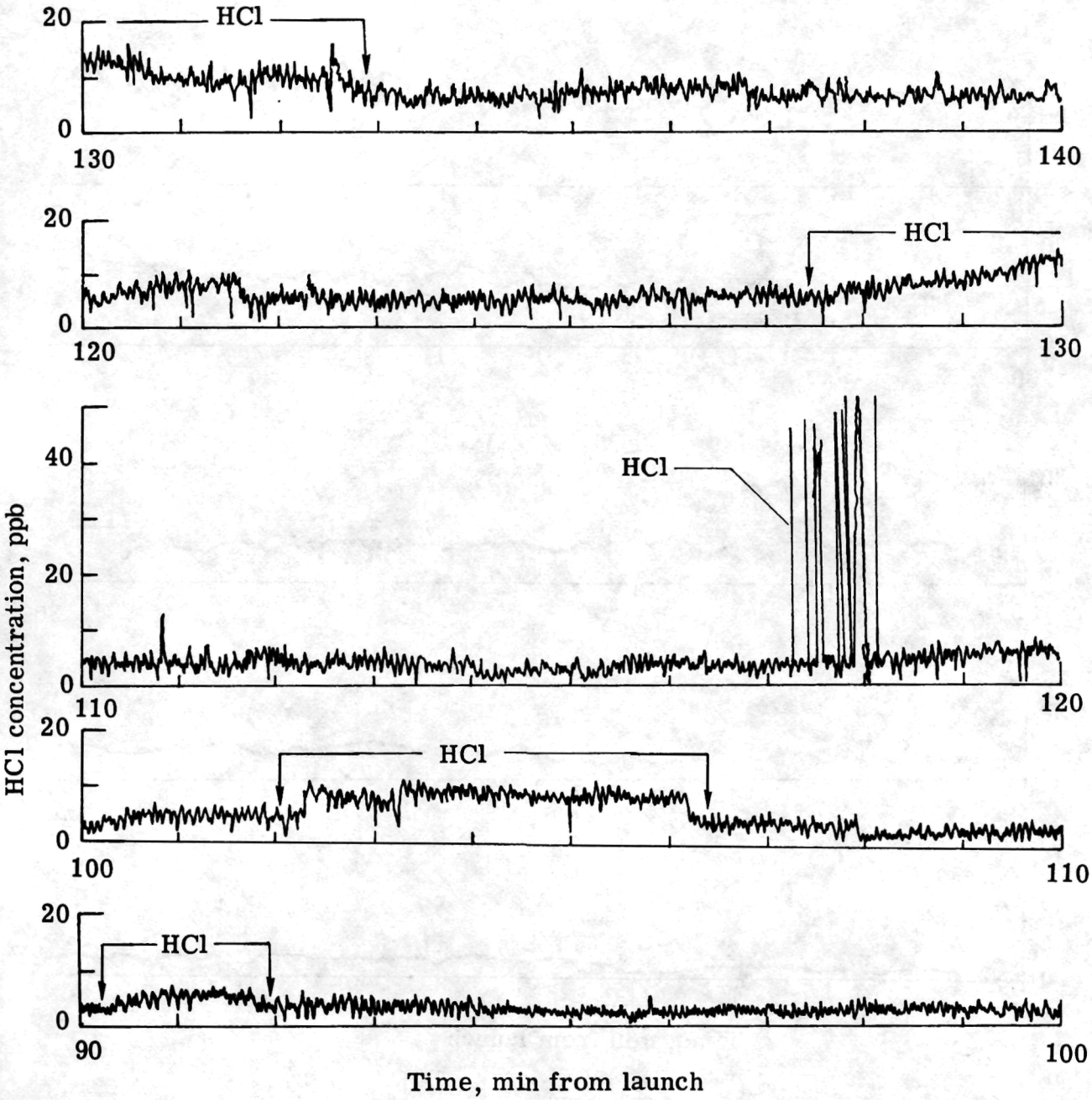

Figure 25.- Concluded.

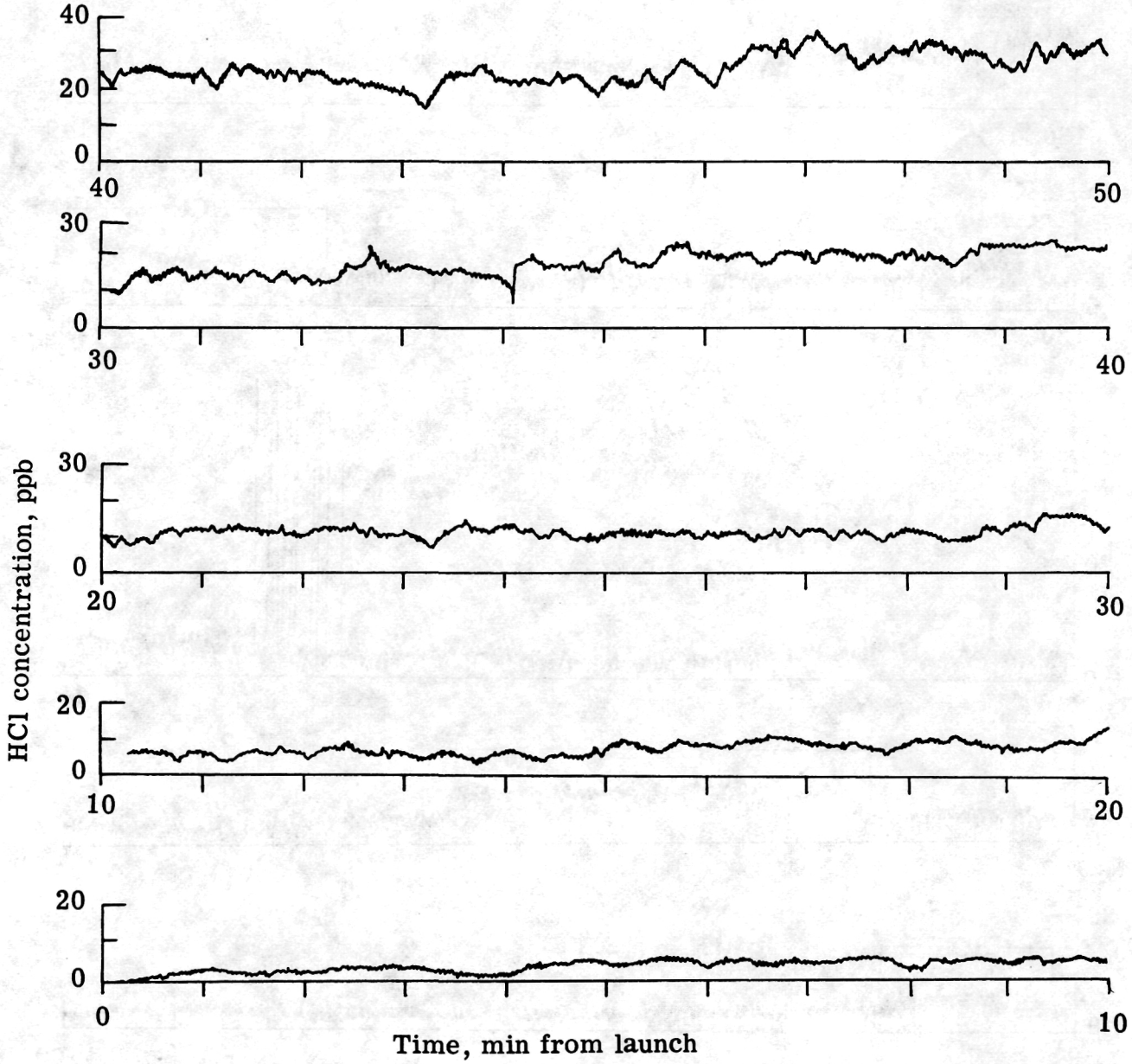

Figure 26.- HCl data trace. Site P-4.

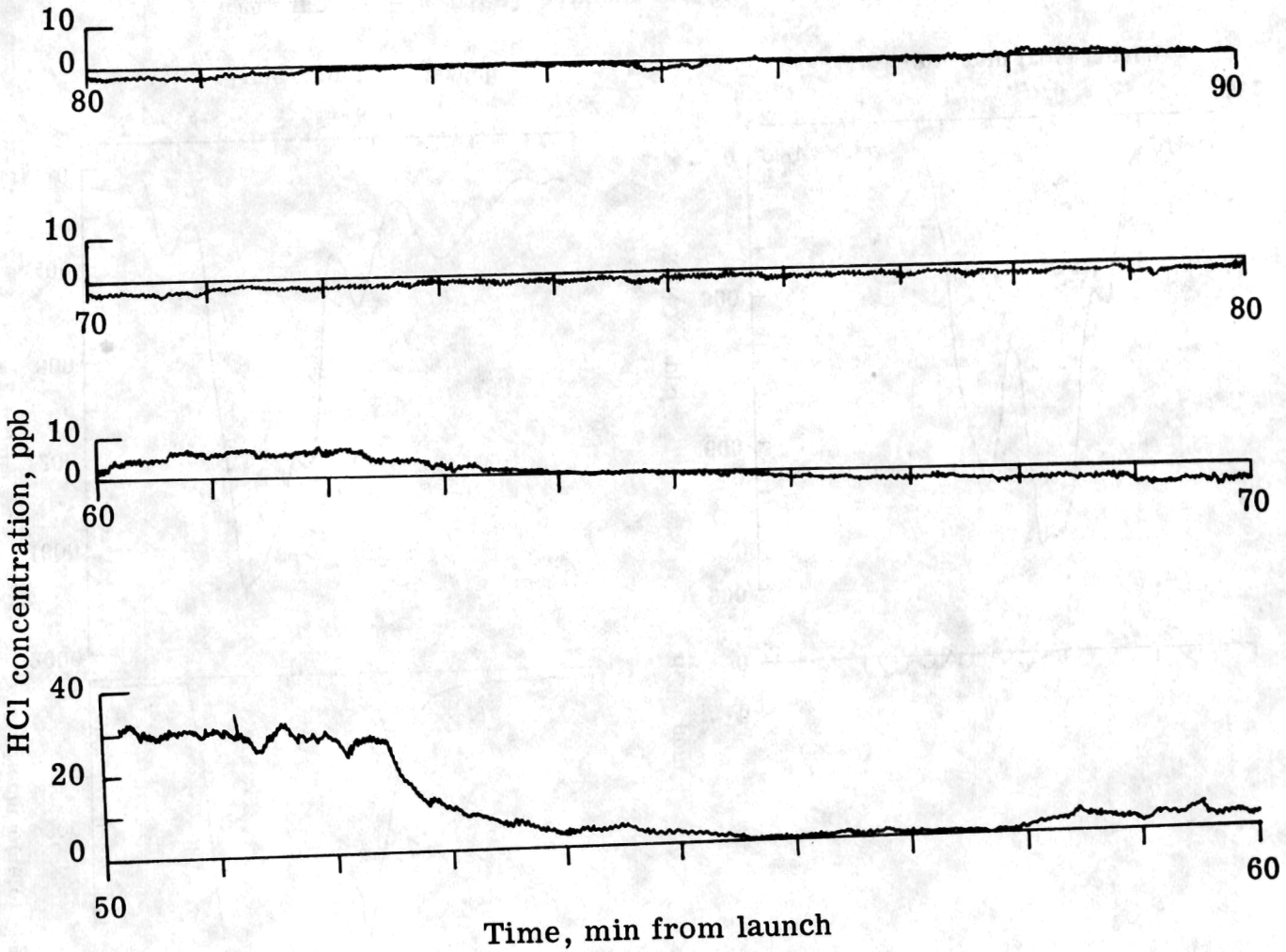

Figure 26.- Concluded.

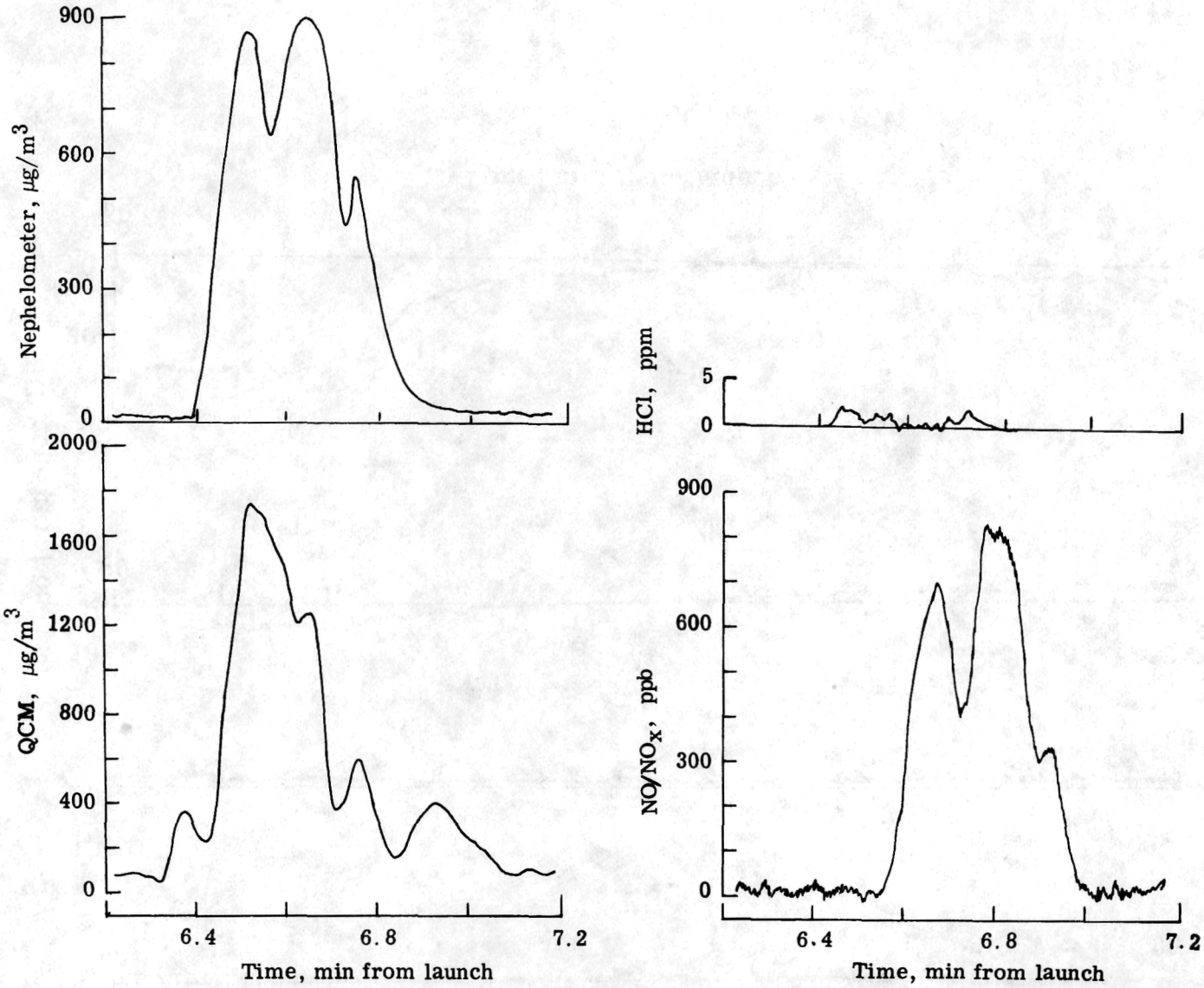

Figure 27.- Typical airborne data. Sampling pass 2.

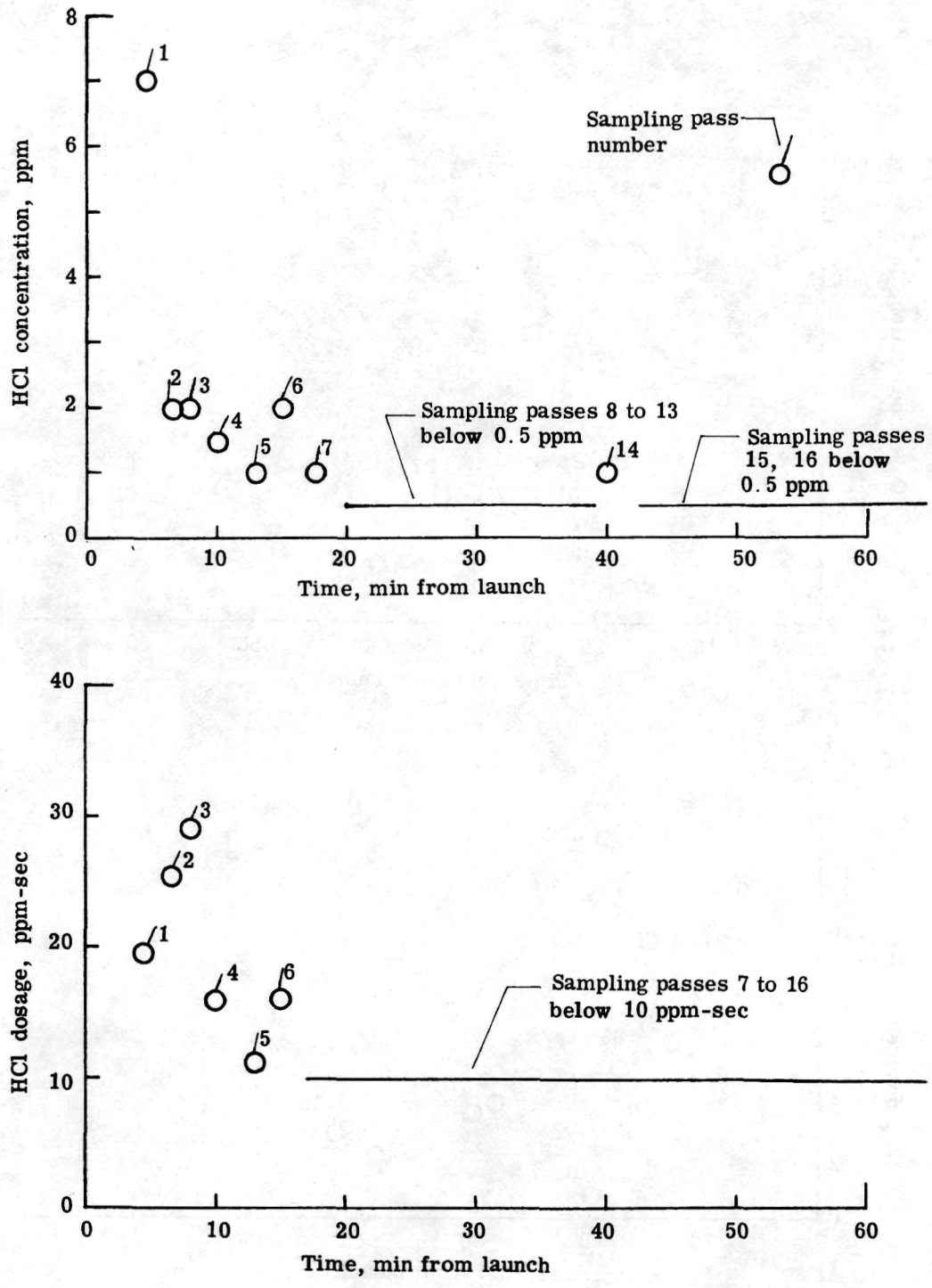

Figure 28.- In-cloud HCl maximum concentration and integrated dosage.

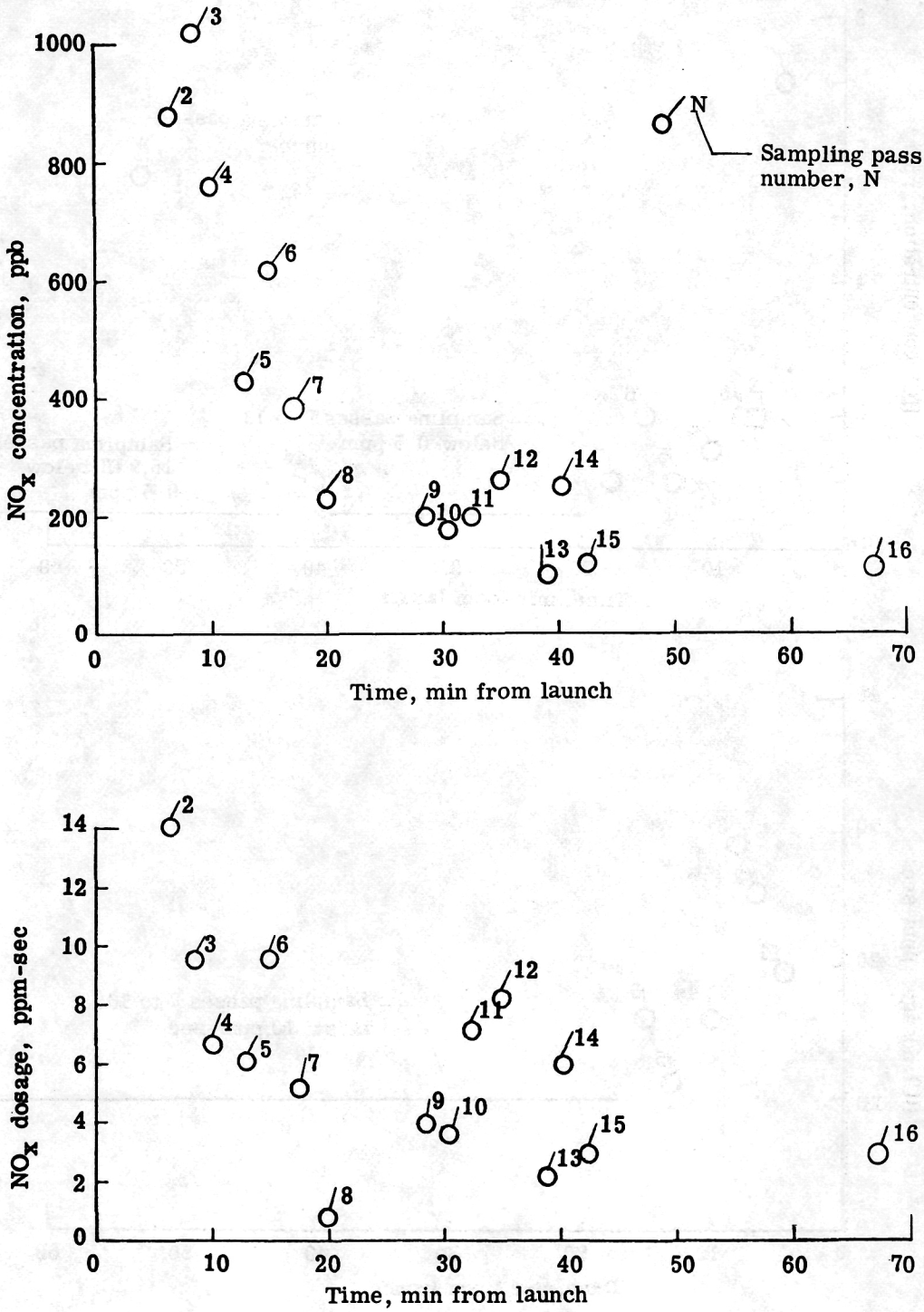

Figure 29.- In-cloud NO_x maximum concentration and integrated dosage.

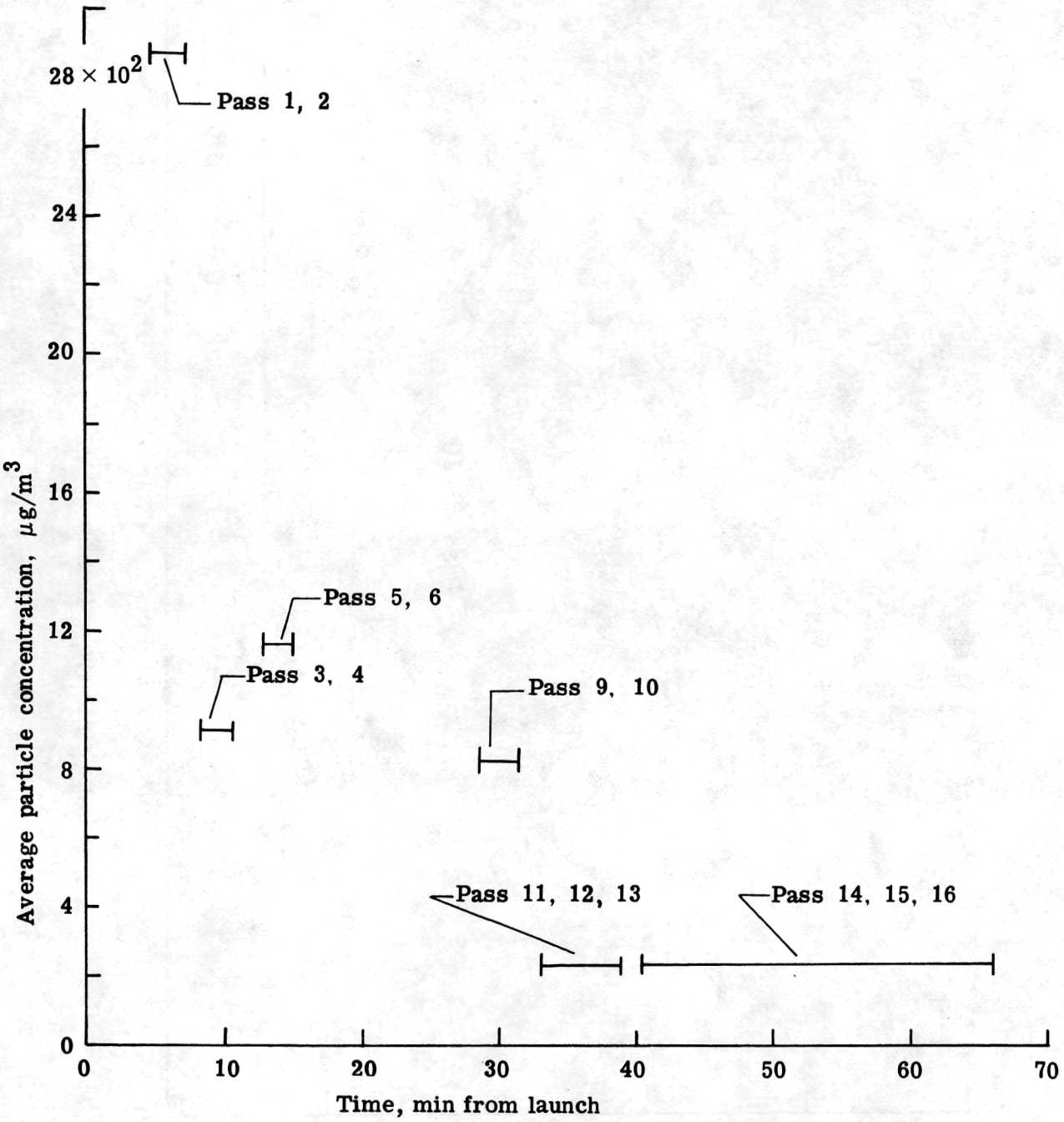

Figure 30.- In-cloud average particulate concentration. Concentrator data.

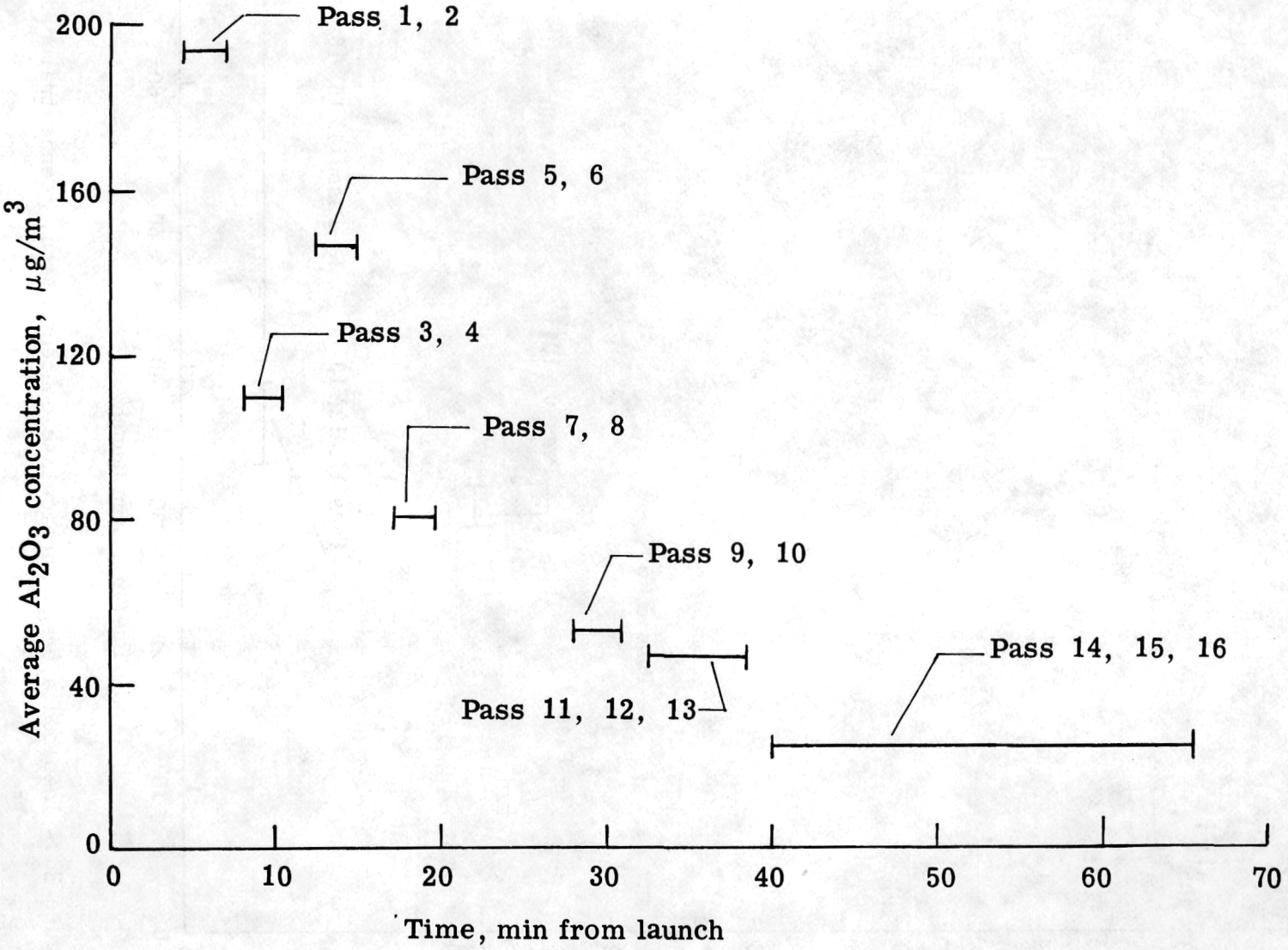

Figure 31.- In-cloud average Al_2O_3 concentration.

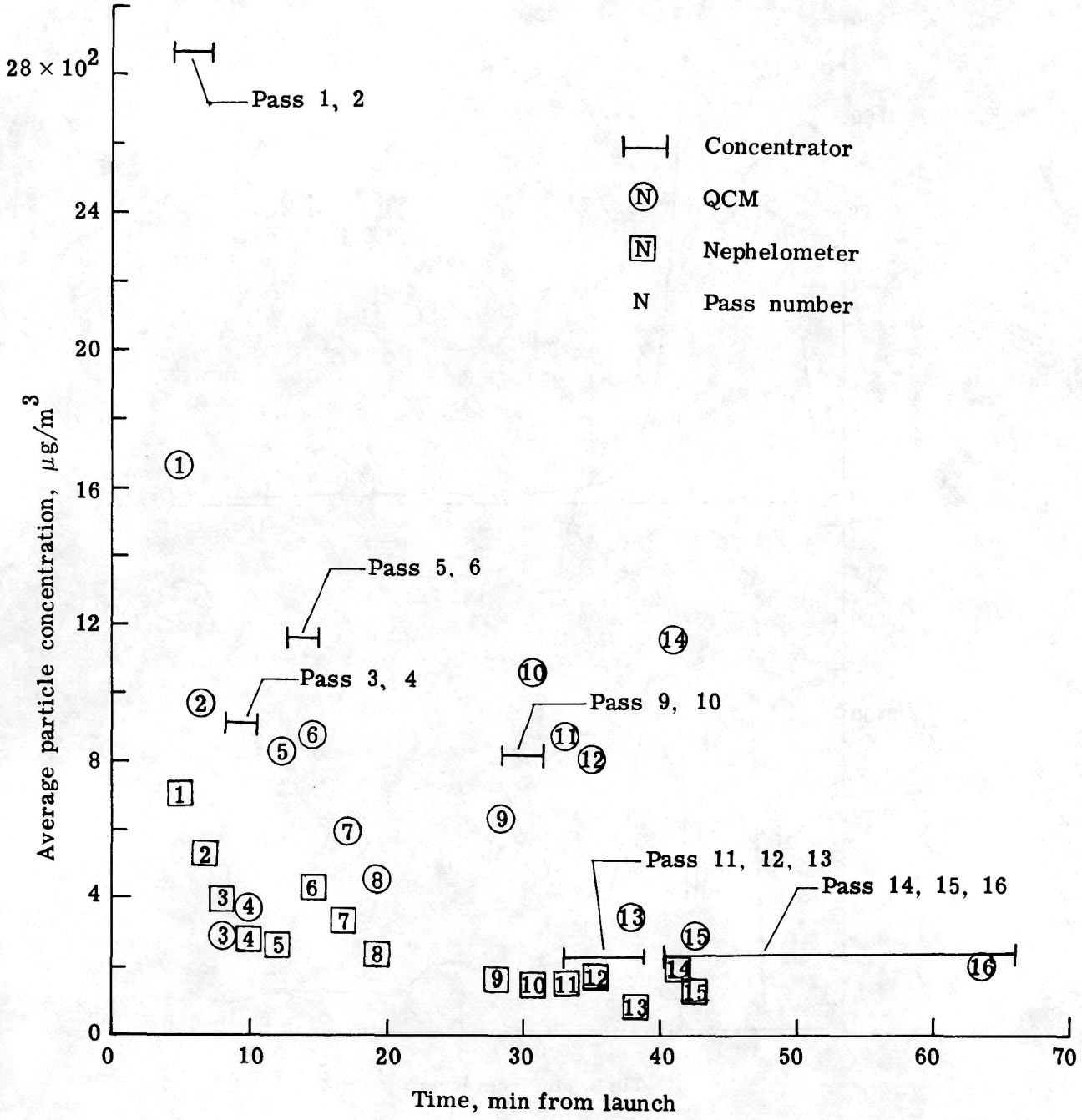

Figure 32.- Comparison of airborne data. Particulates.

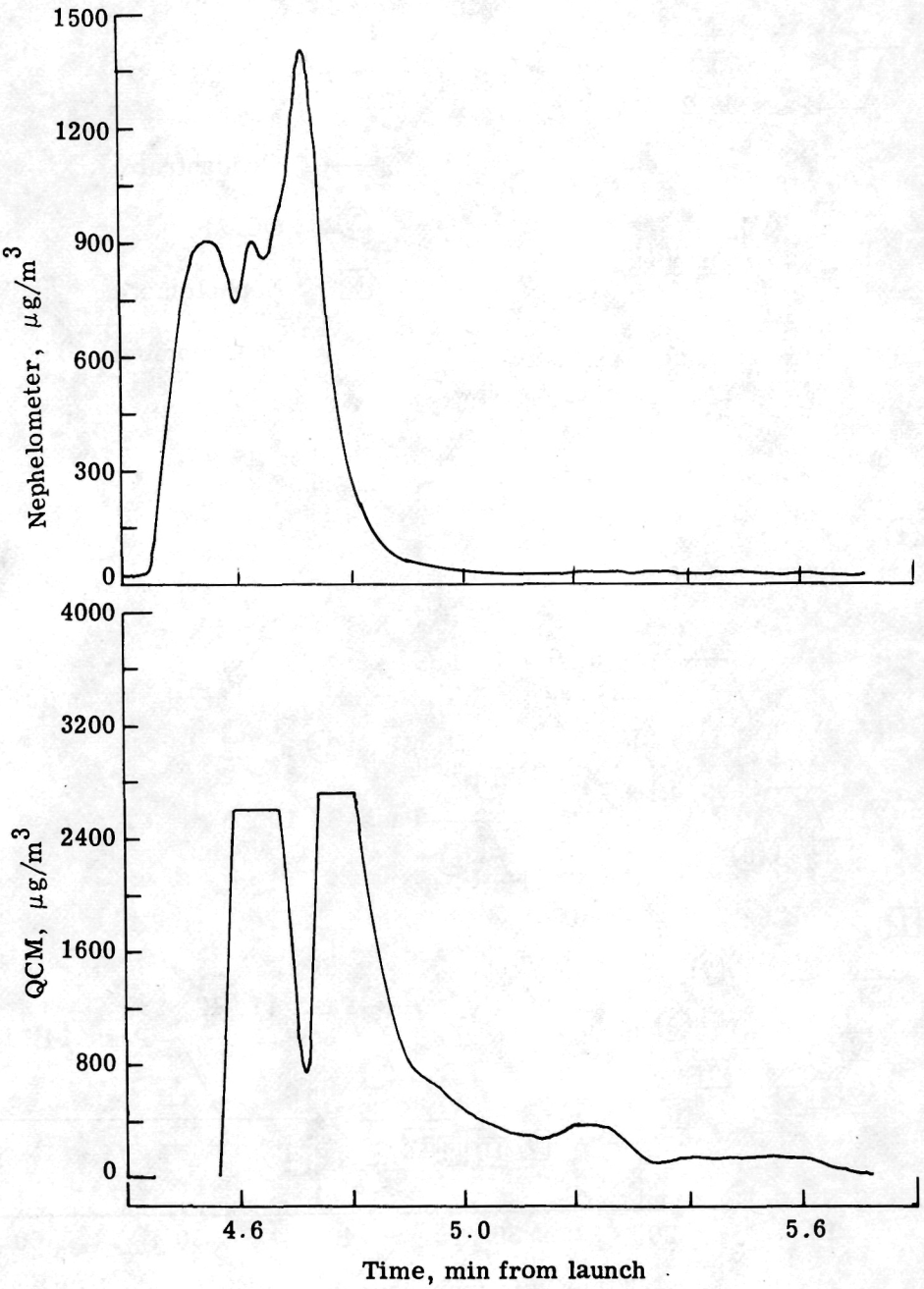

Figure 33.- Airborne data. Sampling pass 1.

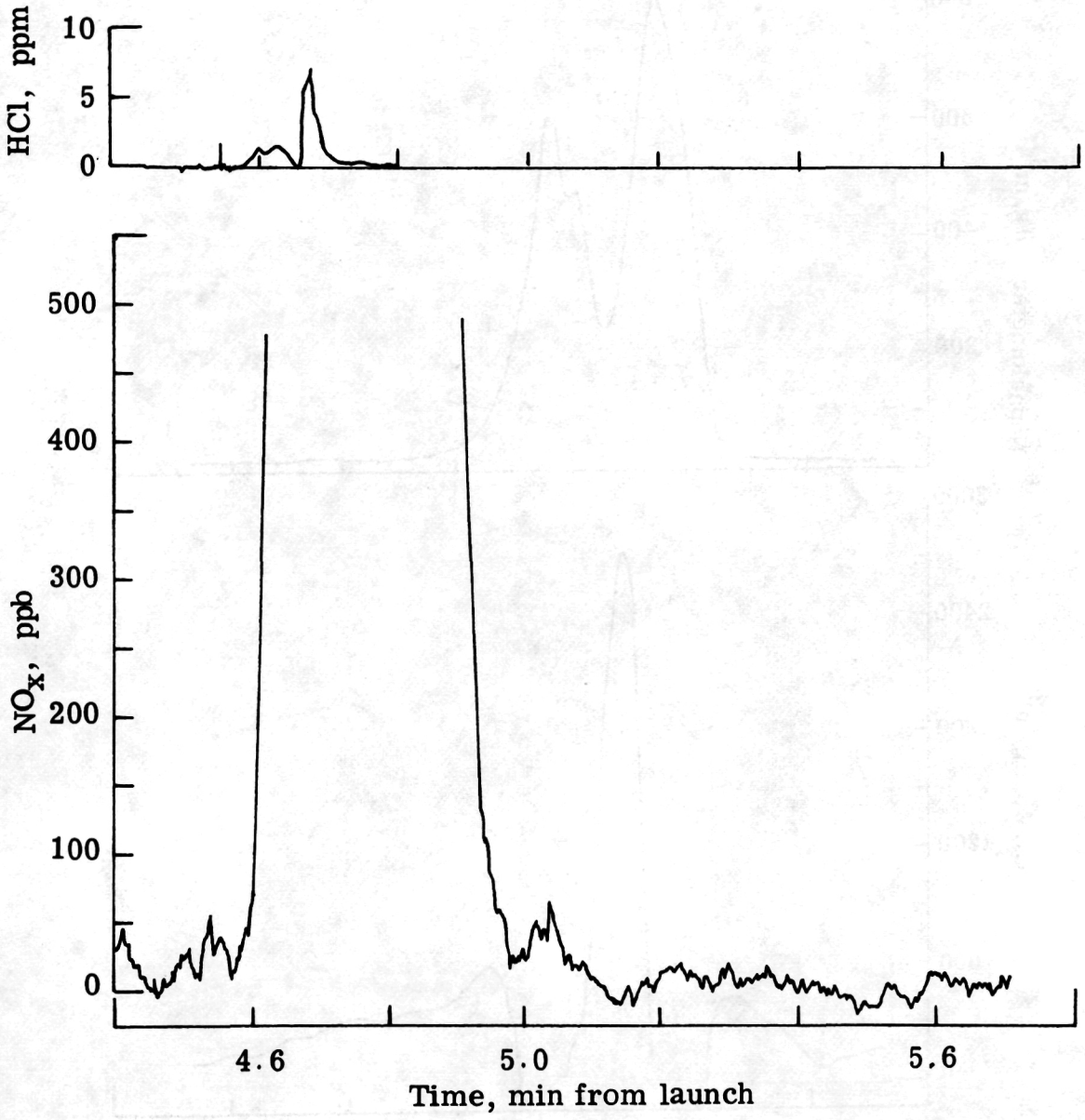

Figure 33.- Concluded.

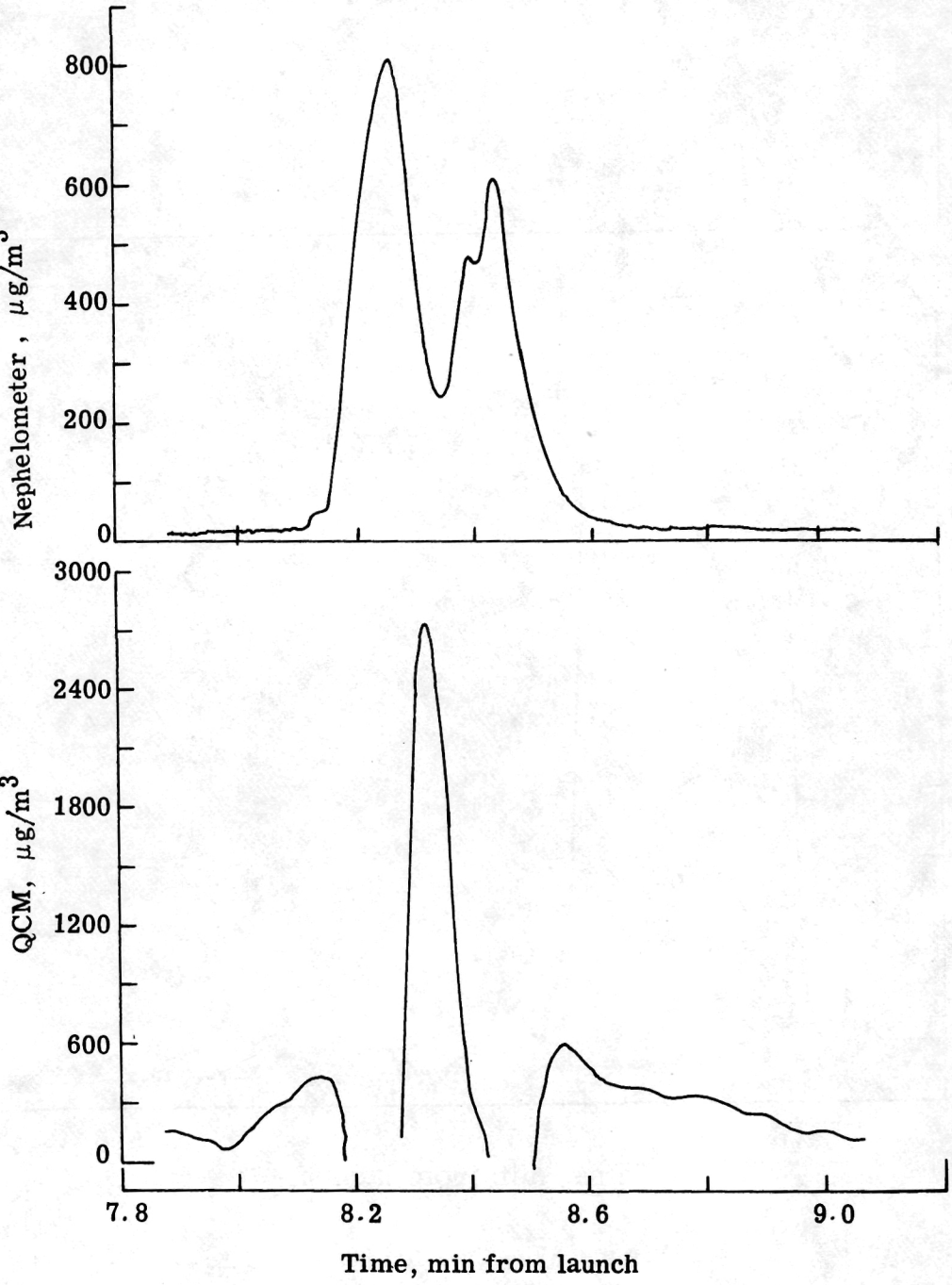

Figure 34.- Airborne data. Sampling pass 3.

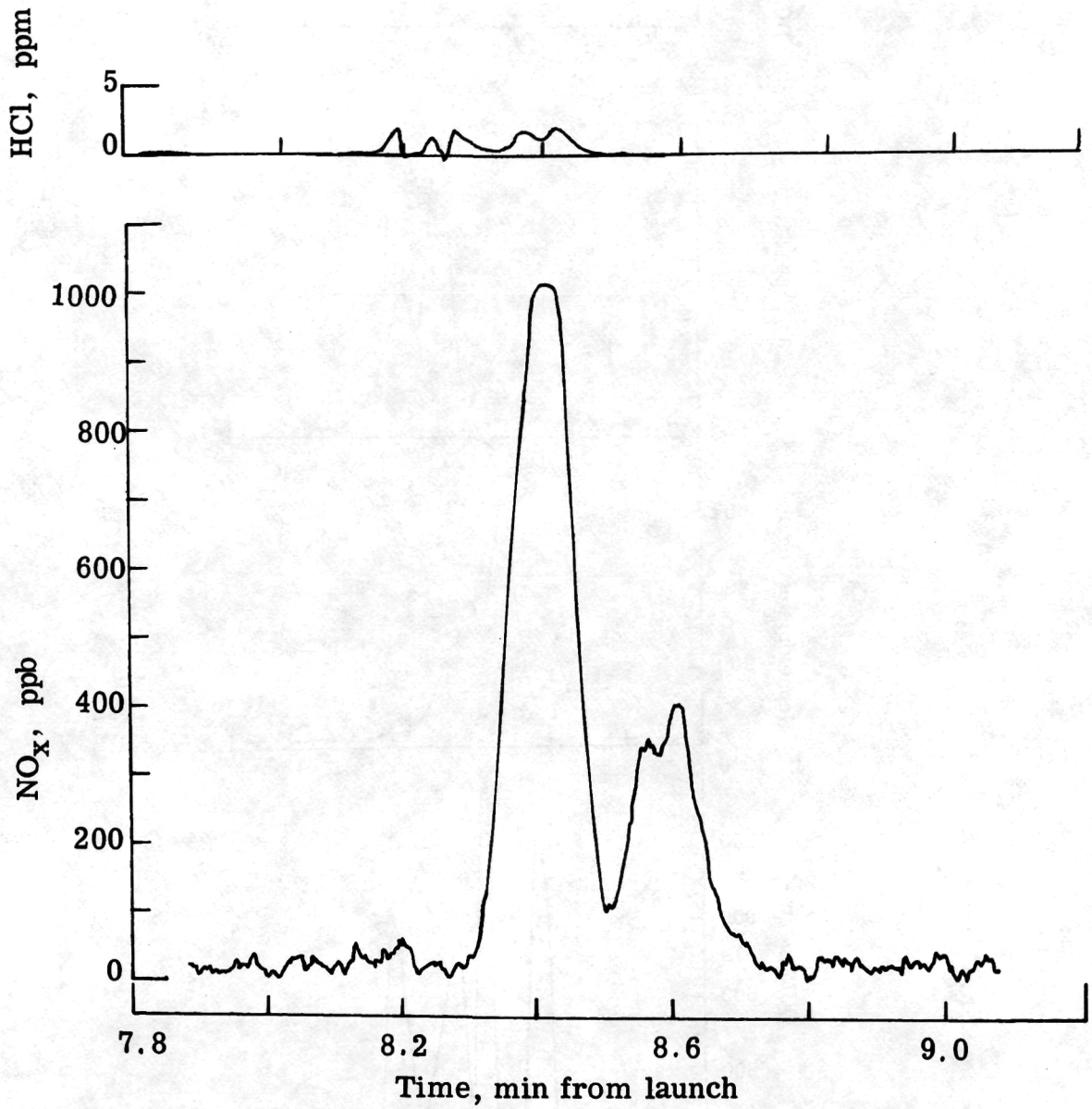

Figure 34.- Concluded.

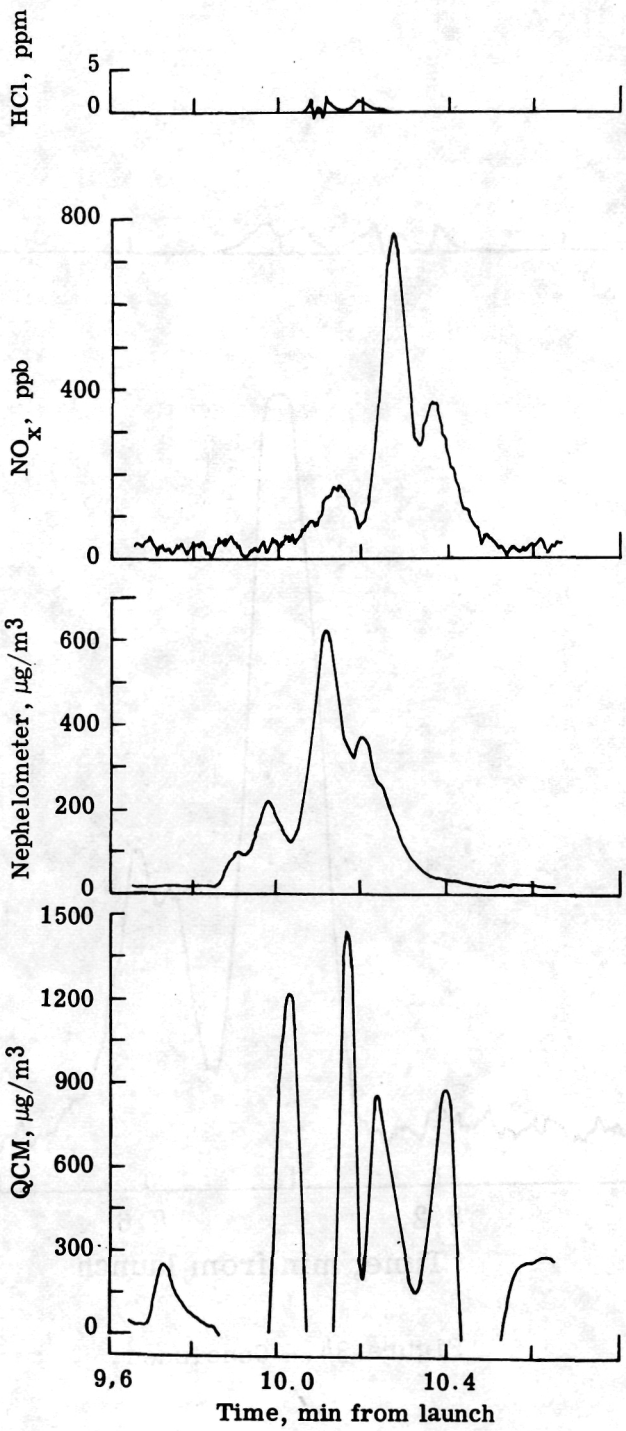

Figure 35.- Airborne data. Sampling pass 4.

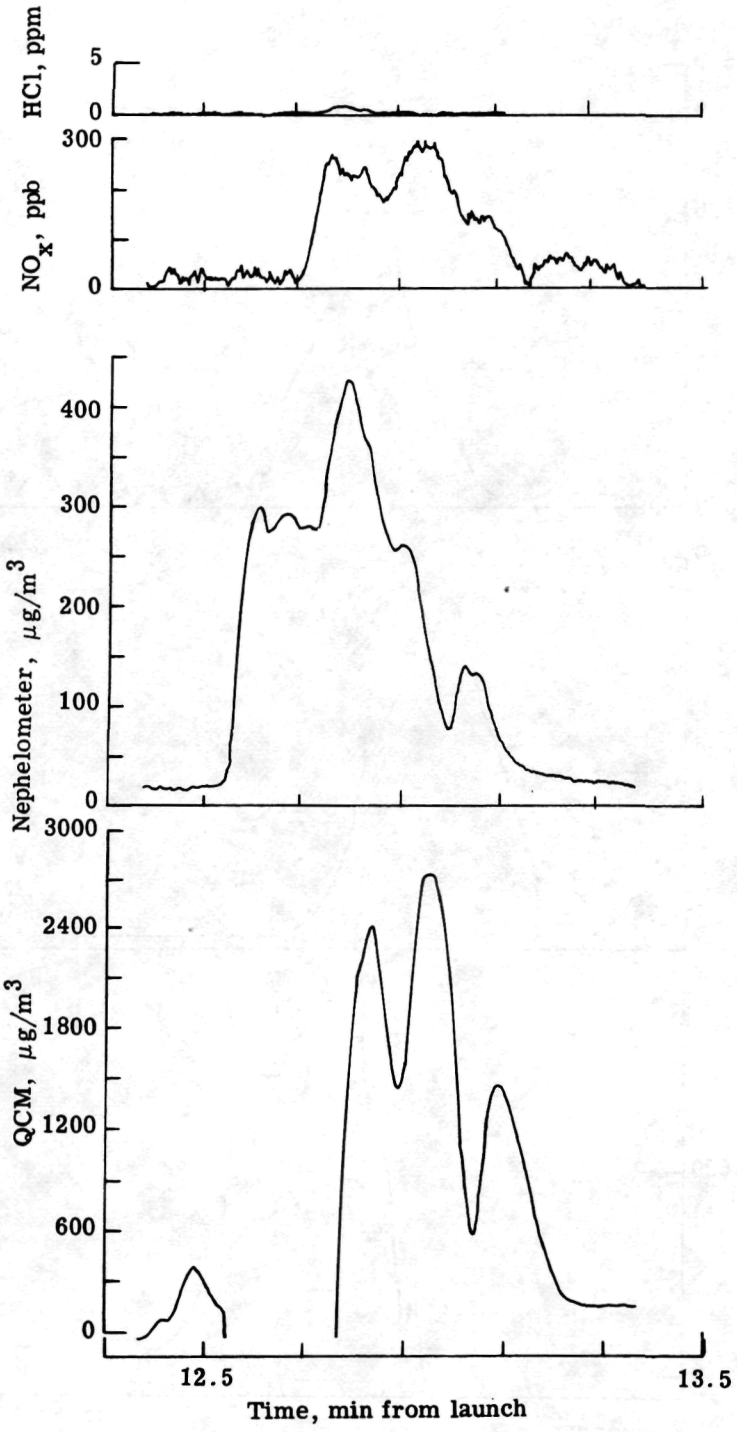

Figure 36.- Airborne data. Sampling pass 5.

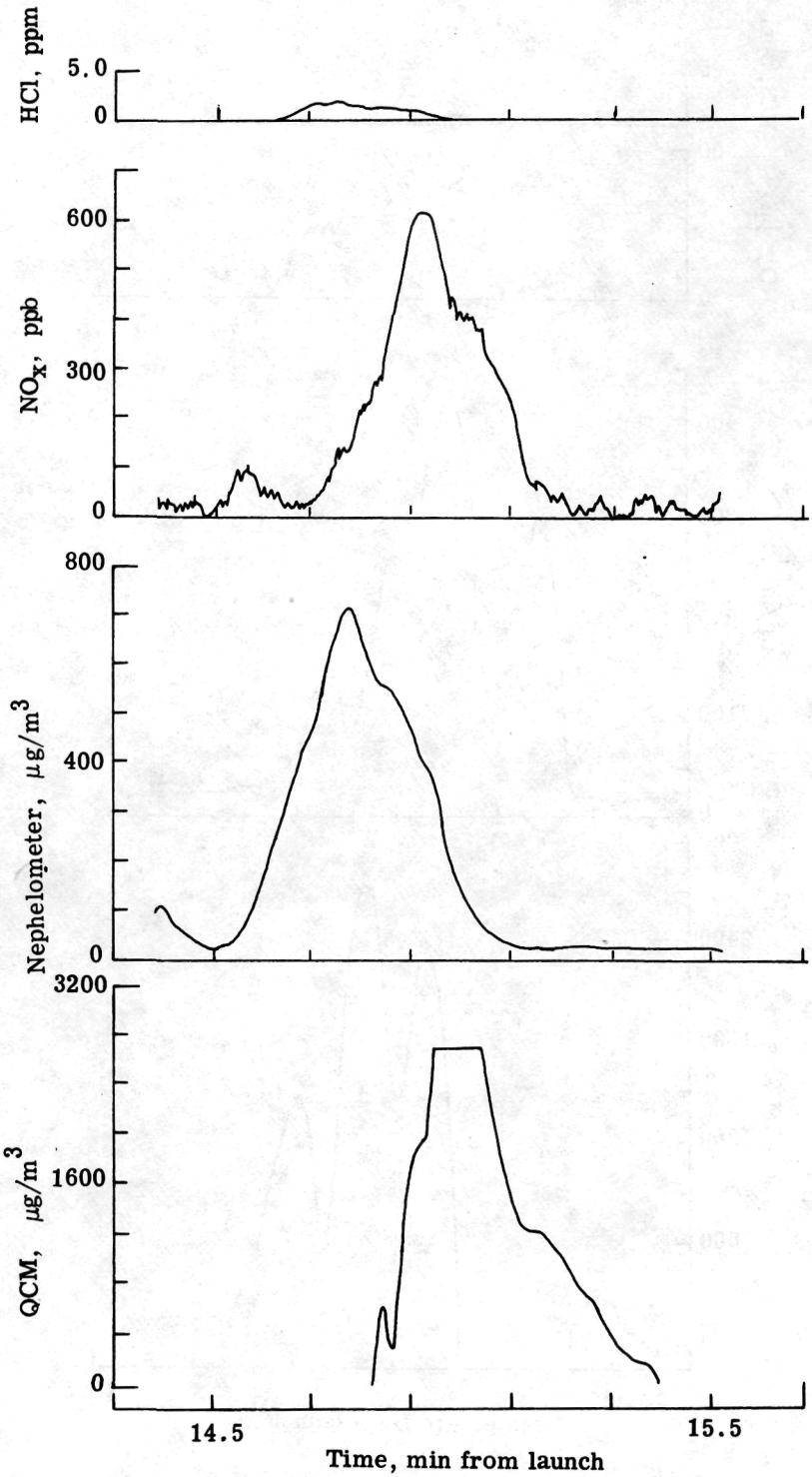

Figure 37.- Airborne data. Sampling pass 6.

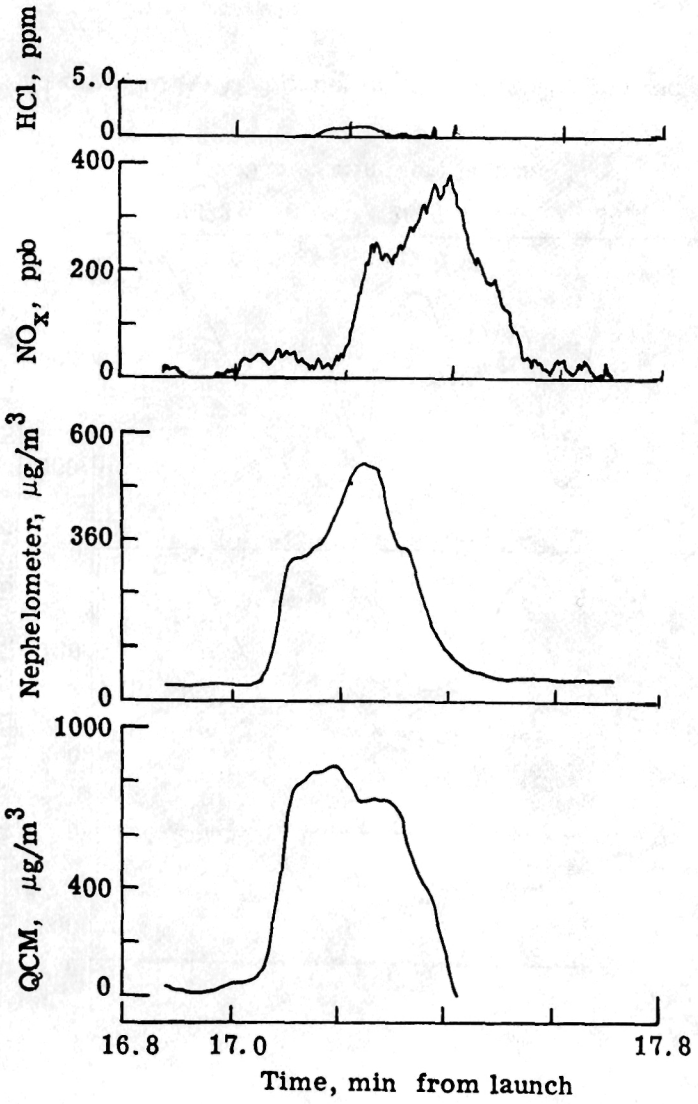

Figure 38.- Airborne data. Sampling pass 7.

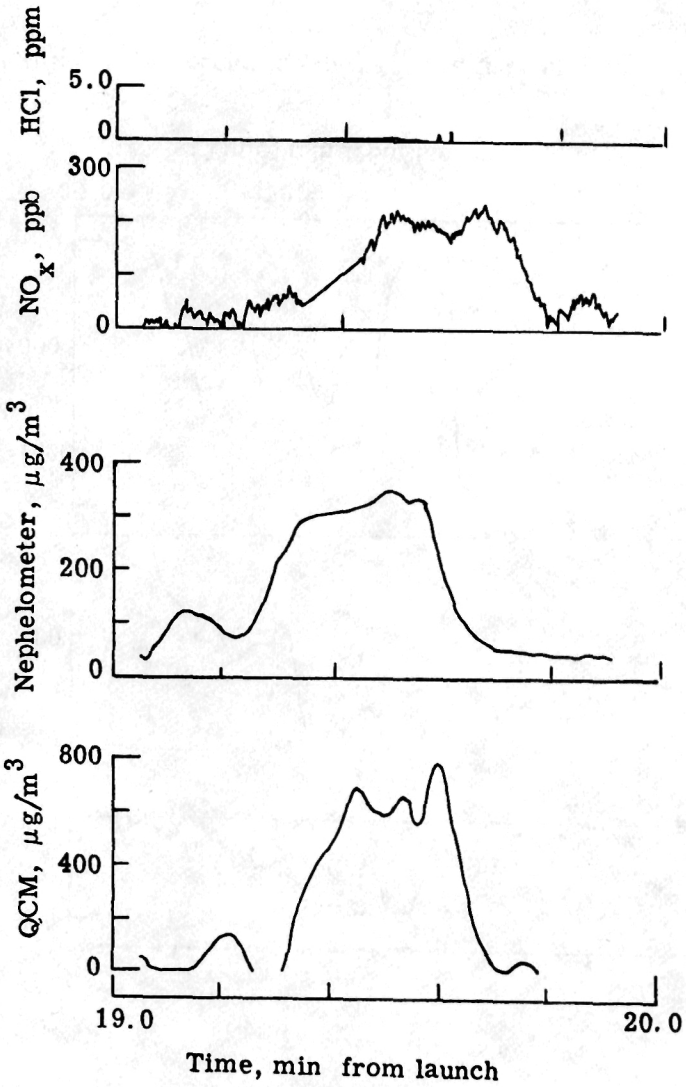

Figure 39.- Airborne data. Sampling pass 8.

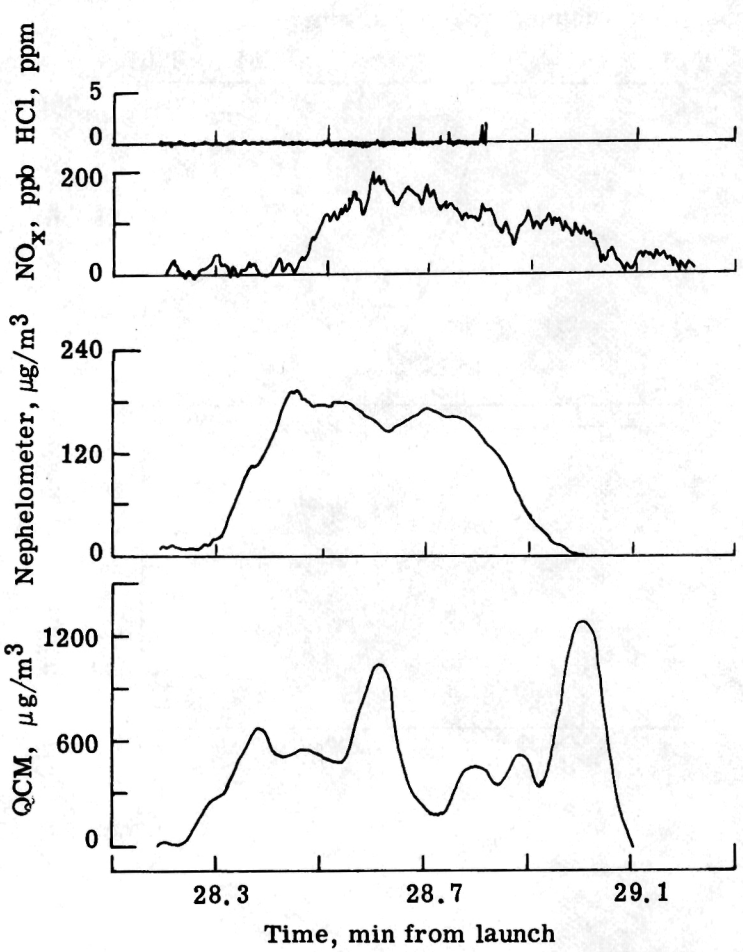

Figure 40.- Airborne data. Sampling pass 9.

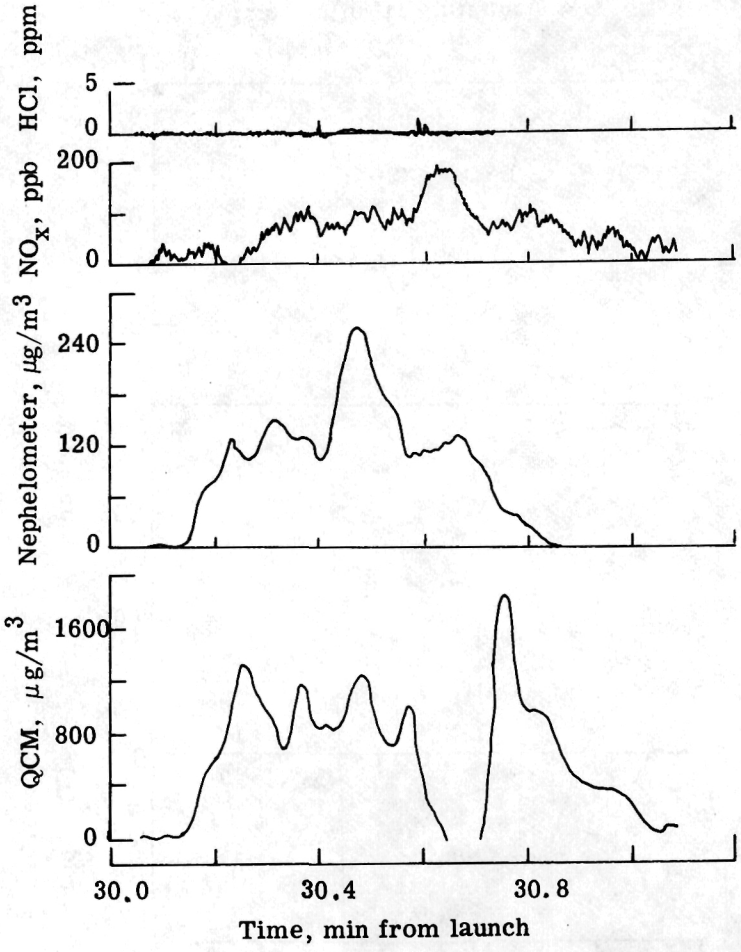

Figure 41.- Airborne data. Sampling pass 10.

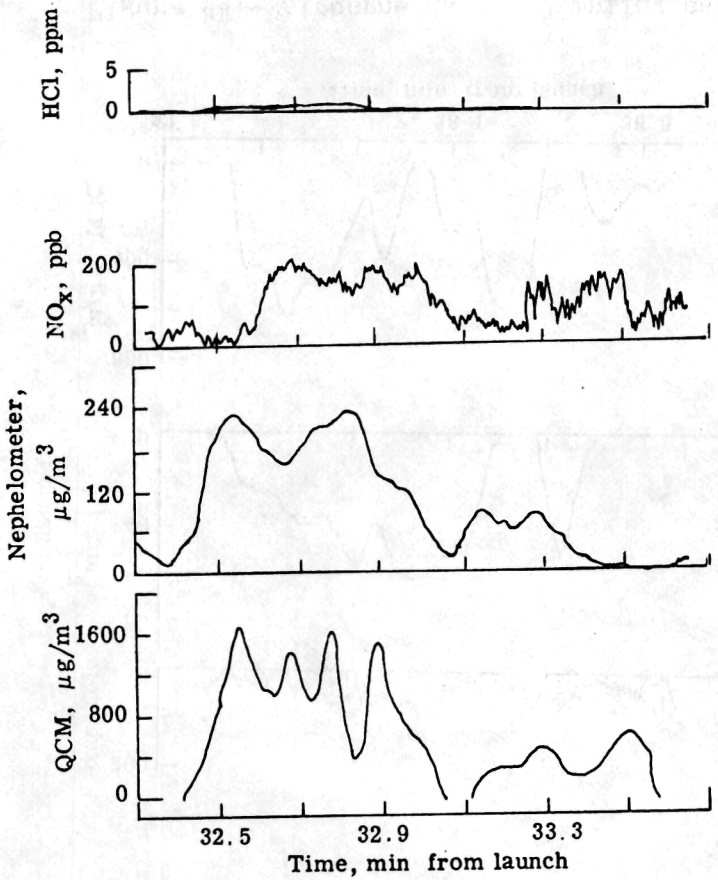

Figure 42.- Airborne data. Sampling pass 11.

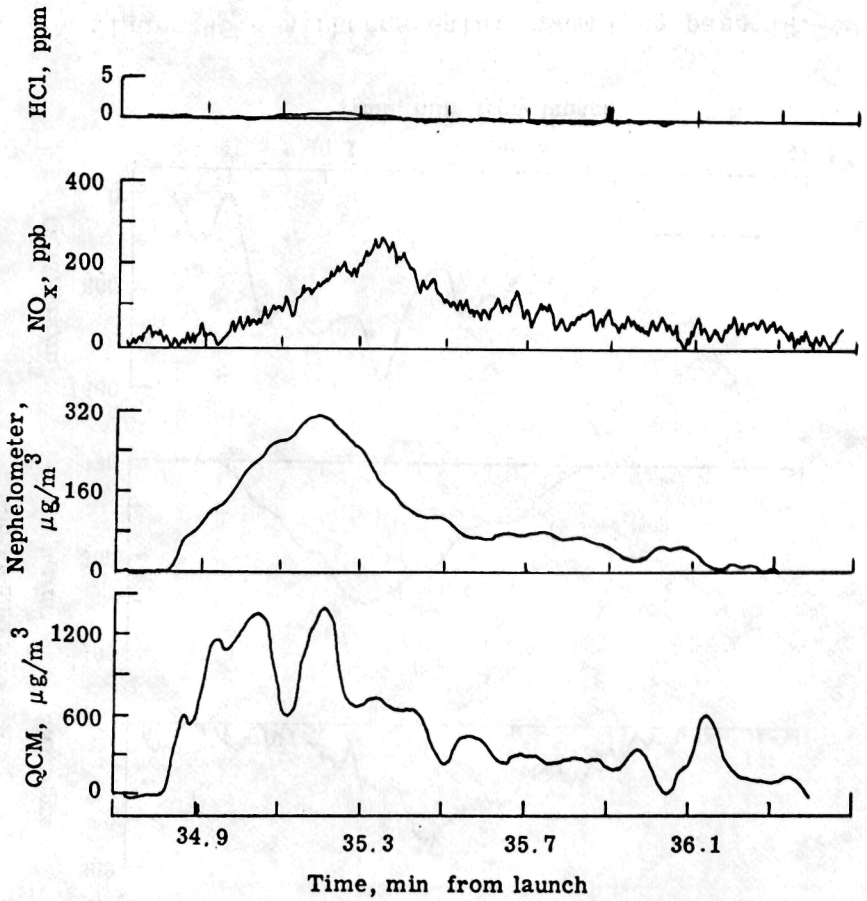

Figure 43.- Airborne data. Sampling pass 12.

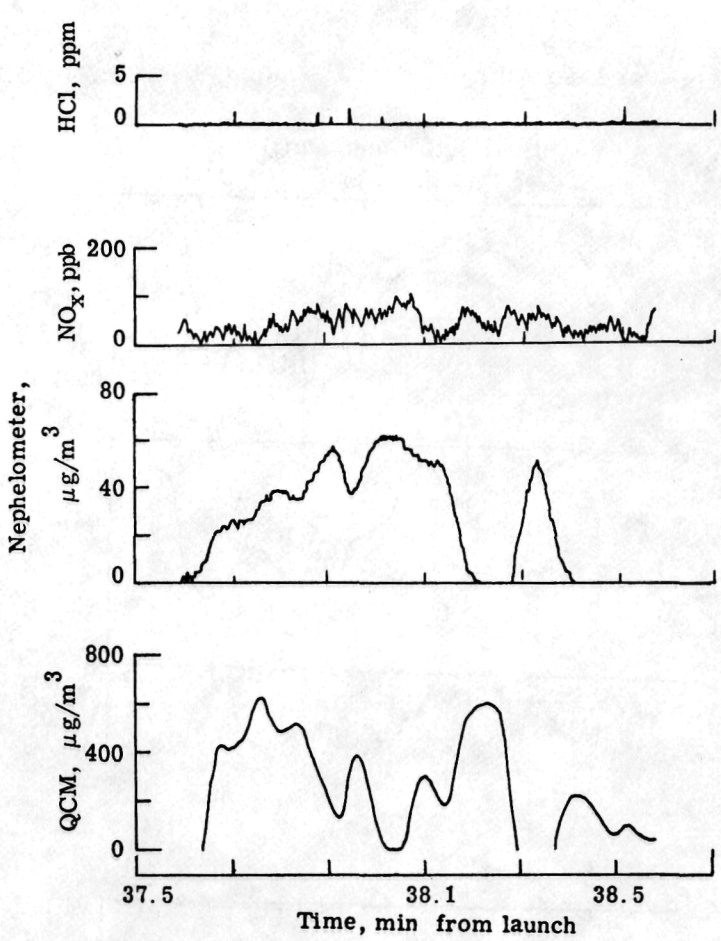

Figure 44.- Airborne data. Sampling pass 13.

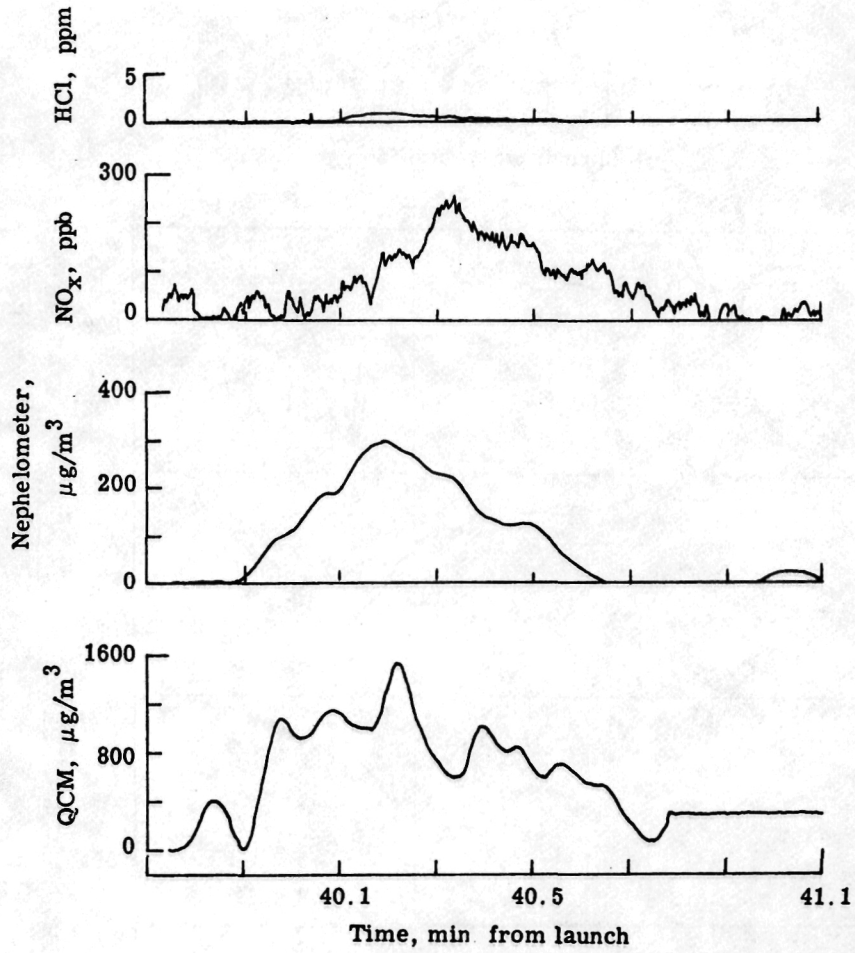

Figure 45.- Airborne data. Sampling pass 14.

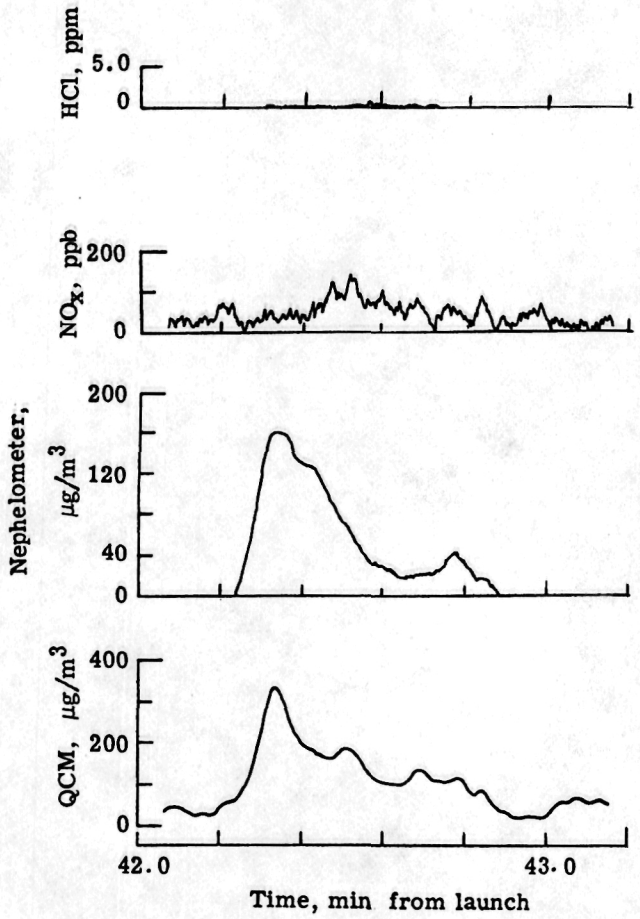

Figure 46.- Airborne data. Sampling pass 15.

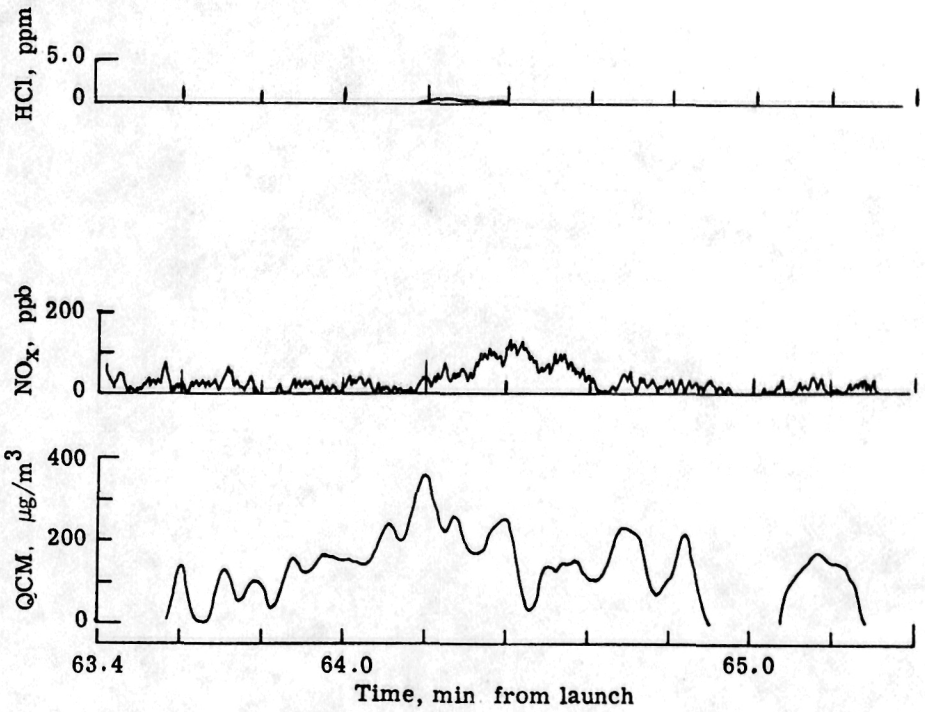

Figure 47.- Airborne data. Sampling pass 16.

1. Report No.	2. Government Accession No.	3. Recipient's Catalog No.
NASA TM-74044		

4. Title and Subtitle	5. Report Date
EXPERIMENTAL MEASUREMENTS OF THE GROUND CLOUD EFFLUENTS AND CLOUD GROWTH FOR THE MAY 20, 1975, TITAN IIIC LAUNCH AT AIR FORCE EASTERN TEST RANGE, FLORIDA	November 1977
	6. Performing Organization Code

7. Author(s)	8. Performing Organization Report No.
Gerald L. Gregory and Richard W. Storey, Jr.	L-11699
	10. Work Unit No. 989-15-20-01

9. Performing Organization Name and Address	11. Contract or Grant No.
NASA Langley Research Center Hampton, VA 23665	
	13. Type of Report and Period Covered
12. Sponsoring Agency Name and Address	Technical Memorandum
National Aeronautics and Space Administration Washington, DC 20546	14. Sponsoring Agency Code

15. Supplementary Notes

16. Abstract

The report summarizes the effluent measurements and tests of ground cloud behavior made during the May 20, 1975, Titan IIIC launch from the Air Force Eastern Test Range, Florida. The launch vehicle effluent monitoring experiments were carried out jointly by Langley Research Center, Marshall Space Flight Center, and Kennedy Space Center, all of the National Aeronautics and Space Administration (NASA). The experiment included surface level and airborne in situ cloud measurements of the exhaust effluents from the Titan IIIC solid rocket boosters. Simultaneous visible spectrum photographic pictures of the ground cloud as well as infrared imaging of the cloud were obtained to study the cloud rise, growth, and direction of travel within the Earth's surface mixing layer. The NASA multilayer diffusion model predictions of cloud growth, direction of travel, and expected surface level effluent concentrations were made prior to launch and after launch using measured meteorological conditions. Prelaunch predictions were used to position the effluent monitoring instruments, and the postlaunch predictions were compared with the measured data. Measurement results showed that surface level effluent values were low, often below the detection limits of the instrumentation. The maximum surface level hydrogen chloride concentration measured 50 parts per billion at about 8 km from the launch pad. The maximum observed in-cloud (airborne measurement) hydrogen chloride concentration was 7 parts per million.

17. Key Words (Suggested by Author(s))	18. Distribution Statement
Effluent sampling Rocket vehicle exhaust Titan IIIC booster exhaust	Unclassified - Unlimited Subject Category 45

19. Security Classif. (of this report)	20. Security Classif. (of this page)	21. No. of Pages	22. Price*
Unclassified	Unclassified	91	$5.00

* For sale by the National Technical Information Service, Springfield, Virginia 22161

NASA-Langley, 1977

National Aeronautics and
Space Administration

Washington, D.C.
20546

Official Business
Penalty for Private Use, $300

THIRD-CLASS BULK RATE

Postage and Fees Paid
National Aeronautics and
Space Administration
NASA-451

7 2 1U,E, 103177 S90344HU
MCDONNELL DOUGLAS CORP
ATTN: PUBLICATIONS GROUP, PR 15246
P O BOX 516
ST LOUIS MO 63166

NASA

POSTMASTER: If Undeliverable (Section 158 Postal Manual) Do Not Return